DESIGN AND MODELING OF A REVERSIBLE 3-PHASE TO 6-PHASE INDUCTION MOTOR FOR IMPROVED SURVIVABILITY UNDER FAULTY CONDITIONS

by

Anushree Anantharaman Kadaba, B.S.E.E.

A Thesis Submitted to the Faculty
of the Graduate School,
Marquette University,
in Partial Fulfillment of
the Requirements for
the Degree of
Master of Science in Electrical and Computer Engineering

Milwaukee, Wisconsin
May, 2008

ABSTRACT

The Conventional standard three-phase induction motors have an inherent drawback in so far as performance under loss of phase conditions. The two-Phase operation of a three-phase induction motor doesn't provide the necessary performance such as torque and output power under applications which require high reliability such as in electric traction applications, electric ship propulsion, etc. Therefore one of the means to overcome this drawback is by the addition of more phases, which forms the main focus of this thesis.

The objective of this thesis is to develop a unique design for an induction motor which can function in both the three-phase and six-phase modes thus obtaining a reversible three-phase to six-phase operation. The functionality of this motor serves the purpose of a reliable operation in the case of loss of phase or phases. In this thesis, a case-study 3-phase, 5-hp squirrel cage, 60hz, 6-pole, induction motor was tested and modeled using time-stepping finite-element simulation. This motor was redesigned in this work for a six-phase stator winding configuration. This redesigned motor was simulated under different types of phase loss scenarios using time-stepping finite-element technique. A comparative analysis of the various phase loss conditions of the six-phase configuration with respect to the healthy six-phase case is presented. The analysis of the torque-ripple content with the help of current-space vector concepts was introduced. The ripple content in the torque is shown to improve with the reversible three-phase to six-phase design under loss of phase conditions. There are some thermal issues with regard to performance under loss of phase conditions which emerged in light of the values of the stator phase currents under such faults.

In conclusion, it was shown that the reversible motor design appears promising in so far as maintaining performance quality under faulty conditions, far better than the conventional three-phase design.. Practical application of such a design would yield better results and an effective means to provide higher performance sustainability /reliability under loss of phase / phases.

ACKNOWLEDGEMENT

To Be Completed

TABLE OF CONTENTS

List of Figures …….. vi

List of Tables …… xiv

Chapter 1: Introduction

1.1 Background …… 1

1.2 Literature Review …….. 1

1.3 Thesis Contribution ……... 6

1.4 Thesis Organization …….. 6

Chapter 2: Design of the three-phase case-study induction motor

2.1 Introduction ……... 8

2.2 Basics of designing polyphase A.C. windings…… 8

2.2.1 Basic rules for designing A.C. windings……. 9

2.3 Design formulations and layout of the 5-HP case-study three-phase induction motor ……. 12

2.3.1 List of symbols ……... 14

2.3.2 Characteristics of motor under study…….....15

2.3.3 Derivation of torque in closed form using design equations……. 16

2.4 Winding of stator…… 20

2.4.1 MMF distribution……... 26

Chapter 3: Reconfiguration of a three-phase induction machine to a six-phase induction machine

3.1 Introduction …… 29

3.2 Steps involved in the stator winding reconfiguration process…….. 30

3.3 Some considerations for the six-phase winding…… 34

3.4 Connection scheme for the six-phase winding configuration……... 36

3.5 The development of the six-phase winding……39

Chapter 4: Design of the six-phase induction motor

4.1 Introduction …… 43

4.2 The constraints and steps involved in the design…….. 43

4.2.1 Some important characteristics of a “good winding”…….. 44
4.3 Parameters of the six-phase induction motor……... 44
4.3.1 Calculation of the number of turns per phase for the design……45
4.3.2 Calculation of the voltage rating of the six-phase motor……. 48
4.4 Design of the stator winding…….49
4.4.1 MMF distribution…… 64
4.5 Connection scheme for the reversible three-phase to six-phase motor…….66
Chapter 5: Fundamentals of the time stepping finite element method
5.1 Introduction ……... 70
5.2 Development of the finite element method……. 70
5.2.1 Basic Principles…….71
5.2.2 Finite element formulation……73
5.2.3 Solution techniques…… 75
5.3 The time stepping finite element method…….. 76
Chapter 6: Experimental and Simulation Results
6.1 Introduction ……. 80
6.2 Comparison of experimental and simulation results of the three-phase operation …… ……. 81
6.3 Comparison of the time-stepping finite element simulation results of the three-phase operation and six-phase operation…….……. 87
6.4 Simulation of the six-phase induction motor under various phase loss scenarios…… 94
6.4.1 5-phase healthy and pne faulty phase operation……94
6.4.2 The four healthy phase-Two faulty phase operation……..98
6.4.2.1 Loss of two adjacent phase…… 98
6.4.2.2 Loss of two-non adjacent phases…… 102
6.4.3 The three-healthy phase and three faulty phase operation……109
6.4.3.1 Loss of three adjacent phases……110
6.4.3.2 Loss of three-non-adjacent phases……114
6.4.4 Simulation of the two-phase healthy operation with one faulty phase in a three-phase motor…….121

6.5 Observations and discussions on the reasons for torque ripples
in the faulty phase operations using current space vector concepts……...125
6.5.1 Harmonic analysis and observations……..131
6.5.2 Discussion about derating of the motor under various fault
scenarios……..135
6.5.2.1 Verification of derating of the motor for the 5-healthy
phase and one faulty phase condition with loss of phase
A by time-stepping finite-element simulation…….137
Chapter 7: Conclusions and Recommendations
7.1 Conclusions ……. 146
7.2 Recommendations for Future Work …… 147
References ……. 149

LIST OF FIGURES

2-1 Single Layer phase layout …… 10

2-2 Double layer phase layout ……..... 12

2-3 Phasor representation of induced emfs on both sides of a single turn in case of short-pithced coil…… 17

2-4 Flux Density Distribution per pole ……..……. 19

2-5 MMF Distribution in the uniform air-gap …… 19

2-6 Phasor diagram of conductor emfs showing slots carrying their respective phases. ……. 21

2-7 Spatial distribution of the Three Phases…… 22

2-8 Cross-Sectional view of stator slots showing the winding distributions of the three phases for the short-pitched design…….. 23

2-9 Cross-Sectional view of stator slots showing the winding distributions of the three phases for the full-pitched design……. 24

2-10 Complete Winding Layout showing the connection of all the coils …… .. 25

2-11 MMF Distribution produced by the Three-Phase winding under study ……. 27

3-1 Y-Connection of the 2 coil groups for Three-Phase Operation …… 30

3-2 Phasor representation Of Voltages In each coil group……..31

3-3 Phasor diagram of Volatge across the coil groups for the high-voltage connection …….. 32

3-4 Phasor diagram of Volatge across the coil groups for the low-voltage connection 33

3-5 Rearrangement Of the Voltage Phasors to form the Six-Phase configuration … 35

3-6 Connection Scheme For the Six-Phase winding …… 36

3-7 Spatial Distribution of phases in the Three-Phase And the Redesigned Six-Phase configurations …….. 38

3-8 Development Of The Six-Phase Winding ……. 40

3-9 Cross-sectional view of the stator slots showing the winding distributions of the Six Phases……..……42

4-1 Phasor diagram of the line and phase voltages in the 6-phase system …… 48

4-2 Six-Phase winding layout with, no. of poles = 6 , no. of slots per pole per phase = 1, Double layered , lap-connected full pitch winding ……..……...50

4-3 Connection Of the different Groups in the three-Phase configuration …….. 51

4-4 Connection Of the different Groups to form the Six-Phase configuration…….. 52

4-5 Connection of the coils of Group I and II constituting Phase A of the three-phase machine …….. 53

4-6 Connection of the coils of Group III and IV constituting Phase B of the three-phase machine …….....54

4-7 Connection of the coils of Group V and VI constituting Phase C of the three-phase machine …….. 55

4-8 Connection of coils of Group I constituting Phase A of the six-phase machine…….. 56

4-9 Connection of coils of Group II constituting Phase D of the six-phase machine….57

4-10 Connection of coils of Group III constituting Phase C of the three-phase machine 58

4-11 Connection of coils of Group IV constituting Phase F of the six-phase machine 59

4-12 Connection of coils of Group V constituting Phase E of the six-phase machine …60

4-13 Connection of coils of Group VI constituting Phase B of the six-phase machine 61

4-14 Cross-sectional view of the stator slots showing the winding distributions of the Six Phases. …… 62

4-15 Complete Winding layout Of The Reconfigured Six-Phase induction machine Showing connections of all the coils…….63

4-16 The mmf distribution produced by the currents in the six windings of the six-phase machine. …… 65

4-17 Connection Scheme For Six-Phase Operation ……. 67

4-18 Connection Scheme For Three-Phase Operation…….69

5-1 Typical triangular finite element connected to other finite elements……74

5-2 Finite-element mesh of a portion of the case-study 5HP induction motor…. 78

6-1 Flow-Chart of types of phase-loss scenarios studied …… 81

6-2 Line voltages obtained from experimental test for the case study 5HP , 3-phase induction conditions ……. 82

6-3 Line voltages obtained from the TSFE simulation for the 5HP, 3-phase induction motor ……. 82

6-4 Phase Currents obtained from experimental test for the 5HP, 3-phase induction motor …….. 83
6-5 Phase Currents obtained from the TSFE simulation for the 5HP, 3-phase induction motor ……. 83
6-6 steady state torque profile from experimental test for the 5HP , 3-phase induction motor …… 84
6-7 steady state torque profile from the TSFE simulation for the 5HP , 3-phase induction motor ……. 84
6-8 Flux plot of the 3-phase machine ……. 88
6-9 Flux plot of the 6-phase machine ……. 88
6-10 Plot of phase voltages in the 3-phase machine…… 89
6-11 Plot of phase voltages in the 6-phase machine …… 89
6-12 Plot of flux-density in the mid-airgap of the 3-phase induction machine from TSFE simulation …….. 90
6-13 Plot of flux-density in the mid-airgap of the 6-phase induction machine from TSFE simulation……. 90
6-14 Phase currents i_a , i_b and i_c of the 3-phase induction machine from TSFE simulation ……. 91
6-15 Phase currents i_a , i_b , i_c , i_d , i_e and i_f of the 6-phase induction machine from TSFE simulation…….. 91
6-16 Torque profile of 3-phase induction motor under rated conditions from TSFE simulation ……..... 92
6-17 Torque profile of 6-phase induction motor under rated conditions from TSFE simulation …… 92
6-18 Speed profile of 3-phase induction motor under rated conditions from TSFE simulation…….. 93
6-19 Speed profile of 6-phase induction motor under rated conditions from TSFE simulation …… 93
6-20 Phasor representation of the voltages in six-phase healthy operation……..95
6-21 Phasor representation of the voltages in the five-phase operation with loss of Phase A …….. ……...95
6-22 Torque profile of the healthy 6-phase case under full-load……. 96

6-23 Torque profile of the 5-healthy phase case with loss of phase A …… 96

6-24 Harmonic spectrum of the torque profile of the healthy 6-phase case …….. 96

6-25 Harmonic spectrum of the torque profile of the 5-healthy phase case with loss of phase A …….. 96

6-26 Phase currents i_a , i_b , i_c , i_d , i_e and i_f of the 5-healthy and one faulty phase operation of the six-phase induction motor …….....97

6-27 Phase currents i_a , i_b , i_c , i_d , i_e and i_f of the healthy six-phase induction motor…...96

6-28 Flow chart summarizing the various cases of 4-phase operations studied.....… 98

6-29 Phasor representation of the voltages in six-phase healthy operation …… 99

6-30 Phasor representation of the voltages in the four-healthy phase operation with loss of adjacent phases A and B ……. 99

6-31 Torque profile of the healthy 6-phase case under full-load……. 100

6-32 Torque profile of the 4-healthy phase case with loss two adjacent phases A and B ……. 100

6-33 Harmonic spectrum of the torque profile of the healthy 6-phase case ……..100

6-34 Harmonic spectrum of the torque profile of the 4-healthy phase case with loss of adjacent phases A and B ……..... 100

6-35 Phase currents i_a , i_b , i_c , i_d , i_e and i_f of the 4-healthy and two faulty phase operation of the six-phase induction motor with loss of adjacent phases A and B…… 101

6-36 Phase currents i_a , i_b , i_c , i_d , i_e and i_f of the healthy six-phase induction motor… 101

6-37 Phasor representation of the voltages in six-phase healthy operation…… 103

6-38 Phasor representation of the voltages in the four-healthy phases with two non-adjacent faulty phase separated by 120^0 *e* operation with loss of phases A and C ……. …… 103

6-39 Torque profile of the healthy 6-phase case under full-load……104

6-40 Torque profile of the 4-healthy phase case with loss two non-adjacent phases separated by 120^0 *e* i.e. phases A and C …… 104

6-41 Harmonic spectrum of the torque profile of the healthy 6-phase case …… 104

6-42 Harmonic spectrum of the torque profile of the 4-healthy phase case with loss of non-adjacent phases A and C …….. 104

6-43 Phase currents i_a , i_b , i_c , i_d , i_e and i_f of the 4-healthy and two faulty phase operation of the six-phase induction motor with loss of non-adjacent phases A and C …… 105

6-44 Phase currents i_a , i_b , i_c , i_d , i_e and i_f of the healthy six-phase induction motor …..105

6-45 Phasor representation of the voltages in six-phase healthy operation……...106

6-46 Phasor representation of the voltages in the four-healthy phase with two non-adjacent faulty phase separated by 180^0 *e* operation with loss of phases A and D ……106

6-47 Torque profile of the healthy 6-phase case under full-load…… 107

6-48 Torque profile of the 4-healthy phase case with loss two non-adjacent phases separated by 180^0 *e* i.e. phases A and D) …….. 107

6-49 Harmonic spectrum of the torque profile of the healthy 6-phase case…… 107

6-50 Harmonic spectrum of the torque profile of the 4-healthy phase case with loss of non-adjacent phases A and D …… 107

6-51 Phase currents i_a , i_b , i_c , i_d , i_e and i_f of the 4-healthy and two faulty phase operation of the six-phase induction motor with loss of non-adjacent phases A and D…….108

6-52 Phase currents i_a , i_b , i_c , i_d , i_e and i_f of the healthy six-phase induction motor… 108

6-53 Flow chart summarizing the various cases of 3-phase operations studied……110

6-54 Phasor representation of the voltages in six-phase healthy operation……...111

6-55 Phasor representation of the voltages in the three healthy phase with three adjacent faulty phase loss operation with loss of phases A, B and C……111

6-56 Torque profile of the healthy 6-phase case under full-load ……..112

6-57 Torque profile of the 3-healthy phase case with loss three adjacent phases separated by 60^0 *e* i.e. phases A , B and C …… 112

6-58 Harmonic spectrum of the torque profile of the healthy 6-phase case……. 112

6-59 Harmonic spectrum of the torque profile of the 3-healthy phase case with loss of three adjacent phases A,B and C ……... 112

6-60 Phase currents i_a , i_b , i_c , i_d , i_e and i_f of the 3-healthy and three faulty phase operation of the six-phase induction motor with loss of adjacent phases A , B and C …… 113

6-61 Phase currents i_a , i_b , i_c , i_d , i_e and i_f of the healthy six-phase induction motor… 113

6-62 Phasor representation of the voltages in six-phase healthy operation…… 115

6-63 Phasor representation of the voltages in the three healthy phase with three non-adjacent phase loss operation separated by120^0 *e* each i.e. with loss of phases A, C and E…….115

6-64 Torque profile of the healthy 6-phase case under full-load ……. 116

6-65 Torque profile of the 3-healthy phase case with loss three non- adjacent phases separated by 120^0 *e* i.e. phases A , C & E…… 116

6-66 Harmonic spectrum of the torque profile of the healthy 6-phase case……..116

6-67 Harmonic spectrum of the torque profile of the 3-healthy phase case with loss of three non-adjacent phases A,C & E …….116

6-68 Phase currents i_a , i_b , i_c , i_d , i_e and i_f of the 3-healthy and three faulty phase operation of the six-phase induction motor with loss of non-adjacent phases A , C and E……. 117

6-69 Phase currents i_a , i_b , i_c , i_d , i_e and i_f of the healthy six-phase induction motor……117

6-70 Phasor representation of the voltages in six-phase healthy operation……...118

6-71 Phasor representation of the voltages in the three healthy phase with three non-adjacent faulty phase loss operation with loss of phases A, B and D…….118

6-72 Torque profile of the healthy 6-phase case under full-load…… 119

6-73 Torque profile of the 3-healthy phase case with loss three non- adjacent phases separated by 120^0 *e* and 60^0 *e* i.e. phases A , B and D…… 119

6-74 Harmonic spectrum of the torque profile of the healthy 6-phase case…… 119

6-75 Harmonic spectrum of the torque profile of the 3-healthy phase case with loss of three non-adjacent phases A,B & D……119

6-76 Phase currents i_a , i_b , i_c , i_d , i_e and i_f of the 3-healthy and three faulty phase operation of the six-phase induction motor with loss of non-adjacent phases A , B and D……120

6-77 Phase currents i_a , i_b , i_c , i_d , i_e and i_f of the healthy six-phase induction motor……120

6-78 Phasor representation of the voltages in three-phase healthy operation……122

6-79 Phasor representation of the voltages in the two healthy phase with loss of phase A. 122

6-80 Torque profile of the healthy 6-phase case under full-load…… 123

6-81 Torque profile of the 2-healthy phase case with loss of phase A…… 123

6-82 Harmonic breakdown of the torque profile of the healthy 6-phase case…… 123

6-83 Harmonic breakdown of the torque profile of the 2-healthy phase case with loss of phase A…… 123

6-84 Phase currents i_a , i_b , i_c of the 2-healthy and one faulty phase operation of the three-phase induction motor with loss of phase A……... 124

6-85 Phase currents i_a , i_b , i_c of the healthy three-phase induction motor……124

6-86 Locus of current space vector in the healthy 6-phase operation in a 6-phase motor…126

6-87 Locus of current space vector in the healthy 3-phase operation in a three-phase motor126

6-88 Locus of current space vector in the one faulty phase operation with loss of phase A in a 6-phase motor…….127

6-89 Locus of current space vector in two faulty phases operation with loss of adjacent phases A and B in a 6-phase motor……127

6-90 Locus of current space vector in the two faulty phases operation with loss of non-adjacent phases separated by 180^0 e i.e. phases A and D in a 6-phase motor…….128

6-91 Locus of the current space vector in the two faulty phases operation with loss of non-adjacent phases separated by 120^0 e i.e. phases A and C, in a 6-phase motor…….128

6-92 Locus of the current space vector in the three faulty phase operation with loss of non-adjacent phases separated by 120^0 e i.e. phases A , C and E, in a 6-phase motor……129

6-93 Locus of the current space vector in the three faulty phases operation with loss of adjacent phases separated by 60^0 e i.e. phases A , B and C, in a 6-phase motor……..129

6-94 Locus of current space vector in the three-faulty phases operation with loss of non-adjacent phases separated by 120^0 e and 60^0 e i.e. phases A, B and D , in a 6-phase motor.130

6-95 Locus of the current space vector in the one-faulty phase operation with loss of Phase A , in a three-phase motor…….130

6-96 Variation of 2nd order harmonic in different cases…….131

6-97 Harmonic spectrum of the 6-phase healthy case…… 132

6-98 Harmonic spectrum of the 5-healthy phase and one faulty phase case……..132

6-99 Harmonic Spectrum of the 4-healthy phase and two adjacent faulty phases A and B...132

6-100 Harmonic Spectrum of the 4-healthy phase and two non-adjacent faulty phases A and C…….132

6-101 Harmonic Spectrum of the 4-healthy phase and two non-adjacent faulty phases A and D…….132

6-102 Harmonic Spectrum of the 3-healthy phase and 3 adjacent faulty phases A ,B and C……132

6-103 Harmonic Spectrum of the 3-healthy phase and 3 non- adjacent faulty phases A ,C and E.....132

6-104 Harmonic Spectrum of the 3-healthy phase and 3 non- adjacent faulty phases A ,B and D…….132

6-105 Harmonic Spectrum of the 2-healthy phase and one faulty phase of a three phase motor…….132

6-106 Summarized chart showing the torque ripple content under different cases……. 133

6-107 Phase currents in the 5-healthy and one faulty phase with loss of phase A before derating the motor from TSFE simulation……..140

6-108 Phase currents in the 5-healthy and one faulty phase with loss of phase A after derating the motor from TSFE simulation……..140

LIST OF TABLES

2-1 Possible slot combinations of 3-phase induction motors which can be readily reconfigured to 6-phase induction motors……..13

3-1 Relationship between Coils of The Three-Phase winding and their corresponding phases in the Six-Phase machine…….....39

6-1 Harmonic breakdown of the experimental versus the TSFE simulation results of the line-to-line voltage for the case study 5hp Induction motor……...85

6-2 Harmonic breakdown of the experimental versus the TSFE simulation results of the phase current for the case study 5hp Induction motor…….86

6-3 Harmonic breakdown of the experimental versus the TSFE simulation results of the torque for the case study 5hp Induction motor……87

6-4 RMS values of phase currents under the various cases considered……134

6-5 Power rating and the corresponding torque under various conditions after derating the motor……144

CHAPTER 1: INTRODUCTION

1.1 BACKGROUND

In general, motors are classified by type and by electrical supply requirements. Basically there are two broad classifications of alternating current machines. One type is the poly-phase synchronous motor, in which the magnetic field associated with the rotor results from a rotor (field) winding excited by direct current via slip rings or brushless exciter from permanent magnets on the rotor structure. The second type of alternating current machine is the poly-phase or single phase induction machine , in which the rotor magnetic field is created by electromagnetic induction effects. Of all the electrical machines, Induction motors are probably the most common in industry due to their simplicity, rugged structure, cheapness and easy maintainability.

1.2 LITERATURE REVIEW

Very early Induction motors had two phases [1], but the three-phase version very soon replaced these, and this eliminated the third harmonic problems associated with two-phase machines and resulted in a motor that was generally better in all performance aspects. Increasing the number of phases beyond three, though may be costly, has advantages which might be worth considering for certain special applications.Among the advantages of poly-phase (more than three) machines are the following

- Improved reliability since loss of one of many phases does not prevent the motor from starting and running

- Reduced torque pulsations and rotor harmonic power loss for inverter supplied motors.
- Reduced current per phase for a given output horsepower without increasing the voltage per phase. This is useful when there is a relatively low upper limit on voltage and current , such as in electric vehicles.
- Reduction in stator copper loss and the additional degrees of freedom enables the injection of harmonic components of current for elimination of specific frequency components of torque ripples (redundancy), or supply multi-motors from a single inverter.

Multi-phase motors (more than three) find their application in areas which require high reliability, power density and high efficiency, some of which are for electric propulsion of electric and hybrid electric vehicles, electric ship propulsion , locomotive traction , electric aircraft and aerospace applications . Although multi-phase motor drives have been around for more than 35 years [2] , it is in the last five years or so that one sees a substantial increase in the volume of research related to these motor drive systems.[3]

For multiphase induction machines, as in three phase induction machines , the constant volts/hertz (V/f) control was extensively studied in the 1970's and 1980's , whereas in recent times the emphasis has shifted to vector (field-oriented) control and direct torque control of induction motors [4], which are elaborated on below:

In vector control schemes, Induction motor is well known to require needs a magnetizing current component and a torque producing current component [5] which are fed to one set of windings: namely the stator phase winding. So the purpose of the vector drive is to separate the two components. This is done by keeping in mind that the magnetizing current component always lags the voltage by 90^0 and that the torque producing current component is always in phase with the voltage. The drive/ controller controls the magnetizing current

component ,Id, the direct-axis current component in one control loop and the torque producing current component ,Iq, the quadrature-axis current component in another control loop The two current component space vectors, Id and Iq , which are always 90^0 apart are then added (vector sum) and their values conveyed to the modulator, which transforms the space vector information into a rotating PWM modulated three-phase voltage system with the correct frequency and rms voltage value. As soon as there is a deviation from the correct speed, or torque, or magnetizing current , is detected by the control loops, the corresponding variable will be changed by the controller to regulate the motor output.

Direct torque control schemes, entail another method used in variable frequency drives to control the torque (and thus finally the speed) of induction motors [6] . This involves calculating an estimate of the motor's magnetic flux and torque based on the measured motor voltage and current. The motor flux and torque are then compared with their reference values. If either the flux or the torque deviates from the reference more than an allowed tolerance, the ineverter switches are turned on and off in such a manner that the flux and torque values will be forced back to within their tolerance bands.[7,8].

A most important area of research is the development of fault-tolerant control techniques for multi-phase motors [9-12]. Control algorithms used for continuous disturbance free operation of multi-phase induction and permanent magnet machines can be found in the literature in references [13,14].

For a three-phase motor to continue operating under loss of one phase , a divided dc bus and neutral connection are required [15]. In other words , a zero sequence component is necessary to provide an undisturbed rotating MMF after a phase is lost. Due to their additional degrees of freedom, multi-phase (more than three) motors are potentially more fault tolerant than their three-phase counterparts. Explained below is the fault tolerant control scheme that has been

developed for continuous and safe operation under closed loop control of multi-phase machines after losing more than one phase [16].This also eliminates the need for accessibility to the neutral line. If one phase of a multi-phase machine is open circuited, the combination of phase currents required to generate an undisturbed forward rotating MMF is no longer unique [17]. The most important consideration then is to establish on optimum set of currents which would produce the same value of MMF as under the healthy conditions .Therefore, with proper current control , an undisturbed forward rotating MMF can be maintained, which can be used to control the electromagnetic torque.

For example , the total stator MMF, *Fs*, of a five-phase machine can be formulated by the following expression:

$$\vec{F}s = NI_a + aNI_b + a^2NI_c + a^3NI_d + a^4NI_e \qquad (1\text{-}1)$$

Where, *N* is the number of turns/phase

I_a is the rms value of current in Phase A

I_b is the rms value of current in Phase B

I_c is the rms value of current in Phase C

I_d is the rms value of current in Phase D

I_e is the rms value of current in Phase E

And a is $1\angle 72^0$

Under normal conditions,

$$\vec{F}s = \frac{5}{2}NI\ e^{j\theta} \qquad (1\text{-}2)$$

Where $\theta = \omega t + \varphi$

Assuming that Phase a suddenly becomes open-circuited, then , after open-circuit , the real and imaginary parts of equation (1-2) are

$$\frac{5}{2}NI\cos\theta = N(I_b^{'} + I_e^{'})\cos 72^0 - N(I_c^{'} + I_d^{'})\cos 36^0 \qquad (1\text{-}3)$$

$$\frac{5}{2}NI\sin\theta = N(I_b^{'} + I_e^{'})\sin 72^0 - N(I_c^{'} + I_d^{'})\sin 36^0 \qquad (1\text{-}4)$$

In this case, By assuming $I_b^{'} = -I_d^{'}$ and $I_c^{'} = -I_e^{'}$, it is possible to maintain the same value of $\vec{F}s$

Similar control algorithms can be worked out for any other multi-phase machine, in the case of an open-circuit .Due to additional degrees of freedom , the current in the remaining phases can be used to control the torque of the machine without the presence of negative-sequence or zero-sequence current.

Some of the other areas of research include modeling of multi-phase induction machine with structural unbalance [18], influence of the loss of a stator phase/phases on the stator current spectrum. This is done through studying the behaviour of some of the frequency components which depend on the speed/slip of the motor. The fluctuation of these frequencies was examined to evaluate the effect of torque ripples generated by the negative sequence component in the stator current which is associated with loss of a phase/phases [19].

In recent years, multi-phase (more than three) induction motors have gained importance in industry because they have proved to be more advantageous when compared to their conventional/standard three-phase counterpart particularly in survivability aspects under faulty conditions. As mentioned earlier, One of their main advantages is an inherent higher reliability at a system level and this is because, a multi-phase machine can operate with an asymmetrical winding configuration even in the case of loss of more than one inverter leg/a machine

phase[20]. Recent research has therefore been centered on improving reliability of operation of induction motors in case of phase-loss scenarios by incorporating the multi-phase (more than three) design concept.

1.3 THESIS CONTRIBUTION

In this study, a novel design has been developed for a 6-phase induction machine,which is based on an existing three-phase design. That is, this approach involves reconfiguration of an existing 3-phase induction machine into a 6-phase induction machine winding design using the same stator core lamination structure. Thus this leads to the development of a stator winding configuration that allows a reversible 3-phase to 6-phase induction machine and vice versa.In particular, the performance of the 6-phase machine is studied under various types of phase-loss conditions like adjacent phase loss (i.e. loss of phases which are next to each other) and non-adjacent phase loss (i.e. loss of phases which are separated by one or two other phases) under drive open loop control or direct line feeding , so that this could later be applied to the investigation of 'Limp Home' startergies without resort to excessive redundancy of system components. The results of this work demonstrate the behaviour of the 6-phase machine under the above mentioned fault conditions. Finally, a comparative analysis between the 3-phase and 6-phase machines from the point of view of motor-drive system reliability is presented

1.4 THESIS ORGANIZATION

Including this introductory chapter, this thesis is organized in seven other chapters. In the second chapter, The design layout of an existing three-phase , 5-hp, 6-pole , induction machine will be presented. In chapter 3, the reconfiguration process of the three-phase induction machine into six-phase motor will be explained in detail . In Chapter 4, the complete design of the reconfigured six-phase induction motor will be shown. In Chapter 5, The fundamentals of the

time-stepping finite element approach used to model both the three-phase and six-phase machines under study will be presented .In Chapter 6 ,the verifyting experimental results and simulation results will be given. In Chapter 7, the conclusions and recommendations for future work are presented.

CHAPTER 2: DESIGN OF THE THREE-PHASE CASE-STUDY INDUCTION MOTOR

2.1 INTRODUCTION

The most common family of motors used in home appliances, office appliances, and industry is that of induction motors. Three-Phase induction motors are today standard primemovers for industrial electrical drives.Cost, reliability, robustness, and maintenance free operation are among the reasons these machines are replacing dc drive systems. Basically an induction motor consists of a stationary member , the stator and rotating member , the rotor. The slots of the stator and rotor cores of induction machines are filled with electric conductors, insulated (in the stator) from cores, and connected in a certain way. This ensemble constitutes the windings. The primary (or the stator) slots contain a polyphase a.c. winding. The rotor may have either a three or two phase winding or a squirrel cage.

2.2 BASICS OF DESIGNING POLYPHASE A.C. WINDINGS

Designing a.c. windings means, in fact, assigning coils in the slots to various phases, establishing the direction of currents in coil sides and coil connections per phase and between phases, and finally calculating the number of turns for various coils and the conductor sizing.

The objective with polyphase a.c. windings is to produce a pure sinusoidally distributed and rotating m.m.f., through proper feeding of various phases with sinusoidal time-varying symmetrical currents. All this is in order to produce constant (ripple-free) torque under steady state operating conditions.

Three-phase windings are layed out in one or two-layers in stator slots, that is single or double-layer windings. The total number of coils equals half the number of stator slots, *Ns*, for single-layer configurations, and is equal to *Ns* for double-layer configurations. Full-pitched and short-pitched coils are used depending on the specific application. Windings for induction machines are built with integer slots per pole per phase and, rarely, fractional slots per pole per phase are used, when cogging or torque-speed characteristic inflection is of concern during starting of such motors.

These windings are characterized by their mmf fundamental amplitude and the space harmonic contents, (the lower the amplitudes of the higher harmonics, the better). The winding factor, *Kw* , characterizes their fundamental harmonic content in terms of the peak mmf value of the entire waveform. Another main concern is to produce balanced resistance and leakage inductance per phase.

2.2.1 BASIC RULES FOR DESIGNING A.C.WINDINGS

1. The basic "winding building block" is represented by coils. It should be pointed out that they may be lap connected or wave connected coils.

2. Coils for single layer windings are always not affected by the pitch factor in so far as the harmonic content of their mmf waveforms.

3. The number of slots per pole per phase could be fractional or an integer whereas the number of slots per pole is usually an integer.

4. As one coil side occupies one slot and its return occupies another slot, the number of coil sides with inward current is obviously equal to the number of coil sides with outward current .

5. The resulting traveling mmf will produce a flux density which will inturn self induce sinusoidal emfs in the stator windings.The emfs induced in coil sides placed in neighbouring slots are thus phase shifted by an angle , α_{es} , expressible in electrical radians as follows:

$$\alpha_{es} = \frac{\pi P}{Ns} \tag{2-1}$$

Where, P = Number of poles and Ns = Number of stator slots.

6. The number of stator slots per phase is N_s / m where m, is the number of phases in the stator winding.Finally the phase shift between the emfs in two coil sides in two adjacent slots in electrical radian measure is also α_{es} , Eq. (2-1)

7. The allocation of slots to phases to produce a symmetrical winding is done as follows:

- For Single-layer windings:

  The slots per pole per phase form a so-called phase belt of coil sides. These coil sides return in another phase belt that is π electrical radians removed from the original aforementioned phase belt, see Figure (2-1)

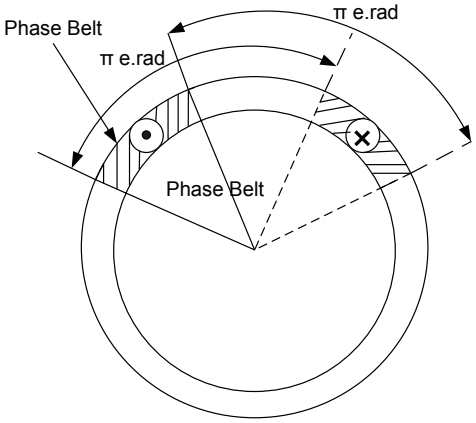

Figure 2-1: Single-Layer Phase Layout

- Double-layer windings

  The slots per pole per phase form a so-called phase belt of coil sides in the one layer.These coil sides return in another phase belt in the another layer which is β electrical radians from the original phase belt. But the start and return of coil sides in the same layer are always separated by π electrical radians, see Figure (2-2)

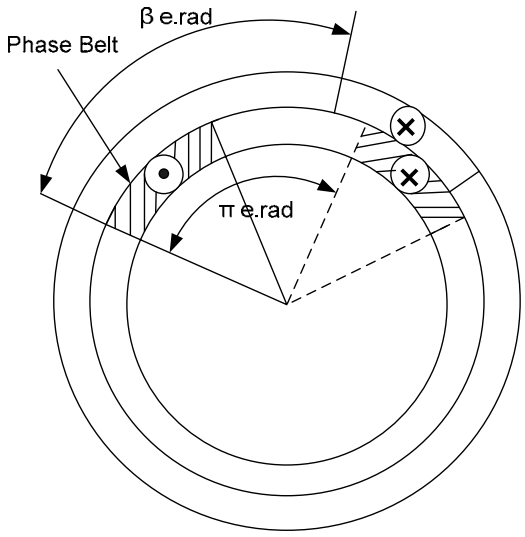

Figure 2-2: Double-Layer Phase Layout

8. Placing the coils in slots:

For single-layer, full pitch windings, the inward and outward coil side occupy entirely the allocated slots from left to right for each phase. There will be (*Ns/2m)* coils/phase ,where, m , is the number of phases in the stator winding of the machine.

For short-pitched or full-pitched double-layer windings, the inward and outward coil sides are placed from left to right of each phase, with one side in one layer (top layer closest to the airgap) and the other side in the second layer(bottom layer farthest from the airgap). These

coil sides are connected by observing the inward and outward directions of currents in their respective positions around the circumference of the machine as depicted in Figures (2-1) nd (2-2) , for single-layer and double-layer windings, respectively.

9. Connecting the coils per phase:

The *Ns/2m* coils per phase for single-layer windings and the *Ns/m* coils per phase for double-layer windings are connected in series (or series/parallel) such that the rules for the top layer and the bottom layer emf polarity / current polarity , again see Figures(2-1) and (2-2) are observed. With all coils per phase connected in series, we obtain a single current path (a = 1). We may obtain "a" current paths if the coils from *Ns/2ma* coils for a number of parallel paths "a" are connected in parallel in a single-layer winding. , and *Ns/ma* coils for a number of parallel paths "a" are connected in parallel in a double-layer winding.

10. If the number of poles ,*P*, the number of slots per pole per phase, *q*, and number of phases for such a design is known then the number of slots, *Ns*, is calculated as :

$$Ns = P \times q \times m \tag{2-2}$$

Again, where, *P* is the number of poles

q is the number of slots per pole per phase,

and *m* is the number of phases in the stator winding

2.3 DESIGN FORMULATIONS AND LAYOUT OF THE 5-HP CASE-STUDY THREE-PHASE INDUCTION MOTOR

It is a known fact that for a balanced three-phase winding, the number of slots should be a multiple of 3 with a minimum of one slot per pole per phase.That is for a simple two-pole machine and *m* phases the minimum number of slots is *mP* (i.e. 6 slots for a 2-pole , three-phase case)

The table below shows the possible slot combinations for a 3-phase induction motors which can be readily reconfigured into 6-phase induction motors.

No. of slots	No. of poles	No. of phases / No. of slots per pole per phase	No. of phases / No. of slots per pole per phase
12	2	3 / 2	6 / 1
	4	3 / 1	6 / Fraction (½) NA
	6	3 / Fraction ($\frac{2}{3}$) NA	6 / Fraction ($\frac{1}{3}$) NA
24	2	3 / 4	6 / 2
	4	3 / 2	6 / 1
	6	3 / Fraction ($\frac{4}{3}$) NA	6 / Fraction ($\frac{2}{3}$) NA
36	2	3 / 6	6 / 3
	4	3 / 3	6 / Fraction ($\frac{3}{2}$)NA
	6	3 / 2	6 / 1
48	2	3 / 8	6 / 4
	4	3 / 4	6 / 2
	6	3 / Fraction ($\frac{8}{3}$) NA	6 / Fraction ($\frac{4}{3}$) NA
60	2	3 / 10	6 / 5
	4	3 / 5	6 / Fraction ($\frac{5}{2}$)NA
	6	3 / Fraction ($\frac{10}{3}$) NA	6 / Fraction ($\frac{5}{3}$) NA
72	2	3 / 12	6 / 6
	4	3 / 6	6 / 3
	6	3 / 4	6 / 2

Table 2-1. Possible slot combinations of 3-phase induction motors which can be readily reconfigured to 6-phase induction motors

As given and suggested in Table 2-1, it is preferable to avoid a fractional value of slots per pole per phase. Therefore combinations like a 12 slot machine with 6 poles or 60 slot machine with 6 poles are not deemed applicable for the reconfigurable 3-phase to 6-phase machine design. The slot and pole combination chosen for the work in this thesis is a Three-Phase , 36 slot induction machine with 6 poles.

In the following chapter the design formulation and layout of an existing 5HP 3-Phase ,36 slot , squirrel cage induction motor ,with 6 poles, is discussed.

2.3.1 LIST OF SYMBOLS

For convenience of the reader the following is a list of symbols used throughout this thesis:

V = Line-Line Voltage (rms)

I = Rated current (rms)

L = length of the motor

g = height of the airgap

D_r = Outer Diameter of the Rotor

D_s = Inner Diameter of the Stator

E_{ph} = Induced Voltage/phase (rms)

f = frequency

P = number of poles

K_w = winding factor

K_d = distribution factor

K_p = pitch factor

q = number of slots per pole per phase

Ns = no. of slots

β = coil span in degrees

γ = slot angle

ϕ_{sr} = Flux originating from one pole

N_{ph} = Number of turns per phase

$B_{sr\,\max}$ = maximum value of fundamental component of flux density

$\vec{F}_s$ = fundamental peak value of the resulting magnetomotive force

$\vec{F}_{s\,\max}$ = maximum value of stator mmf per pole

$T_{\max}$ = maximum torque developed.

2.3.2 CHARACTERISTICS OF THE MOTOR UNDER STUDY

This case-study motor is a 36-slot, 6-pole, 5-HP squirrel cage induction motor rated at 460 V (rms value of line-to-line voltage) with a rated current of 6.8 A per phase.

The Inner diameter of the stator bore, D_s = 5.75 inches.The stator winding is a lap connected distributed winding with 20 turns per coil and 12 coils per phase. Therefore, the number of turns per phase, N_{ph} = 240. Here,

q = 2 slots per pole per phase.

The Dimensions of the rotor are as follows:

D_r = 5.72 inches

L = 5 inches

g = 0.015 inches

2.3.3 DERIVATION OF TORQUE IN CLOSED FORM USING DESIGN EQUATIONS

It is known that the induced phase voltage is the voltage induced in one conductor multiplied by the number of turns N_{ph}. The equation for the induced voltage is,

$$E_{ph} = 4.44\, f \phi_{sr} N_{ph} \tag{2-3}$$

This is true if the winding is full-pitched and the slots per pole per phase, $q = 1$

If $q > 1$, then the voltage induced in one coil of a phase winding will have the same magnitude as that of an adjacent coil but shifted by phase angle , α_{es}, because of the spatially distributed sinusoidal flux density waveform in the air gap. Thus the series connection of coils does not give the algebraic sum of the induced voltages but a lesser value. Therefore the calculated value has to be multiplied by the winding distribution factor , K_d .Here, the phase angle between the induced voltages in two neighbouring slots is,

$$\gamma = \frac{P \times 180^0}{Ns} \tag{2-4}$$

Where, P = number of poles

Therefore, in this case, $$\gamma = \frac{6 \times 180^0}{36} = 30^0 \tag{2-5}$$

Hence the distribution factor,

$$K_d = \frac{E_{ph}}{q\, E_{coil}} = \frac{\sin(q\, \gamma/2)}{q \sin(q\, \gamma/2)} \tag{2-6}$$

where, $\gamma \times q$ = phase belt angle

Therefore, $$K_d = \frac{\sin(2 \times 30^0/2)}{30^0 \times \sin(2 \times 30^0/2)} = 0.966 \tag{2-7}$$

Phasor representation of induced emfs on both sides of a single turn in case of short-pitched coils where the induced emfs will not be in 180^0 e (π e. radians) time phase with respect to each other is represented in Figure 2-3,

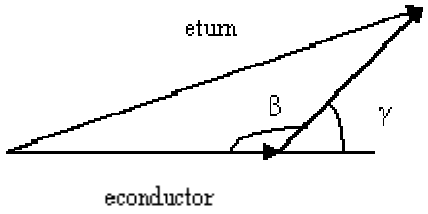

Figure 2-3. Phasor representation of induced emfs on both sides of a single turn in case of short-pithced coil

From Figure 2-3, The Pitch Factor can be defined as ,

$$K_p = e_{turn} \Big/ 2 \times e_{cond} = \sin(\beta \Big/ 2) \tag{2-8}$$

Where , $$\beta = \frac{\tau_c}{\tau_p} \times 180^0 \; e \tag{2-9}$$

Here $\tau_c = coil\,pitch \quad and \quad \tau_p = pole\,pitch$

In this case, since the winding is full-pitched, $\tau_c = \tau_p$

Therefore, $\beta = 180^0$ and $K_p = 1$

The Winding Factor , K_w, is accordingly defined as,

$$\begin{aligned} K_w &= K_p \times K_d \\ &= 1 \times 0.966 = 0.966 \end{aligned} \tag{2-10}$$

Now , Equation (2-3) yielding the induced emf per phase becomes

$$E_{ph} = 4.44\, f \phi_{sr} N_{ph} K_w \tag{2-11}$$

In this case, $$E_{ph} = V_{L-L} \Big/ \sqrt{3} = 460 \Big/ \sqrt{3} = 265 \text{ V} \quad (2\text{-}12)$$

From Equations (2-11) and (2-12),

$$\phi_{sr} = \frac{E_{ph}}{4.44 f N_{ph} K_w} = \frac{265}{4.44 \times 60 \times 240 \times 0.966} = 0.0043 Wb \quad (2\text{-}13)$$

It is known that the flux per pole, $\phi_{sr} = \frac{2}{\pi} \tau_p L B_{sr}$, from which maximum flux density per pole, B_{sr} can be expressed as ,

$$B_{sr} = \frac{\pi \times \phi_{sr}}{2 \times \tau_p \times L} \quad (2\text{-}14)$$

where, the pole-pitch , τ_p , is,

$$\tau_p = \frac{\pi \times D}{P} \quad (2\text{-}15)$$

Here, the diameter , D , is

$$D = D_{midairgap} = D_r + g = 5.72" + 0.015" = 5.735" \; or \; 0.145 m \quad (2\text{-}16)$$

Consequently,

$$\tau_p = \frac{\pi \times 0.145}{6} = 0.0762 m \quad (2\text{-}17)$$

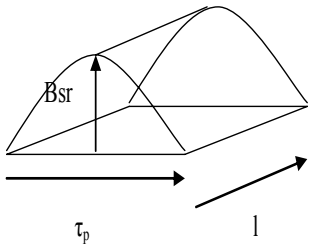

Figure 2-4. Flux Density Distribution per pole

Therefore, The maximum flux density per pole , B_{sr} , is ,

$$B_{sr} = \frac{\pi \times 0.0043}{2 \times 0.0762 \times 0.127} = 0.7 Wb/m^2 \quad \text{(Tesla)} \tag{2-18}$$

Figure 2-5 shows the MMF distribution in the uniform air-gap

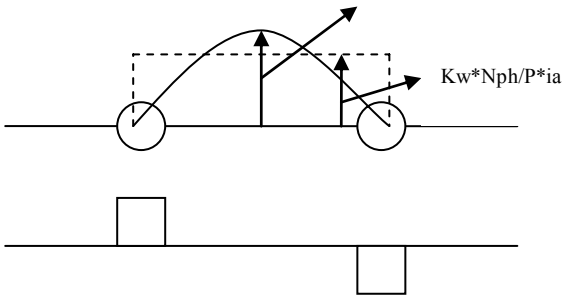

Figure 2-5. MMF Distribution in the uniform air-gap

From Figure 2-5 , The maximum value of stator MMF , $F_{s\max}$, can be expressed as follows [21]:

$$F_{s\max} = \frac{4 \times K_w \times N_{ph} \times I \times \sqrt{2}}{\pi \times P} \tag{2-19}$$

Therefore, $$F_{s\max} = \frac{4 \times 0.966 \times 240 \times 6.8 \times \sqrt{2}}{\pi \times 6} = 473.12 \ AT/Pole \tag{2-20}$$

In Balanced Three-Phase Induction Motors, The peak (amplitude) of the resultant stator mmf , F_s is given by [21]:

$$F_s = \frac{3}{2} \times F_{s\max} = \frac{3}{2} \times 473.12 = 709.6\, AT / Pole \tag{2-21}$$

The Expression for maximum value of the developed electromechanical torque developed can be expressed as follows [21]:

$$T_{\max} = \frac{\pi}{2} \times (\frac{P}{2})^2 \times \phi_{sr} \times \vec{F}_s \quad Nm \tag{2-22}$$

Therefore, the maximum value of the developed electromechanical torque is computed as:

$$T_{\max} = \frac{\pi}{2} \times (\frac{6}{2})^2 \times 0.0043 \times 709.6 = 43.13 \quad Nm \tag{2-23}$$

2.4 WINDING OF THE STATOR

The winding designed for the motor case at hand is a double-layered, distributed, lap-connected winding with full –pitched coils. Following the rules of designing the windings as explained earlier in Section 2.2.1, it follows that the number of slots per pole per phase , $q = 2$, the number of phases , $m = 3$, and the number of poles, $P = 6$, Therefore, from Equation 2-3, number of slots $Ns = 2 \times p \times q \times m = 2 \times 3 \times 2 \times 3 = 36\ slots$. From Equation (2-2) ,

$$\alpha_{es} = \frac{2\pi p}{Ns} = \frac{2\pi \times 3}{36} = \frac{\pi}{6} \tag{2-24}$$

The star of conductor emfs in the various 36 slots of the stator can be depicted as shown in Figure 2-6. This Figure bares a direct relationship to the winding layout labels shown in the machine cross-section with the respective phase labeling, *A, -A, B,-B,C,-C* shown in Figure 2-9.

Phasor diagram of conductor emf showing phasors which slot contains which phase

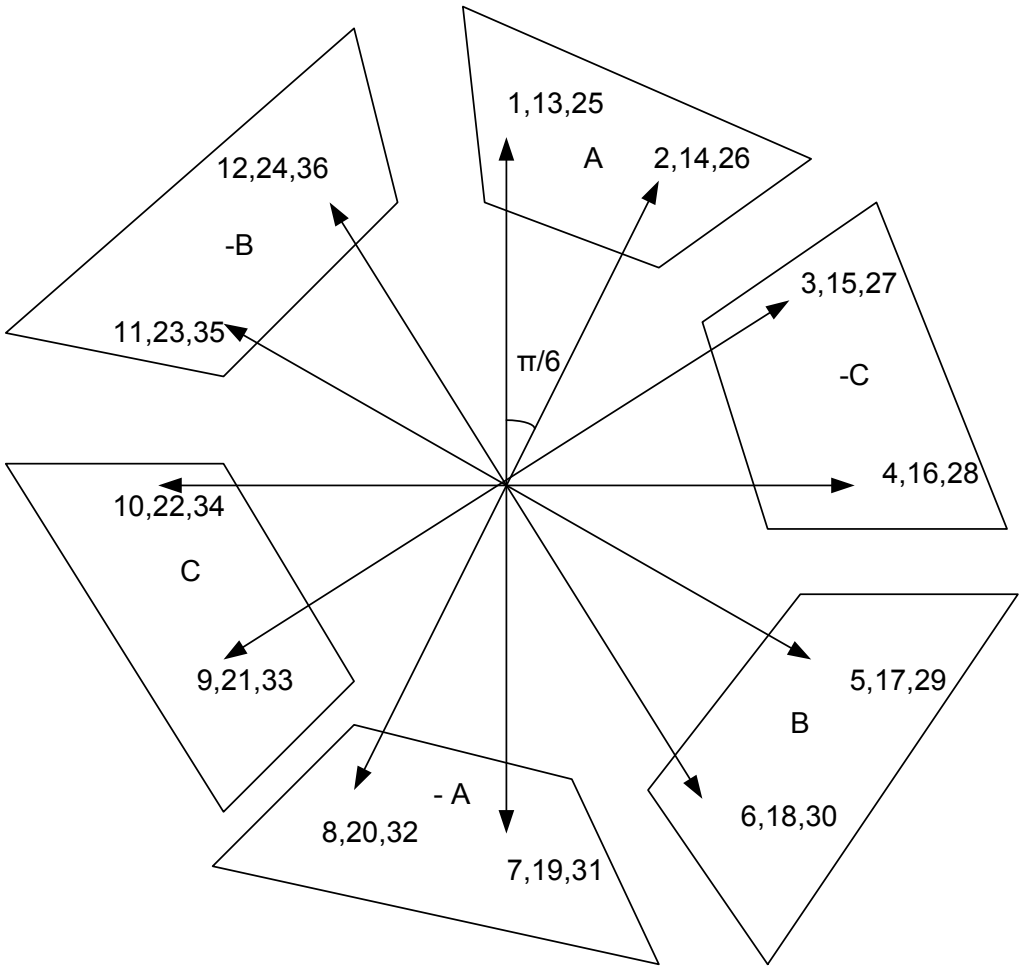

Figure 2-6. Phasor diagram of conductor emfs showing slots carrying their respective phases.

In the case of the 36 slot motor, considering 2 slots per pole per phase and a double-layered winding configuration, the total number of coils per phase will be 12 . Placing the subsequent coils for each winding will depend on the coil span which is 6 slot pitches .

Placement of coils of the other phases is done based on the spatial distribution of the windings. Figure 2-7 shows how the phases are distributed in space and their associated angles in a simple 2-pole , 6-slot , winding layout .Meanwhile, from this principle depicted in Figure 2-7 , one can obtain the winding configuration for a 36-slot , 6-pole , full-pitched coil stator depicted in the motor cross-section of Figure 2-9, and its associated developed diagram / table shown below this cross-section. The corresponding developed diagram of the winding layout for the case with full-pitched coils is shown for completeness in Figure 2-10. Furthermore , this Figure will be helpful in understanding the forthcoming 6-phase motor winding layout.

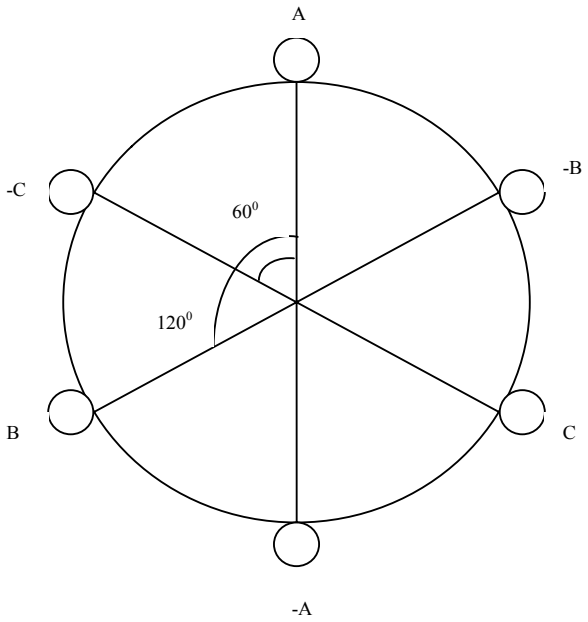

Figure 2-7. Spatial distribution of the Three Phases

Meanwhile for a corresponding short-pitched winding distribution for the case-study three phase induction machine with 36 slots and a coil span of 150^0 is shown in Figure 2-8. This is the actual design of the winding of the 3-phase motor being simulated and tested in this work.

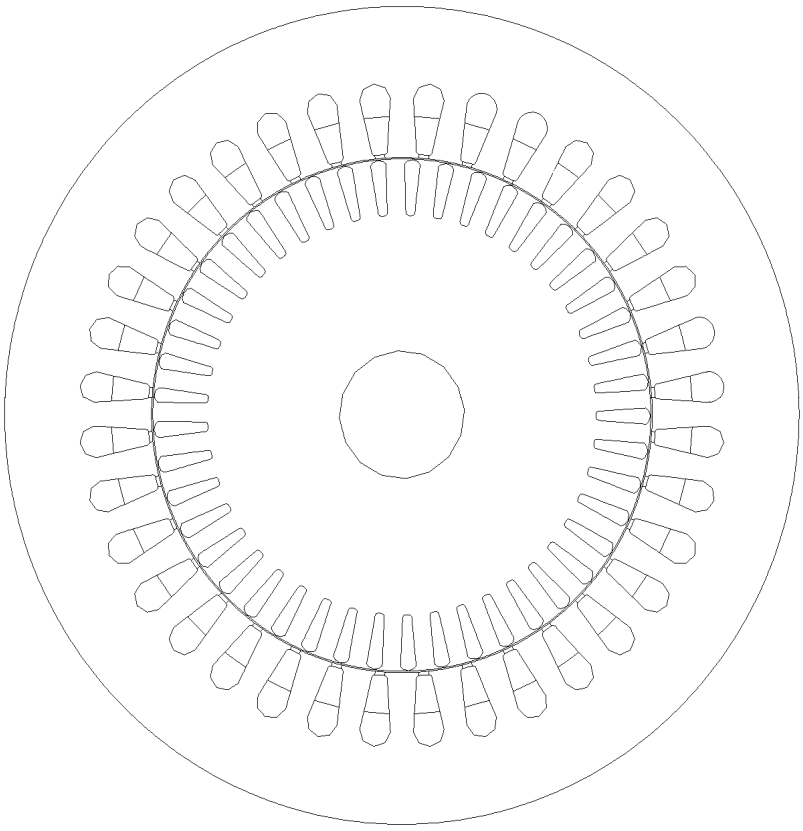

	1	2	3	4	5	6	7	8	9	10	11	12	13	14	15	16	17	18
Top	A7	C5-	C6-	B8	B7	A1-	A2-	C12	C11	B1-	B2-	A12	A11	C1-	C2-	B12	B11	A3-
Bottom	A1	A2	C12-	C11-	B1	B2	A12-	A11-	C1	C2	B12-	B11-	A3	A4	C10-	C9-	B3	B4
	19	20	21	22	23	24	25	26	27	28	29	30	31	32	33	34	35	36
Top	A4-	C10	C9	B3-	B4-	A10	A9	C3-	C4-	B10	B9	A5-	A6-	C8	C7	B5-	B6-	A8
Bottom	A10-	A9-	C3	C4	B10-	B9-	A5	A6	C8-	C7-	B5	B6	A8-	A7-	C5	C6	B8-	B7-

Figure 2-8. . Cross-Sectional view of stator slots showing the winding distributions of the three phases for the short-pitched design

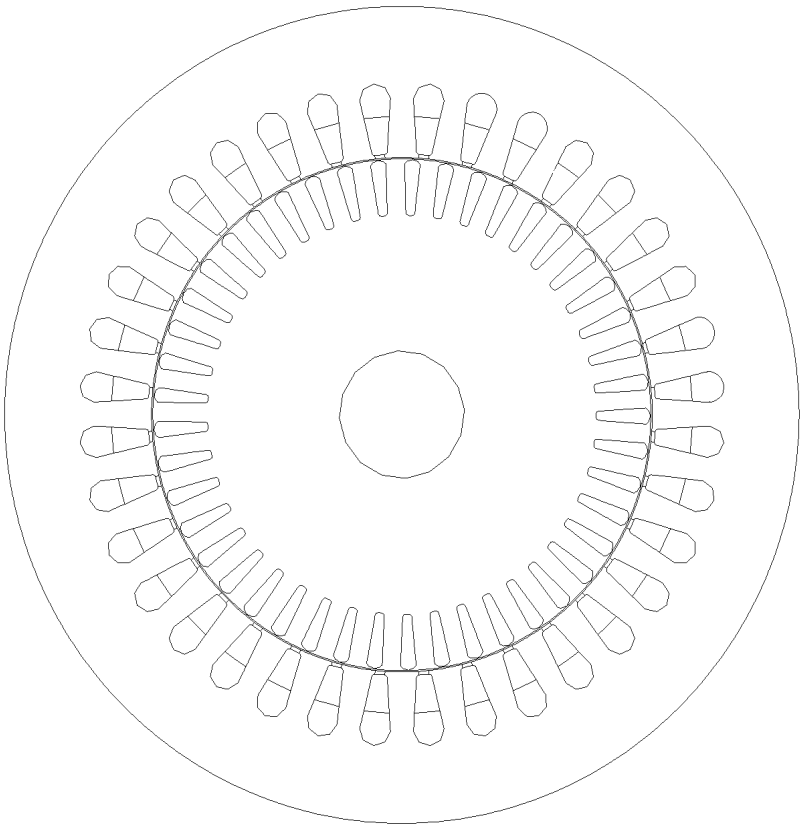

	1	2	3	4	5	6	7	8	9	10	11	12	13	14	15	16	17	18
Top	A8	A7	C5-	C6-	B8	B7	A1-	A2-	C12	C11	B1-	B2-	A12	A11	C1-	C2-	B12	B11
Bottom	A1	A2	C12-	C11-	B1	B2	A12-	A11-	C1	C2	B12-	B11-	A3	A4	C10-	C9-	B3	B4
	19	20	21	22	23	24	25	26	27	28	29	30	31	32	33	34	35	36
Top	A3-	A4-	C10	C9	B3-	B4-	A10	A9	C3-	C4-	B10	B9	A5-	A6-	C8	C7	B5-	B6-
Bottom	A10-	A9-	C3	C4	B10-	B9-	A5	A6	C8-	C7-	B5	B6	A8-	A7-	C5	C6	B8-	B7-

Figure 2-9. Cross-Sectional view of stator slots showing the winding distributions of the three phases for the full-pitched design.

Shown below in Figure 2-10 is the complete winding layout showing all the three phases for the full-pitched design :

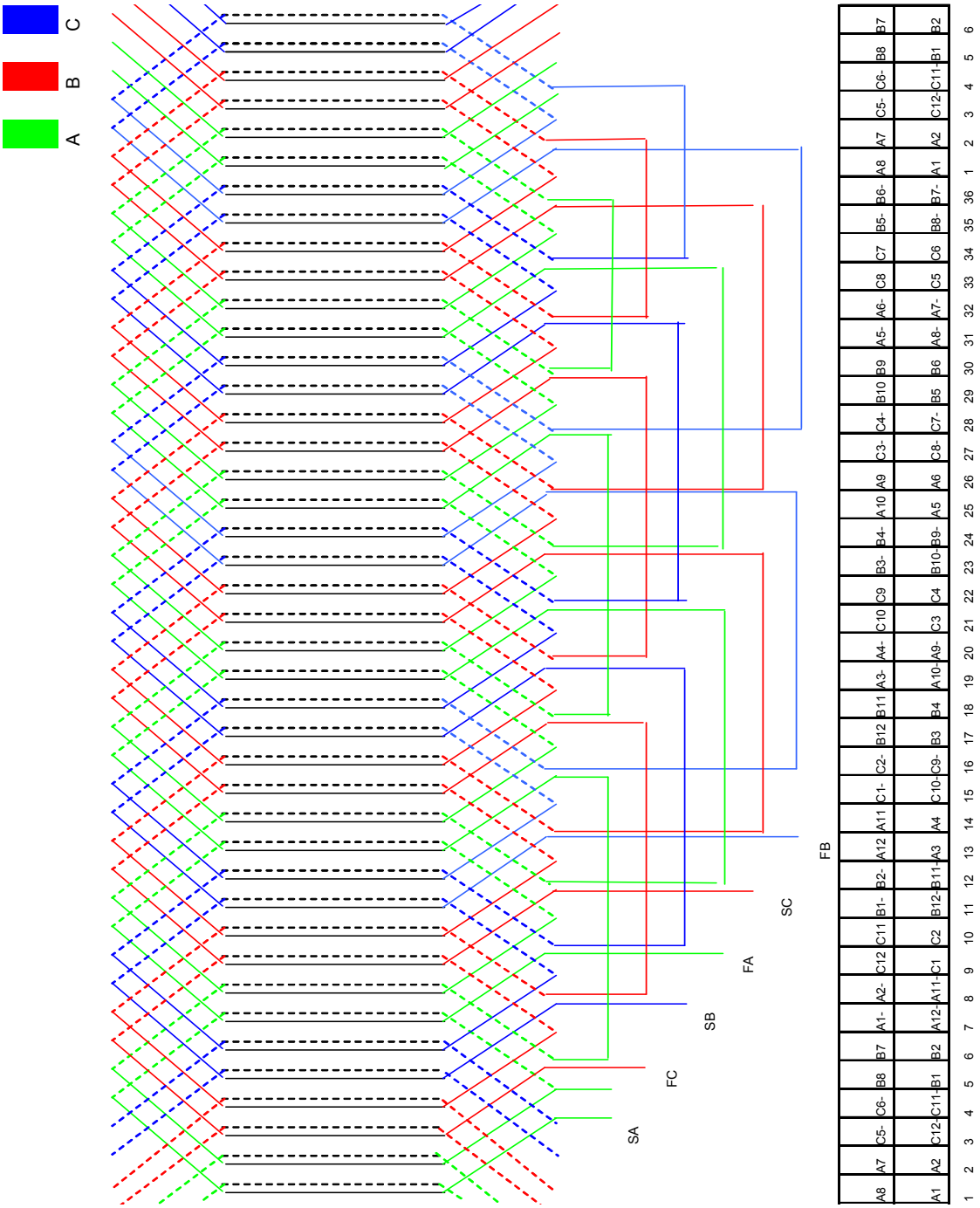

Figure 2-10. Complete Winding Layout showing the connection of all the coils.

2.4.1 MMF DISTRIBUTION

As mentioned earlier, the objective of a poly-phase a.c. winding is to produce a rotating MMF with a profile that is as close as possible to a sinusoidally shaped waveform. The equation representing a rotating MMF of a distributed phase winding with *q* slots per pole per phase, and electrical angular slot pitch, α , with short-pitched coils of span angle β is [21] :

$$F_{ph}(\theta,t) = \frac{4}{\pi} \times \frac{N_{ph}}{P} \times \frac{I_{ph}}{m} \times \sum_{h=1}^{k} \frac{1}{h} [\sin(h \cdot \frac{\beta}{2}) \times \frac{\sin(q \cdot h \cdot \frac{\alpha}{2})}{q \times \sin(h \cdot \frac{\alpha}{2})} \times \sin(h \cdot \frac{\pi}{2}) \times \cos(h \cdot \theta) \times \cos(h \cdot \omega \cdot t)]$$

which can inturn be written as: (2-25)

$$F_{ph}(\theta,t) = F_{\max} \times \sum_{h=1}^{k} \frac{1}{h} [K_{ph} \times K_{dh} \times K_{sh} \times \cos(h \cdot \theta) \times \cos(h \cdot \omega \cdot t)] \quad (2\text{-}26)$$

or $F_{ph}(\theta,t) = F_{\max} \times \sum_{h=1}^{k} \frac{1}{h} [K_{wh} \times \cos(h \cdot \theta) \times \cos(h \cdot \omega \cdot t)]$ (2-27)

where, N_{ph} is the Number of turns per phase

P is the Number of Poles

m is the Number of phases

$$F_{\max} = \frac{4}{\pi} \times \frac{N_{ph}}{P} \times \frac{I_{ph}}{m} \times \sqrt{2}\ AT / Pole \quad (2\text{-}28)$$

and h is the harmonic number , for $h = 1$, $\vec{F}_{ph}(\theta,t) = \vec{F}_{fundamental}$

For a three-phase system the a,b,c mmfs are:

$$F_a(\theta,t) = F_{\max} \times \sum_{h=1}^{k} \frac{1}{h} [K_{wh} \times \cos(h \cdot \theta) \times \cos(h \cdot \omega \cdot t)] \quad (2\text{-}29)$$

$$F_b(\theta,t) = F_{\max} \times \sum_{h=1}^{k} \frac{1}{h} [K_{wh} \times \cos(h \cdot \theta - \frac{2\pi}{3}) \times \cos(h \cdot \omega \cdot t - \frac{2\pi}{3})] \quad (2\text{-}30)$$

$$F_c(\theta,t) = F_{\max} \times \sum_{h=1}^{k} \frac{1}{h}[K_{wh} \times \cos(h \cdot \theta - \frac{4\pi}{3}) \times \cos(h \cdot \omega \cdot t - \frac{4\pi}{3})] \quad (2\text{-}31)$$

Therefore it can be shown that, The resultant / total stator MMF , $\vec{F}_s$, can be exprseed as follows:

$$F_s = F_a(\theta,t) + F_b(\theta,t) + F_c(\theta,t) = \frac{3}{2} \times F_{\max} \times \cos(\theta - \omega t) \quad (2\text{-}32)$$

The MMF distribution produced by the three-phase a, b and c windings under study is shown versus the phase winding locations in Figure 2-11:

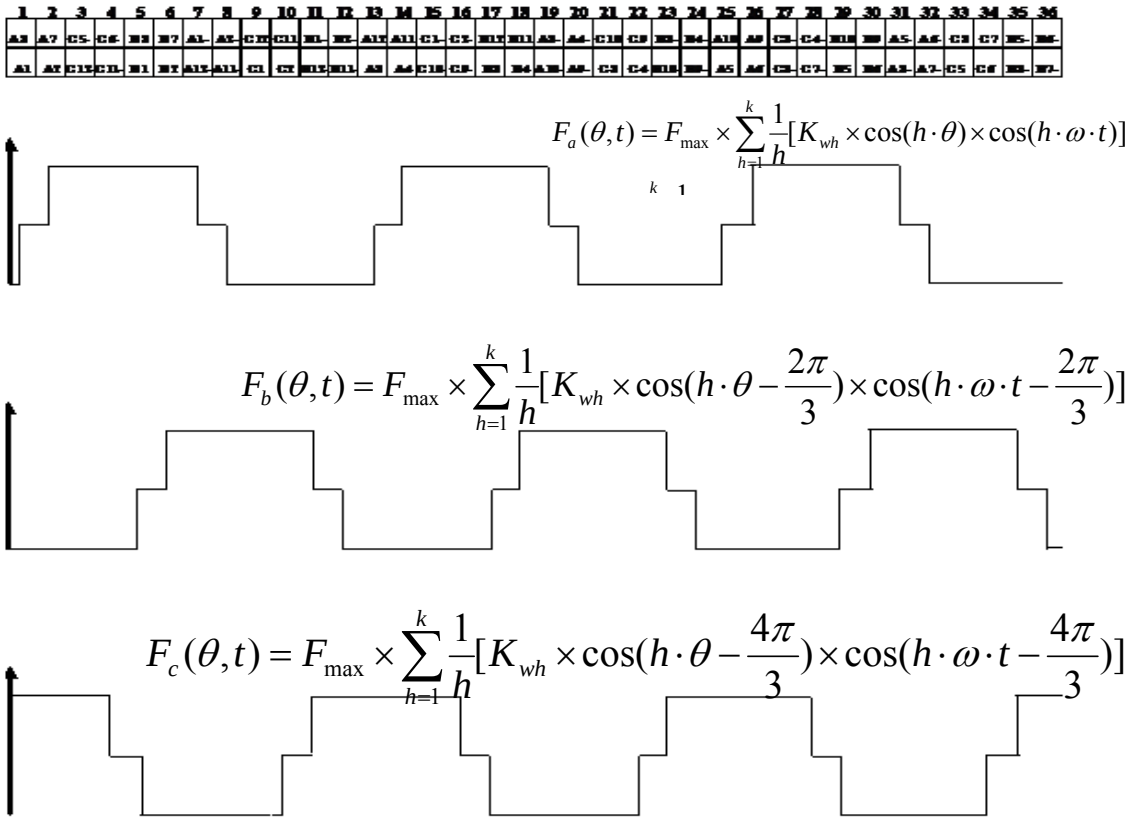

Figure 2-11.MMF Distribution produced by the Three-Phase winding under study.

In Figure 2-11, the currents in the slots are considered to be infinitely thin elements so that the mmf takes step-type jumps along the middle of each slot. The mmf distribution is symmetrical in successive half waveforms and therefore the mmf is balanced.

The rectangular mmf distribution can be decomposed into harmonics for each phase.By increasing the number of steps in the mmf waveform , it is possible to reduce the harmonic content.

In summary, in this chapter the winding design of the existing 5-HP three-phase induction motor was presented . This is a suitable introduction to the next chapter in which the reconfiguration of the three-phase winding into a six-phase winding is presented.

CHAPTER 3: RECONFIGURATION OF A THREE-PHASE INDUCTION MACHINE INTO A SIX-PHASE INDUCTION MACHINE

3.1 INTRODUCTION

Power switching converters are sensitive to different types of failures. In A.C. a motor-drive systems, these failures can occur at the converter side or at the control subsystem side. The reliability of the motor-drive system is an important factor in applications where continuous operation is mandated. When an open circuit fault occurs in the winding of an induction machine, the electromagnetic torque exhibits very oscillatory behaviour with high torque ripple content , and consequently the machine operation may have to be stopped for maintenance. In order to reduce the costs related to maintenance stops and for purposes of increasing the reliability of the motor-drive system it is necessary to introduce some fault tolerance characteristics [22]. Frequently systems with redundancy are used. In recent years, several research teams have focused on the development of fault-tolerant power conversion systems [23-25]. Main attention has been given to the development of new analysis techniques, fault detection, fault isolation and compensation of faults using the standard three-phase winding configuration [26,27]. Many configurations include topologies with redundancy of components such as switches/phases , cascaded inverters , four-leg inverter topology and systems with multiple-phases were proposed and implemented in prototypes [24,25] .Machines with multiple phases present inherent redundancy and can be used to provide fault tolerance [1-3,16]. This

Chapter proposes a method to redesign the three-phase induction motor described in the previous chapter by reconfiguring its stator winding into a six-phase configuration.

3.2 STEPS INVOLVED IN THE STATOR WINDING RECONFIGURATION PROCESS

The reconfiguration process basically involves an approach which converts the existing three-phase winding described in the previous chapter into a six-phase winding. Consider a 2-pole machine with 12 stator slots. In a three-phase winding configuration with a double-layer , lap-type winding , there would exist 4 coils that belong to each of the three-phases , A, B , and C. These coils would be connected into two groups per phase , each consisting of two coils connected in series per group. This would form the coil groups A1, A2, B1, B2, C1, and C2 depicted in the connection of Figure 3-1 for the high voltage/460V line-line arrangement.

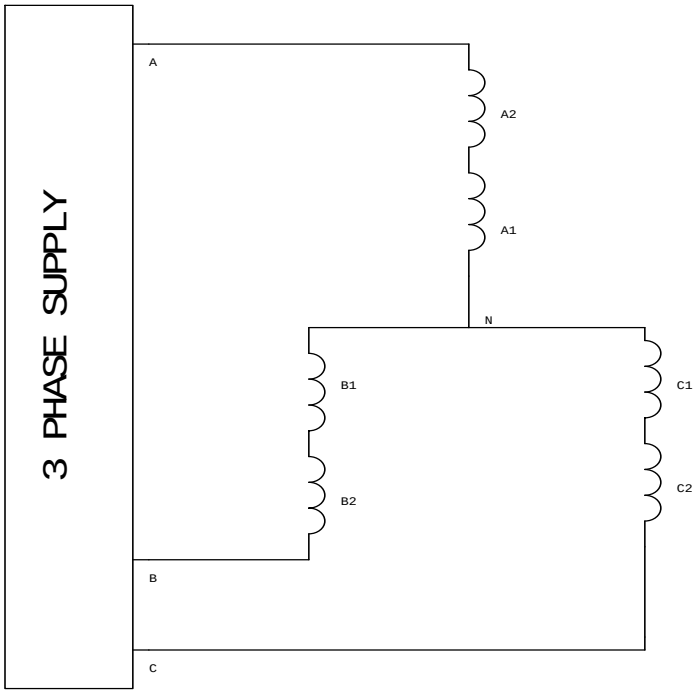

Figure 3-1.Y-Connection of the 2 coil groups for Three-Phase Operation**.**

In a balanced three-phase winding, such as the one depicted in Figure 3-1 supplied from a balanced three-phase supply , the A,B and C voltages are:

$$V_A = \sqrt{2} \times V \times \cos(\omega \cdot t) \ \ V \qquad (3\text{-}1)$$

$$V_B = \sqrt{2} \times V \times \cos(\omega \cdot t - \frac{2\pi}{3}) \ \ V \qquad (3\text{-}2)$$

$$V_C = \sqrt{2} \times V \times \cos(\omega \cdot t - \frac{4\pi}{3}) \ \ V \qquad (3\text{-}3)$$

Where, V is the rms line to neutral voltage applied from the supply.

and $\omega = 2\pi f$, the angular frequency in rad/sec.

The voltage phasors in each of the aforementioned coil groups of Figure 3-1 can be represented schematically and in voltage phasor form as in Figure 3-2

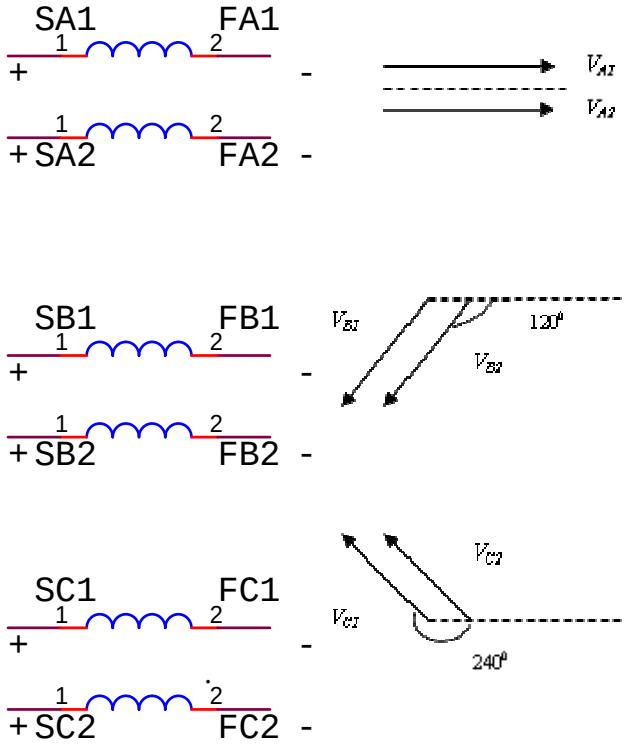

Figure 3-2.Phasor representation Of Voltages In each coil group**.**

The two coil-groups can be further connected in two arrangements depending on the current and voltage requirements, these two arrangements namely are:

1. The low voltage connection
2. The high voltage connection

In the high voltage connection, the 2 coil groups are connected in series so that the voltage in each of the coils VA1 and VA2 is 230V and the total voltage VA = VA1+VA2 is 460V (Line-Line). Here, Figure 3-3 shows the phasor diagram of voltages across the coils for the high voltage connection

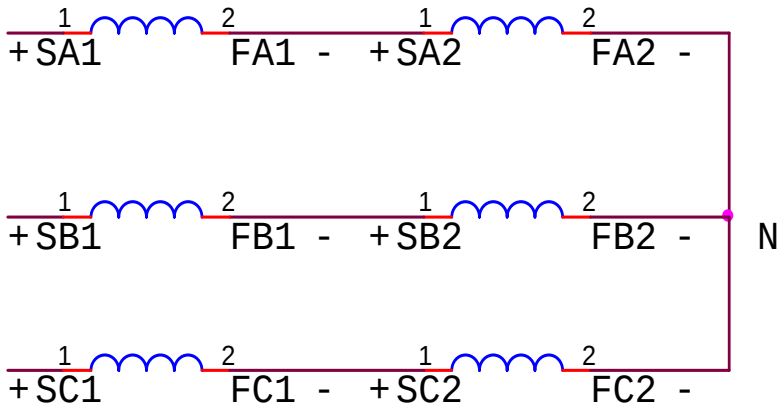

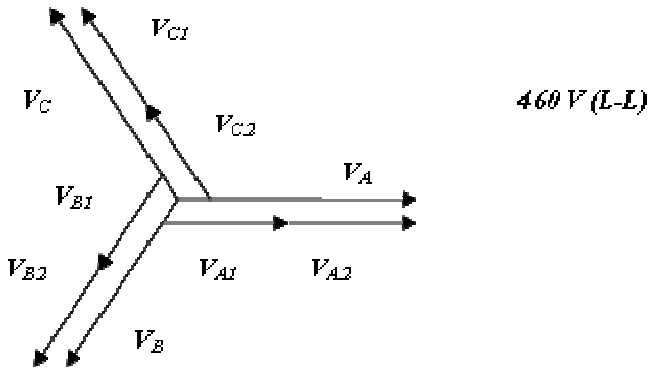

Figure 3-3.Phasor diagram of Volatge across the coil groups for the high-voltage connection.

In the Low-Voltage Connection the two coil groups are connected in parallel so that voltage in each coil V_{A1} and V_{A2} is 230 V(L-L) and the total voltage V_A is also 230V (L-L). Figure 3-4 shows the phasor diagram of voltages across the coils for the low voltage connection.

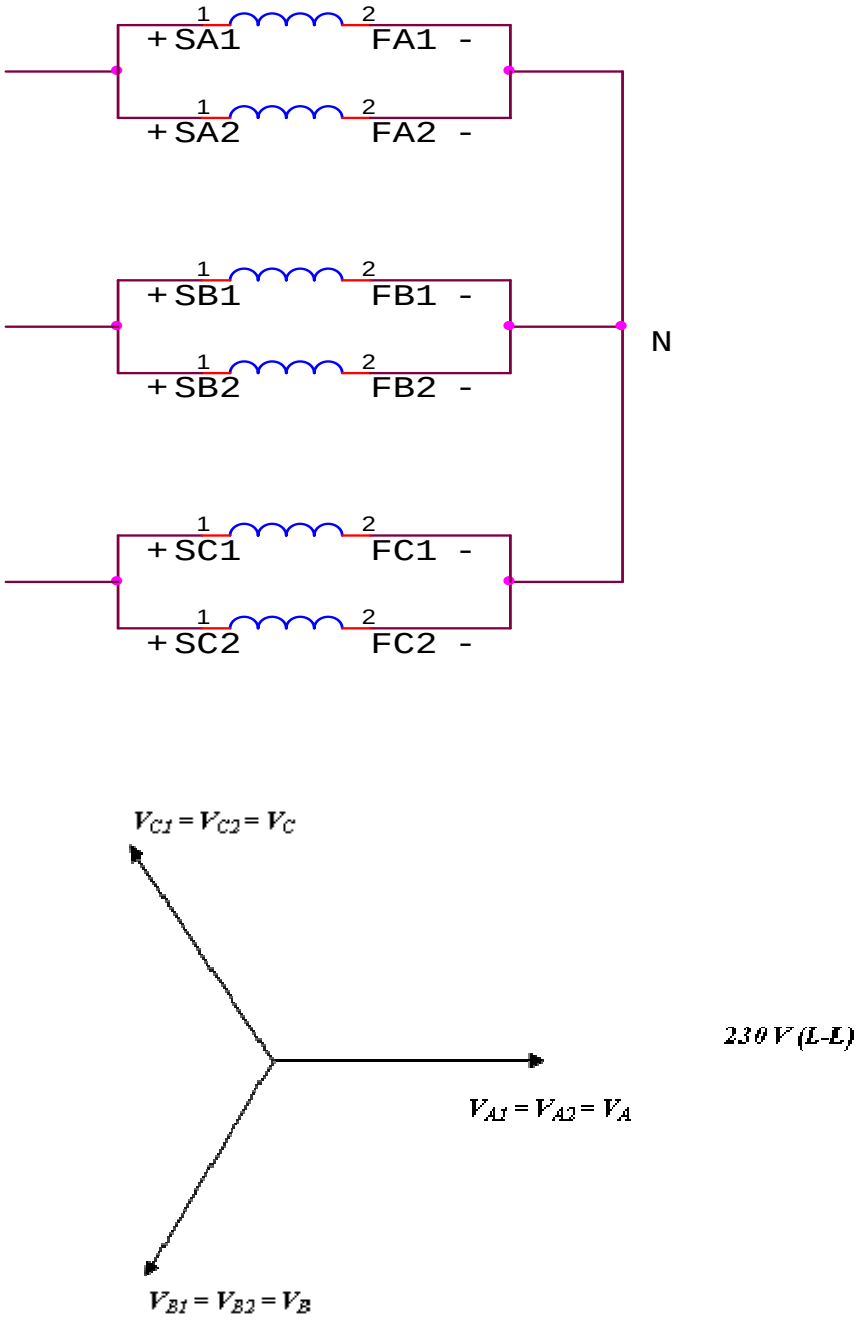

Figure 3-4.Phasor diagram of Volatge across the coil groups for the low-voltage connection.

3.3 SOME CONSIDERATIONS FOR THE SIX-PHASE WINDING

It is well known that the number of phases in a machine is assumed to be the same as the number of stator terminals or leads, excluding the neutral. However , giving the number of phases or leads is not always the adequate description. This is because ,for a given number of phases in a machine, two versions are possible based on the two possible values of the phase belt angle.For example three-phase motors can be wound with a phase belt angle of either 120^0 or 60^0. Since the phase belt angle governs certain harmonic characteristics, the 120^0 case is different from the 60^0 case [2].

In dealing with the phase belt angle, it is convenient to specify the number of phase belts per pole which is

$$q = \frac{180^0}{\psi} \qquad \text{(3-4) Where, } \beta \text{ is the phase belt angle.}$$

In this thesis, the design for the six-phase machine was chosen such that there is a symmetrical 60^0 displacement between the windings and the phase belt angle is 60^0.

For transforming the 3-phase winding configuration into a 6-phase one, the voltage phasors discussed in Figure 3-3 for the 2-pole , 12 stator slot example can be rearranged in a way such that they form the a six-phase system with a phase belt angle of 60^0. The voltage phasors in each of the coil groups can then be represented as shown in Figure 3-5

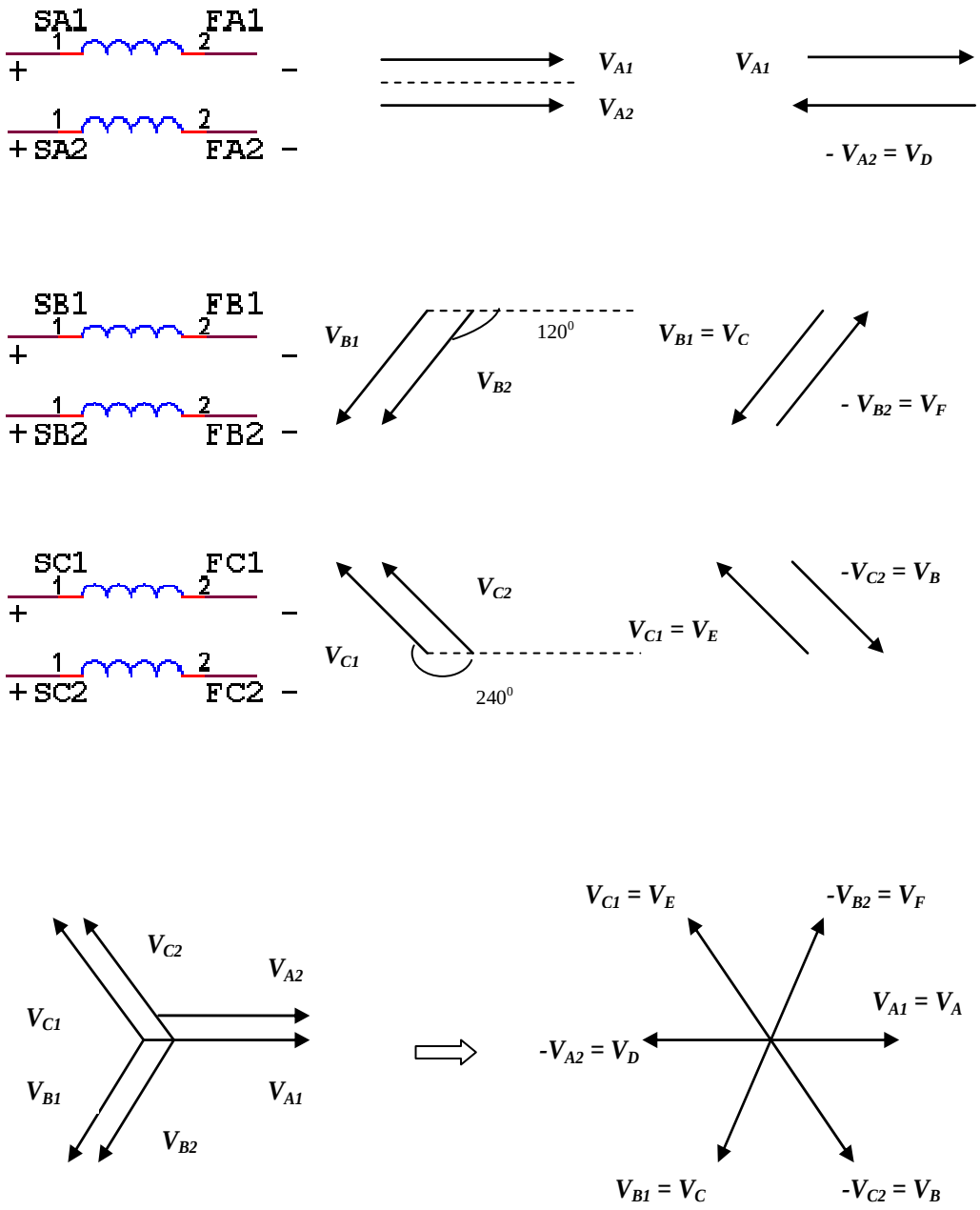

Figure 3-5.Rearrangement Of the Voltage Phasors to form the Six-Phase configuration.

3.4 CONNECTION SCHEME FOR THE SIX-PHASE WINDING CONFIGURATION

In order to achieve the 60^0 displacement between the voltage phasors, each of the two coil-groups in the three-phase system is separated and the starts and finishes of these coil are connected as shown , to form the winding which is depicted schematically in Figure 3-6

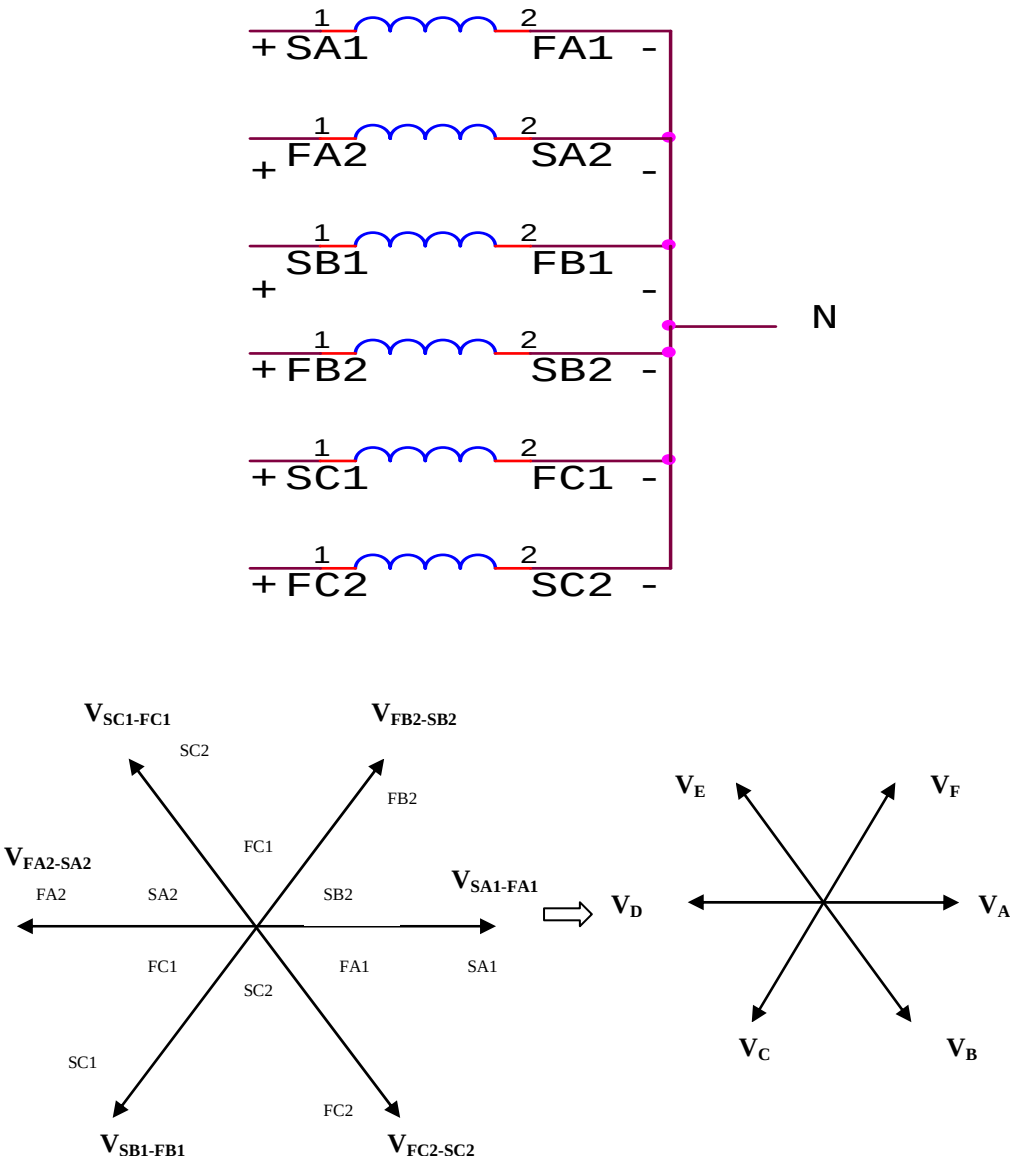

Figure 3-6.Connection Scheme For the Six-Phase winding

From the above arrangement , it is clear that Phase A and Phase D are separated by 180^0, Phase B and Phase E are separated by 180^0 & Phase C and Phase F are separated by 180^0 .Therefore,the spatial distribution of the phases in the six-phase machine can be represented as in shown in Figure 3-7

Three-Phase Case:

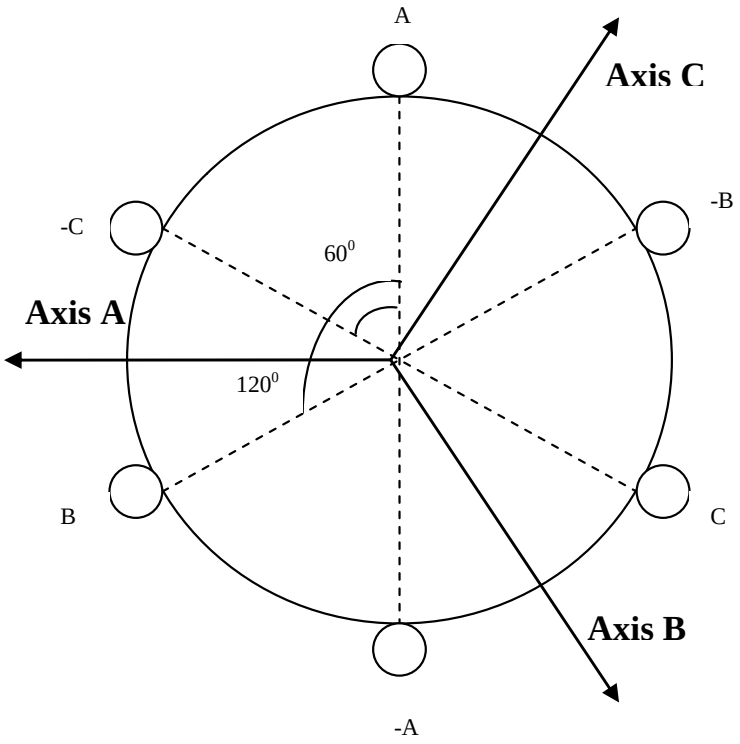

1	2	3	4	5	6	7	8	9	10	11	12	1	2
A	**A**	**-C**	**-C**	**B**	**B**	**-A**	**-A**	**C**	**C**	**-B**	**-B**	**A**	**A**
A	**A**	**-C**	**-C**	**B**	**B**	**-A**	**-A**	**C**	**C**	**-B**	**-B**	**A**	**A**

Six-Phase Case:

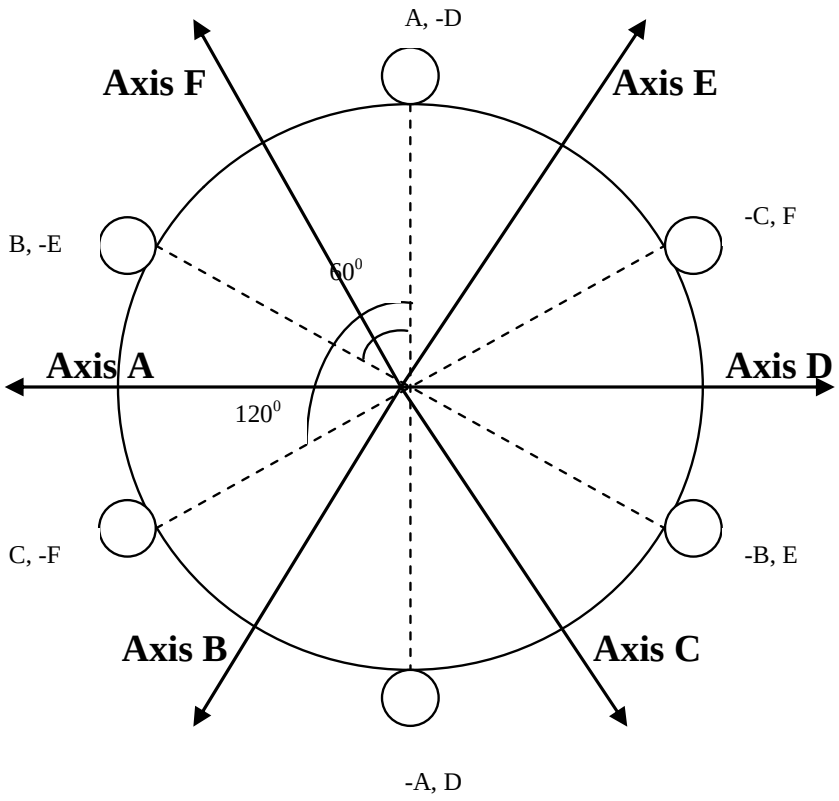

1	2	3	4	5	6	7	8	9	10	11	12	1	2
-D	**-D**	**-E**	**-E**	**-F**	**-F**	**-A**	**-A**	**-B**	**-B**	**-C**	**-C**	**-D**	**-D**
A	**A**	**B**	**B**	**C**	**C**	**D**	**D**	**E**	**E**	**F**	**F**	**A**	**A**

Figure 3-7 Spatial Distribution of phases in the Three-Phase And the Redesigned Six-Phase configurations

3.5 THE DEVELOPMENT OF THE SIX-PHASE WINDING

From the above analysis, phases A and D lie in the same slot, phases B and E lie in the same slot and phases C and F lie in the same slot. Table 3-1 relates the coils of the existing Three-Phase winding and its corresponding phase in the six-phase connection.

COIL NAME	NAME OF THE PHASE (3-PHASE)	NAME OF THE PHASE (6-PHASE)
A1	Phase A	Phase A
A2	Phase A	Phase D
B1	Phase B	Phase C
B2	Phase B	Phase F
C1	Phase C	Phase E
C2	Phase C	Phase B

Table 3-1 . Relationship between Coils of The Three-Phase winding and their corresponding phases in the Six-Phase machine.

From Table 3-2 and Figures 3-6 and 3-7 , one can proceed with the development of the Six-Phase winding .A logical representation of this kind of connection is presented in Figure 3-8.In this figure, each slot is represented by two two blocks on top of each other representing the double-layer nature of the winding, in which each slot is occupied by two coil-sides that may or may not belong to the same phase. Also, in Figure 3-8 the slots are numbered from right to left #1 through #12 ,for an example 12 slot per pair of poles stator winding configuration.

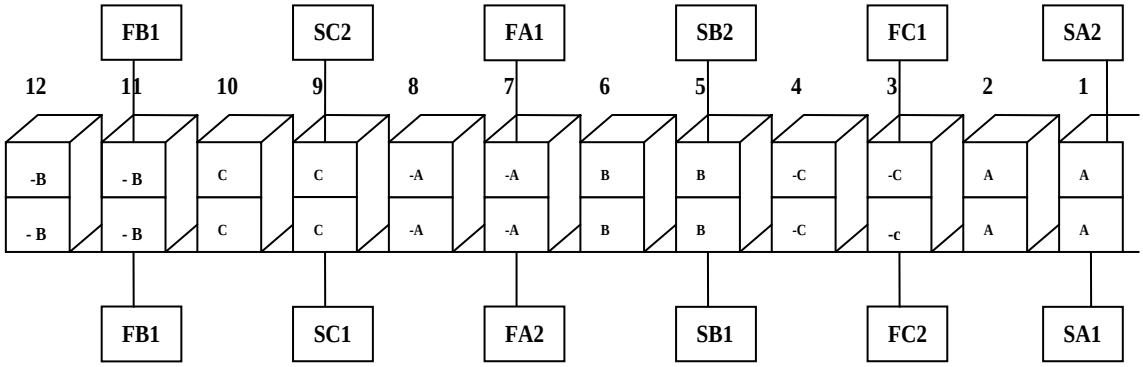

(a) Starts and finishes of each coil in the 3-phase machine

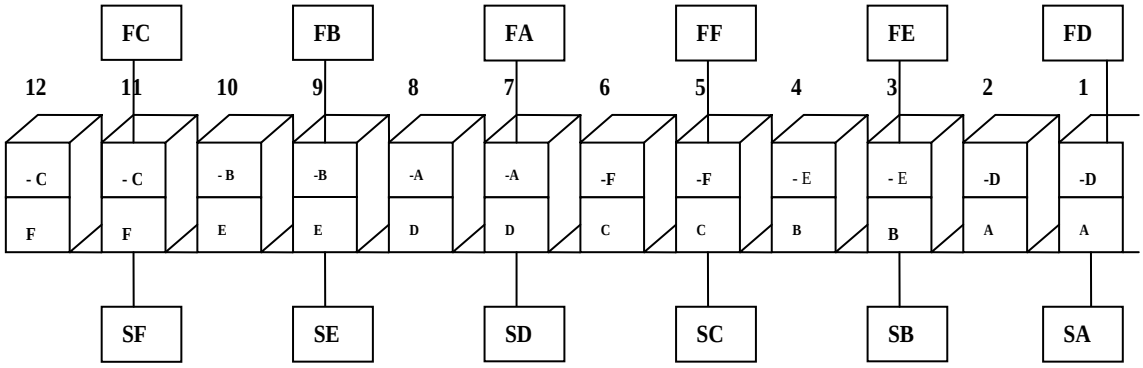

(b) Corresponding Starts and finishes of each phase to form the 6-phase winding

Figure 3-8 Development Of The Six-Phase Winding

From Figure 3-8 , the following can be deduced :

(1) The start of the coil A1 of the 3-phase winding corresponds to the start of phase A of the 6-phase winding,

(2) The start of the coil A2 of the 3-phase winding corresponds to the finish of phase D of the 6-phase winding,

(3) The start of the coil B1 of the 3-phase winding corresponds to the start of phase C of the 6-phase winding,

(4) The start of the coil B2 of the 3-phase winding corresponds to the finish of phase F of the 6-phase winding,

(5) The start of the coil C1 of the 3-phase winding corresponds to the finish of phase E of the 6-phase winding,

(6) The start of the coil C2 of the 3-phase winding corresponds to the start of phase B of the 6-phase winding,

(7) The finish of the coil A1 of the 3-phase winding corresponds to the finish of phase A of the 6-phase winding,

(8) The finish of the coil A2 of the 3-phase winding corresponds to the start of phase D of the 6-phase winding,

(9) The finish of the coil B1 of the 3-phase winding corresponds to the finish of phase C of the 6-phase winding,

(10) The finish of the coil B2 of the 3-phase winding corresponds to the start of phase F of the 6-phase winding,

(11) The finish of the coil C1 of the 3-phase winding corresponds to the start of phase E of the 6-phase winding, and

(12) The finish of the coil C2 of the 3-phase winding corresponds to the finish of phase B of the 6-phase winding,

Following the above scheme, the six-phase machine winding is designed.Accordingly, in this section , the development of the connection diagram for the reconfiguration of the three-phase machine has just been presented. Hence, the 36 slot,6-pole,6-phase armature double-layer winding can best be shown in cross-section as given in Figure 3-9, which is explained in detail in the next chapter.

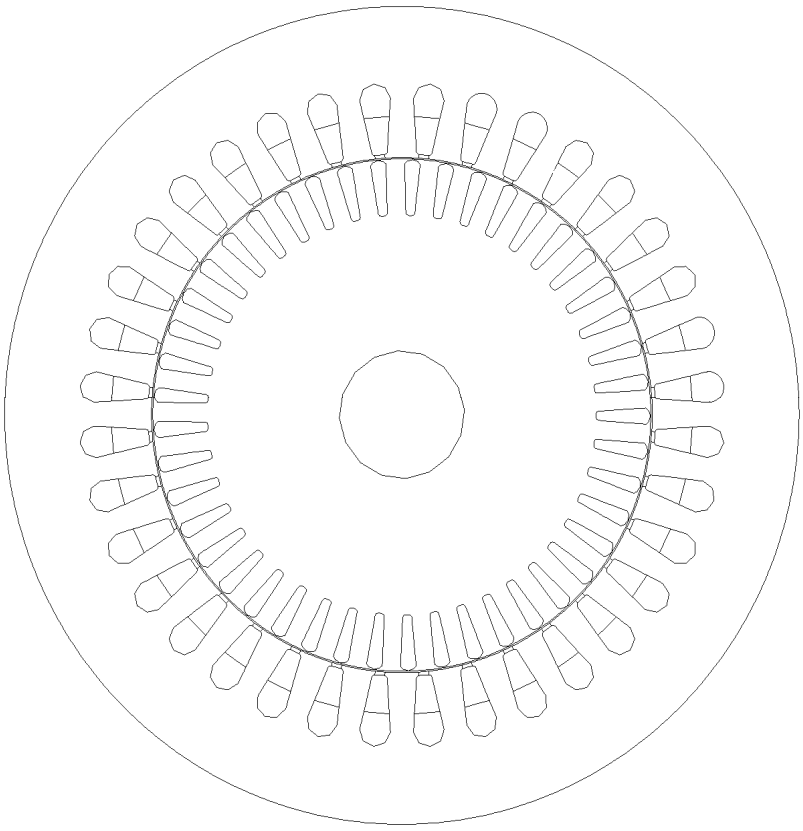

	1	2	3	4	5	6	7	8	9	10	11	12	13	14	15	16	17	18
Top	D5-	D6-	E5-	E6-	F5-	F6-	A1-	A2-	B1-	B2-	C1-	C2-	D1-	D2-	E1-	E2-	F1-	F2-
Bottom	A1	A2	B1	B2	C1	C2	D1	D2	E1	E2	F1	F2	A3	A4	B3	B4	C3	C4
	19	20	21	22	23	24	25	26	27	28	29	30	31	32	33	34	35	36
Top	A3-	A4-	B3-	B4-	C3-	C4-	D3-	D4-	E3-	E4-	F3-	F4-	A5-	A6-	B5-	B6-	C5-	C6-
Bottom	D3	D4	E3	E4	F3	F4	A5	A6	B5	B6	C5	C6	D5	D6	E5	E6	F5	F6

Figure 3-9:Cross-sectional view of the stator slots showing the winding distributions of the Six Phases.

CHAPTER 4: DESIGN OF THE SIX-PHASE INDUCTION MOTOR

4.1 INTRODUCTION

In this chapter, the complete design layout of the reconfigured six-phase induction motor is described. The main purpose of this chapter is to calculate the major design parameters of the six-phase induction machine, and arrive at the actual design of the stator winding by following the approach described in the previous chapter.

4.2 THE CONSTRAINTS AND STEPS INVOLVED IN THE DESIGN

The following are some constraints and aonsepts that were adhered t o in arriving at the design of the reconfigured six-phase winding layout :

- The main constraint is to keep the same values of the output torque and the same maximum mid-airgap flux density of the existing 3-phase machine in the new reconfigured 6-phase machine.
- The output power of the reconfigured 6-phase machine is also maintained at the same value as the existing 3-phase machine.
- From the available design data of the 3-phase machine which were detailed in the Chapter 2, the closed form equations of torque and magneto motive force are used here to find the actual number of turns required for the 6-phase design.

- The winding is designed keeping in mind, the winding reconfiguration scheme which was illustrated in detail in the previous chapter, including the required phase shifts between the different phases, A,B,C,D,E and F, respectively.

4.2.1 SOME IMPORTANT CHARACTERISTICS OF A " GOOD WINDING "

The following are some of the important features that a designer should keep in mind while choosing a particular winding layout configuration:

- The winding should preserve symmetry in every phase. (This will occur only if the electric angle between the phase voltages is exactly 360^0/m.)
- The phase voltage induced in the distributed phase windings with a given flux density should be as large as possible; i.e. the winding factor should be high.
- The mmf waveform created by the winding should be identical for every pair of poles balanced and should contain as few harmonic components as possible with a substantial fundamental component.

4.3 PARAMETERS OF THE SIX-PHASE INDUCTION MOTOR

Stator and rotor core cross sections and airgap height and mean diameter are the same for both the six-phase and the three-phase machines. The six-phase machine is also a 36 stator slot machine. Following the constraints discussed in section 4-2, the power rating of the six-phase motor is maintained at a value of 5-HP. It has six poles and the number of slots per pole per phase, q , is accordingly given by:

$$q = Ns / P / m = 36 / 6 / 6 = 1 \text{slots/pole/phase} \qquad (4\text{-}1)$$

In the first step of the design , the number of turns per phase has to be calculated from the closed form design equations . In the second step , the operating voltage of the motor is obtained. Finally , the stator winding layout is arrived at.

4.3.1 CALCULATION OF THE NUMBER OF TURNS PER PHASE FOR THE DESIGN

From Equation 2-24, it is known that the maximum value of electromechanical torque developed is expressed as, follows:

$$T_{\max} = \frac{\pi}{2} \times (\frac{P}{2})^2 \times \phi_{sr} \times \bar{F}_s \quad Nm \qquad (4\text{-}2)$$

in which all terms have been previously defined in Chapter 2.Since one constraint is to keep the torque and flux density the same as in the 3-phase case,it follows from Equation 2-16, that the peak resultant flux density at mid-airgap level , $B_{sr\ 6\ phase,}$ for the new six-phase design is as follows:

We have, From equation 2-2

$$B_{sr\ 6\,phase} = \frac{\pi \times 0.0043}{2 \times 0.0762 \times 0.127} = 0.7\,Wb/m^2\,(Tesla) \qquad (4\text{-}3)$$

where $\tau_p = 0.0762\ m$ and $L = 0.127\ m$ are remaining the same as in the 3-phase original design

In addition the maximum torque for the six-phase design can also be written based on Equation 4-2 as follows:

$$T_{\max\ 6\,phase} = \frac{\pi}{2} \times (\frac{6}{2})^2 \times 0.0043 \times 709.6 = 43.13 \quad Nm \qquad (4\text{-}4)$$

which is the same value as given earlier in Equation (2-25) in Chapter 2.

Since the core dimensions of the six-phase machine are the same as the three-phase machine , it follows that the flux per pole , ϕ_{sr} **,** as discussed in Chapter 2 is also of the same value as for the 3-phase machine. That is,

$$\phi_{sr\ 6\,phase} = 0.0043 \quad Wb \qquad (4\text{-}5)$$

Hence , It follows from equation 4-2 that one can compute the peak stator mmf , $\vec{F}_{s\,6\,phase}$, as follows:

$$\vec{F}_{s\ 6\,phase} = \frac{T_{\max 6\,phase} \times 8}{P^2 \times \phi_{sr\ 6\,phase}} = \frac{43.13 \times 8}{6^2 \times 0.0043} = 709.6 \ \ AT/Pole \qquad (4\text{-}6)$$

For a balanced six-phase machine , maximum phase value of the stator mmf , $\vec{F}_{s\max}$, is related to the total stator mmf per pole, $\vec{F}_{s\,6\,phase}$, by the following expression:

$$\vec{F}_{s\,6\,phase} = \frac{6}{2} \times \vec{F}_{s\max 6\,phase}$$

Therefore ,

$$\vec{F}_{s\max 6\,phase} = \frac{2}{6} \times \vec{F}_{s\,6\,phase} = \frac{2}{6} \times 709.6 = 236.5\ AT \qquad (4\text{-}7)$$

However , From Equation (2-21), $\vec{F}_{s\max}$ is also equal to,

$$\vec{F}_{s\max 6\,phase} = \frac{4 \times K_w \times N_{ph} \times I \times \sqrt{2}}{\pi \times P} \qquad (4\text{-}8)$$

Therefore,

$$\vec{F}_{s\max 6\,phase} = \frac{4 \times K_w \times N_{ph} \times I \times \sqrt{2}}{\pi \times P} = 236.5\ AT \qquad (4\text{-}9)$$

From (4-9) The product $K_w \times N_{ph}$ is found to be,

$$K_{w\,6\,phase} \times N_{ph\,6\,phase} = \frac{\pi \times P \times \vec{F}_{s\max 6\,phase}}{4 \times I \times \sqrt{2}} = \frac{\pi \times 6 \times 236.5}{4 \times 6.8 \times \sqrt{2}} = 115.6 \qquad (4\text{-}10)$$

Since the rated current , *I*, is maintained the same as in the 3-phase case , which is equal to 6.8A , and the winding factor , $K_{w\,6\,phase}$ can be written as follows:

$$K_{w\,6\,phase} = K_{p\,6\,phase} \times K_{d\,6\,phase} \qquad (4\text{-}11)$$

where, $K_{p\,6\,phase} = \sin(\frac{\beta}{2})$ and $\beta = \frac{\tau_c}{\tau_p} \times 180^0$

Hence, in the above case, because the chosen winding is full pitched , $\tau_c = \tau_p$, that is $\beta = 180^0$, it follos that $K_{p\,6\,phase} = 1$.In addition , from equation 2-8 it follows that ,

$$K_{d\,6\,phase} = \frac{\sin(q_{6\,phase} \times \gamma_{6\,phase}/2)}{q_{6\,phase} \times \sin(q_{6\,phase} \times \gamma_{6\,phase}/2)} \qquad (4\text{-}12)$$

where, $\gamma_{6\,phase}$, the slot angle is equal to 30^0 and $q_{6\,phase}$, the number of slots per pole per phase is equal to 1, hence $K_{d\,6\,phase} = 1$, and based on Equation 4-11, $K_{w\,6\,phase} = 1$ (4-13)

Hence the Number of turns per phase is found to be, $N_{ph\ 6\,phase} = 115.6 \approx 120$

Thus , the chosen number of turns per phase for the six-phase design is 120.

4.3.2 CALCULATION OF THE VOLTAGE RATING OF THE SIX-PHASE MOTOR

Since one of the constraints is to keep the same value of power rating for the six-phase machine as the rating of the three-phase machine, one can state the following,

Volt-Ampere Output Of Three-Phase Machine = Volt-Ampere Output Of Six-Phase Machine

i.e. $$3 \times V_{ph\,3phase} \times I_{ph\ 3phase} = 6 \times V_{ph\,6phase} \times I_{ph\,6phase} \quad (4\text{-}14)$$

From previous analysis, it is known that

$$V_{ph\,3phase} = 265\,V \quad \text{and} \quad I_{ph\,3phase} = 6.8\ A \quad (4\text{-}15)$$

However, From section 4-2, one knows that $I_{ph\,6phase} = I_{ph\,3phase}$, Therefore, the rated value of the phase current in the 6-phase machine , $I_{ph\,6phase} = 6.8\ A$

Hence, from Equation 4-14,

$$V_{ph\,6phase} = \frac{3}{6} \times \frac{V_{ph\,3phase} \times I_{ph\,3phase}}{I_{ph\,6phase}} = \frac{3}{6} \times \frac{265 \times 6.8}{6.8} = 132.5\,V \quad (4\text{-}16)$$

Furthermore, the line-to-line voltage can be deduced from the 6-phase voltage phasor diagram shown in Figure 4-1

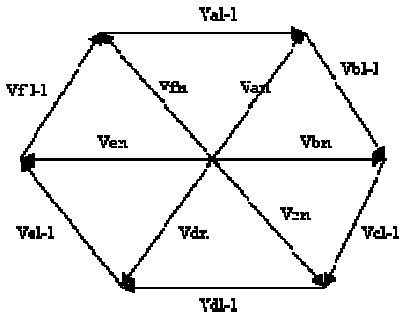

Figure 4-1. Phasor diagram of the line and phase voltages in the 6-phase system

In Figure 4-1, it can be observed that each triangle formed by any two phase voltage phasors and a line-to-line voltage phasor is an equilateral triangle. Therefore, as a result the $V_{line-line\,6\,phase}$ will be equal to $V_{phase\,6\,phase}$.

Hence $V_{line-line\,6\,phase} = V_{phase\,6\,phase} = 132.5\,V$ (4-17)

4.4 DESIGN OF THE STATOR WINDING

In the case of the 36 slot motor with 6 poles and 6 phases, the number of slots per pole per phase is equal to one (1). Since the stator winding design is a double-layered layout, the total number of coils per phase is 6 which is equal to half the number of coils per phase of the three-phase machine . Also as derived earlier , each coil has half the number of turns of the three-phase machine, that is each coil has 120 turns.

The slot pitch angle for the six-phase machine is accordingly calculated as follows:

$$\gamma_{6\,phase} = \frac{360^0}{Ns} = \frac{360^0}{36} = 10^0\,mechanical$$
$$or \quad \gamma_{6\,phase} = 10^0\,mechanical \times \frac{P}{2} = 10^0\,mechanical \times \frac{6}{2} = 30^0\,electrical \qquad (4\text{-}18)$$

Therefore, if coil (1) of phase A starts in slot (1) , then coil (1) of phase B which is 60^0 away from phase A is placed in slot (3) . Similarly, coil (1) of phase C is placed in slot (5) , coil 1 of Phase D is placed in slot (7) , coil 1 of Phase E is placed in slot (9) and coil 1 of phase F is placed in slot (11), see Figure 4-2 . Again a full –pitched winding design is adopted.Therefore, the end of each coil is 180^0 *e* away from the start of the coil and hence the coil span is (6) slot pitches. For clarity, the layout of the first six pairs of coils in such a six-phase winding is shown in Figure 4-2.

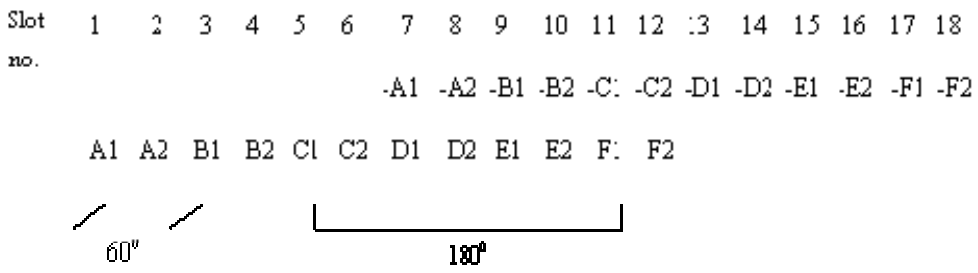

Figure 4-2 . Six-Phase winding layout with, no. of poles = 6 , no. of slots per pole per phase = 1, Double layered , lap-connected full pitch winding .

Placement of coils of the six phases is done based on the spatial distribution of the windings in accordance with the following considerations:

- As discussed in chapter 2 , the three-phase machine under study has 12 coils per phase . To reconfigure this winding into a six-phase layout, which has 6 coils per phase, the 12 coils of the three-phase are split into two groups each containing 6 coils. They can be denoted as follows:

  Group I --- Coils A1- A6

  Group II --- Coils A7-A12

  Group III --- Coils B1-B6

  Group IV --- Coils B7-B12

  Group V --- Coils C1-C6

  Group VI --- Coils C7-C12.

  These groups are connected for three-phase operation as shown in Figure 4-3

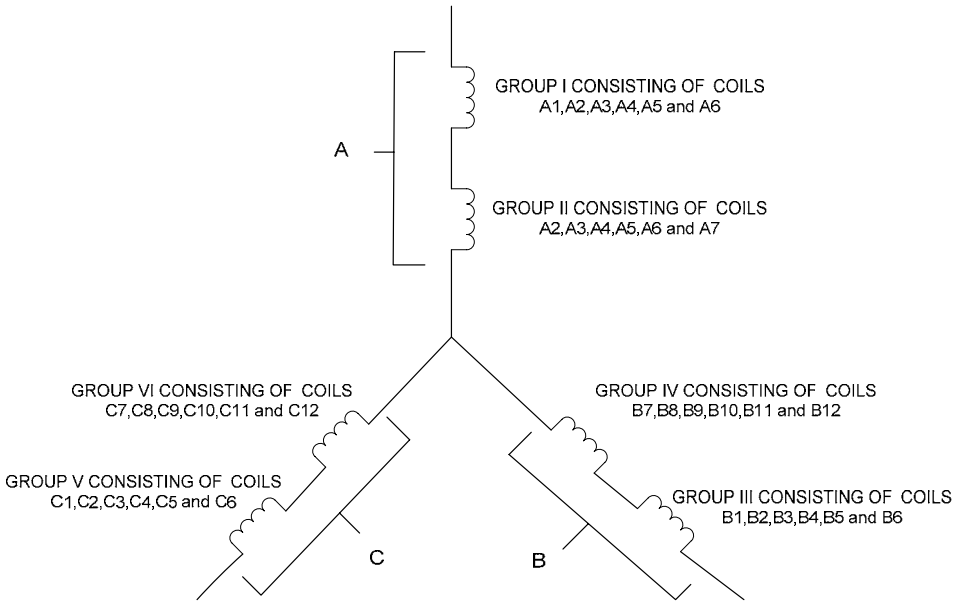

Figure 4-3. Connection Of the different Groups in the three-Phase configuration.

To reconfigure this grouping of coils into a six-phase winding , the terminal connections of the coil Groups II , IV and VI are reversed (start becomes a finish and a finish becomes a start) . Therefore , these groups of coils are connected to form the coils of phases D, F and B whereas Groups I , V and III of coils are connected to form phases A, E and C. The rearrangement of this coil grouping to form the 6-phase winding is best understood upon examination of the schematic diagram shown in Figure 4-4.

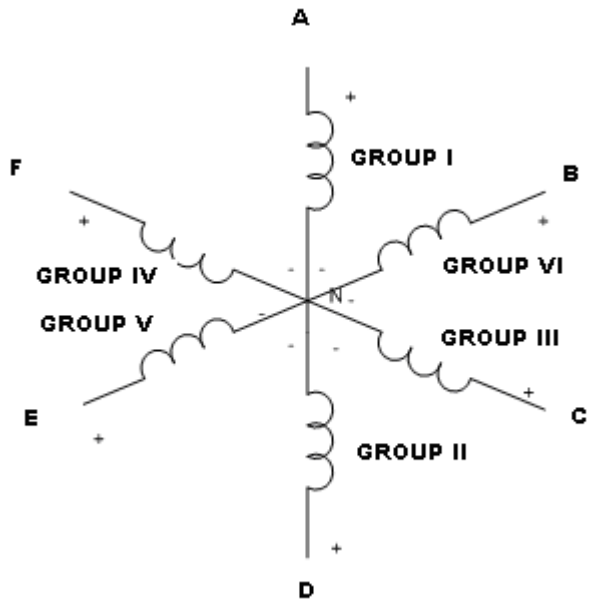

Figure 4-4. Connection Of the different Groups to form the Six-Phase configuration.

The connection of the coils of belonging to Group I and II constituting phase (A) in the 3-phase machine are shown in Figure (4-5), the connection of the coils belonging to Group III and Group IV constituting phase (B) in the 3-phase machine are shown in Figure (4-6) and the connection of the coils belonging to Group V and Group VI constituting phase (C) in the 3-phase machine are shown in Figure (4-7). Meanwhile , the connection of coils of Group I constituting phase(A) in the 6-phase machine is shown in Figure (4-8) , the connection of coils of Group II constituting phase (D) in the 6-phase machine is shown in Figure (4-9) , the connection of coils of Group III constituting phase (C) in the 6-phase machine is shown in Figure (4-10) , the connection of coils of Group IV constituting phase (F) in the 6-phase machine is shown in Figure (4-11) , the connection of coils of Group V constituting phase (E) in the 6-phase machine is shown in Figure (4-12) and the connection of coils of Group VI constituting phase (B) in the 6-phase machine is shown in Figure (4-13).

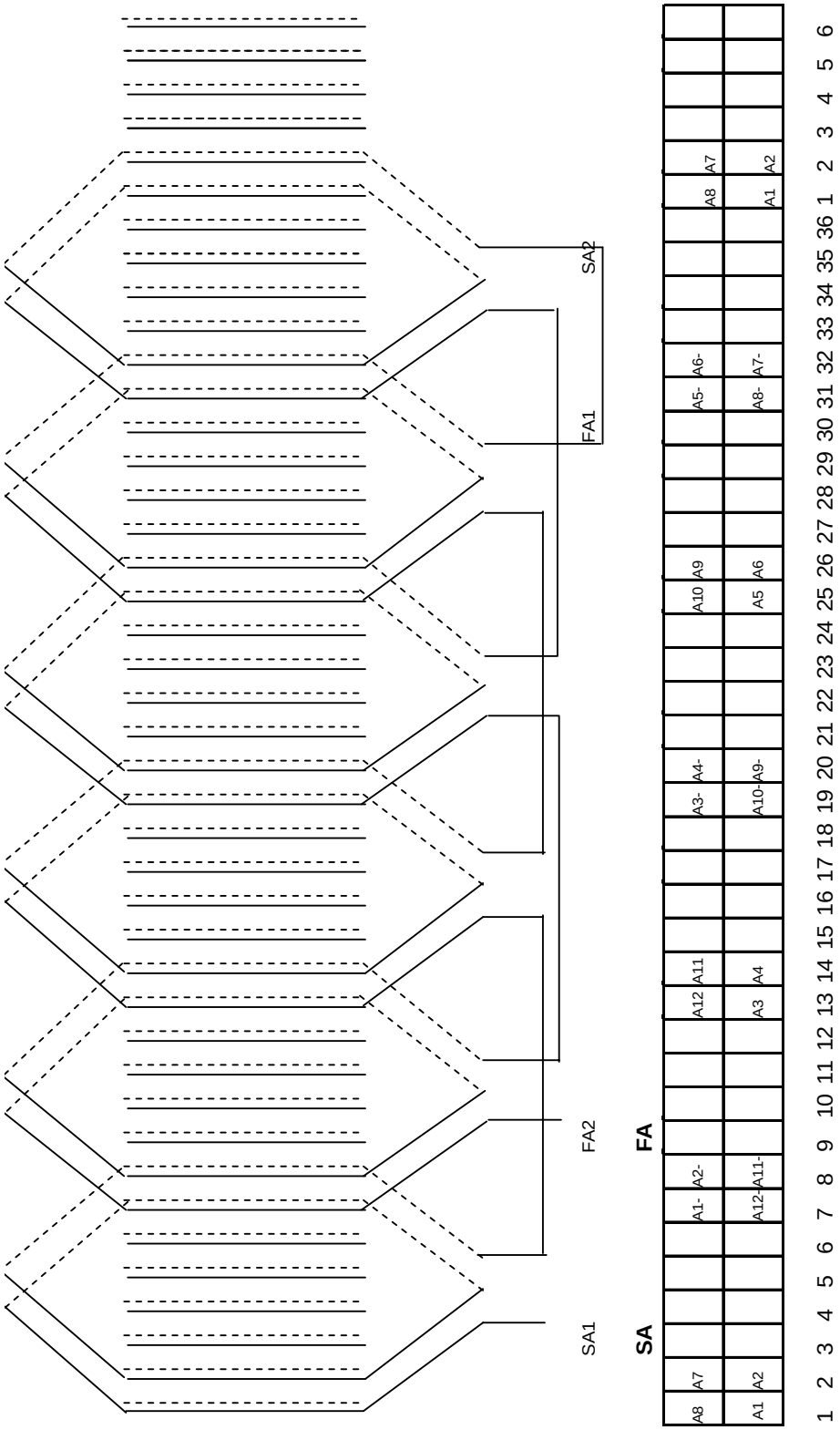

Figure 4-5. Connection of the coils of Group I and II constituting Phase A of the three-phase machine

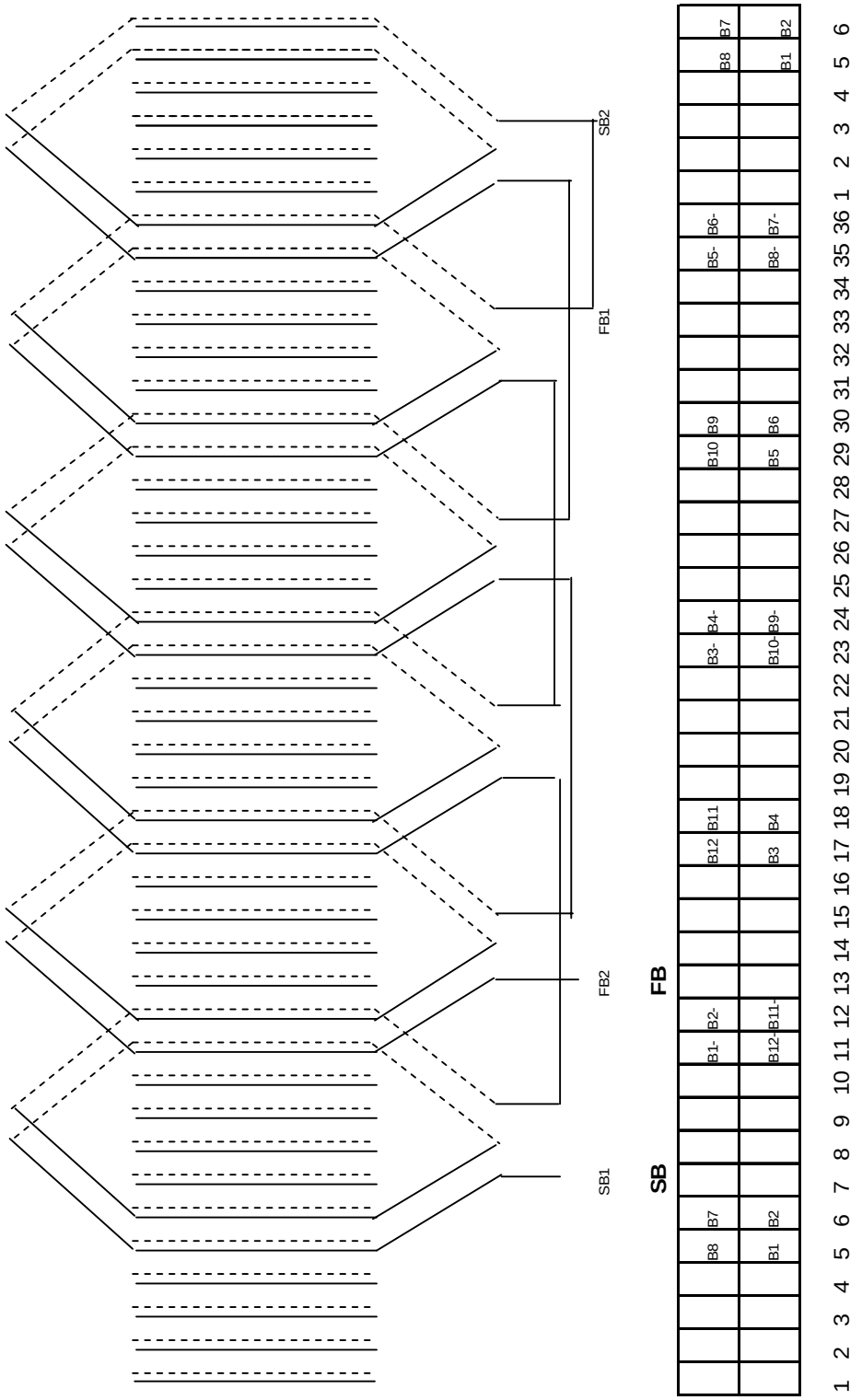

Figure 4-6. Connection of the coils of Group III and IV constituting Phase B of the three-phase machine

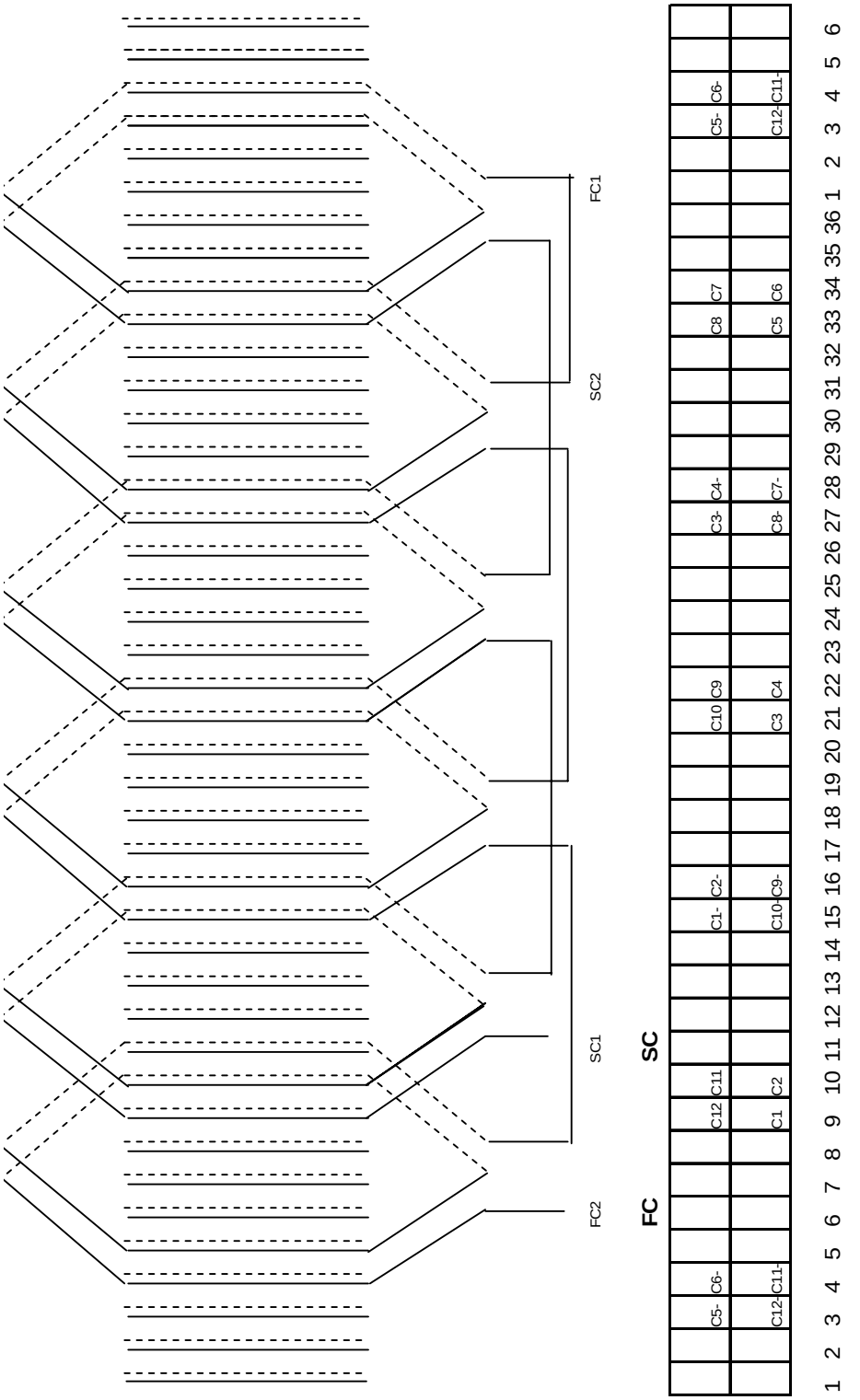

Figure 4-7. Connection of the coils of Group V and VI constituting Phase C of the three-phase machine.

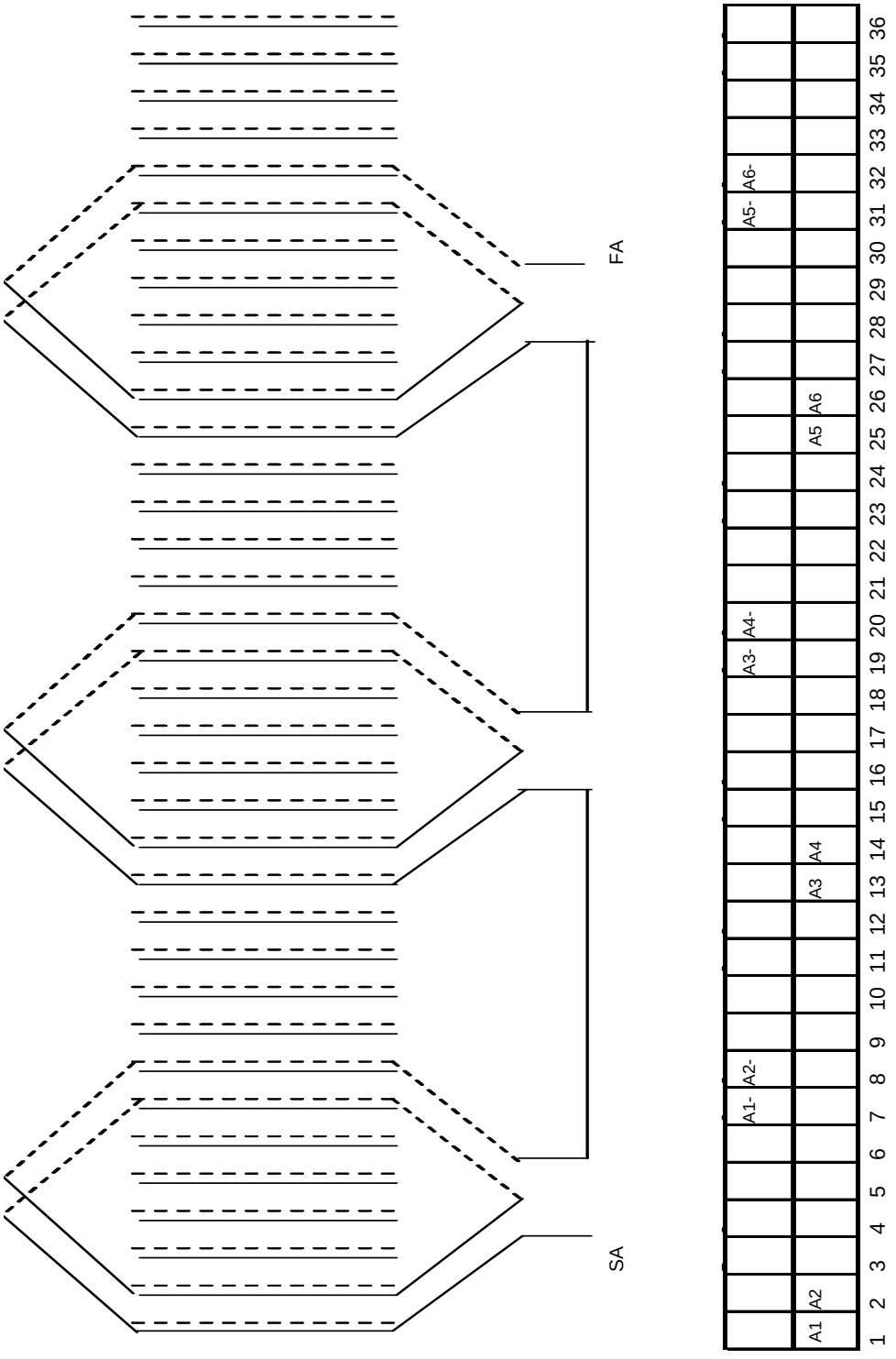

Figure 4-8. Connection of coils of Group I constituting Phase A of the six-phase machine.

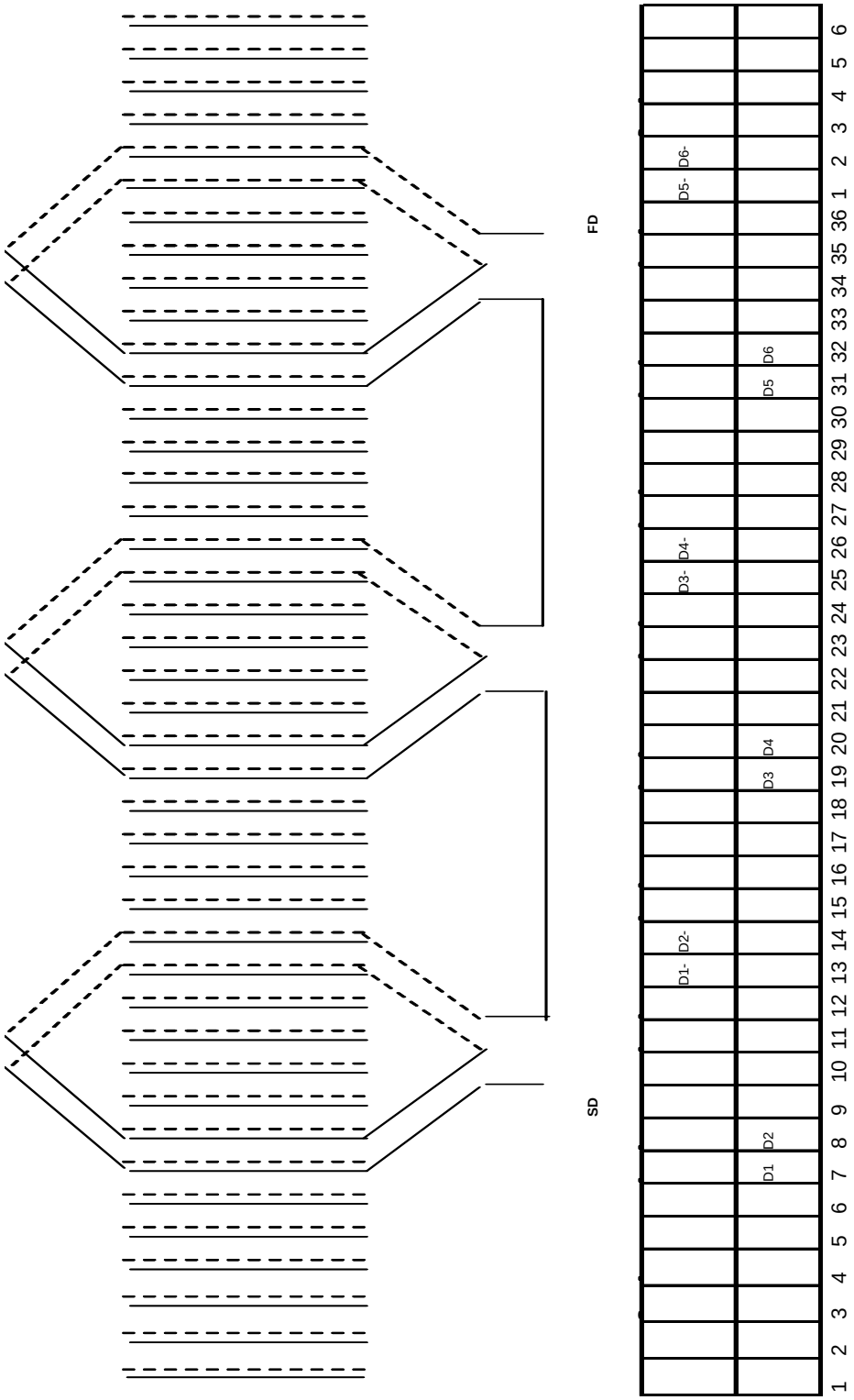

Figure 4-9. Connection of coils of Group II constituting Phase D of the six-phase machine.

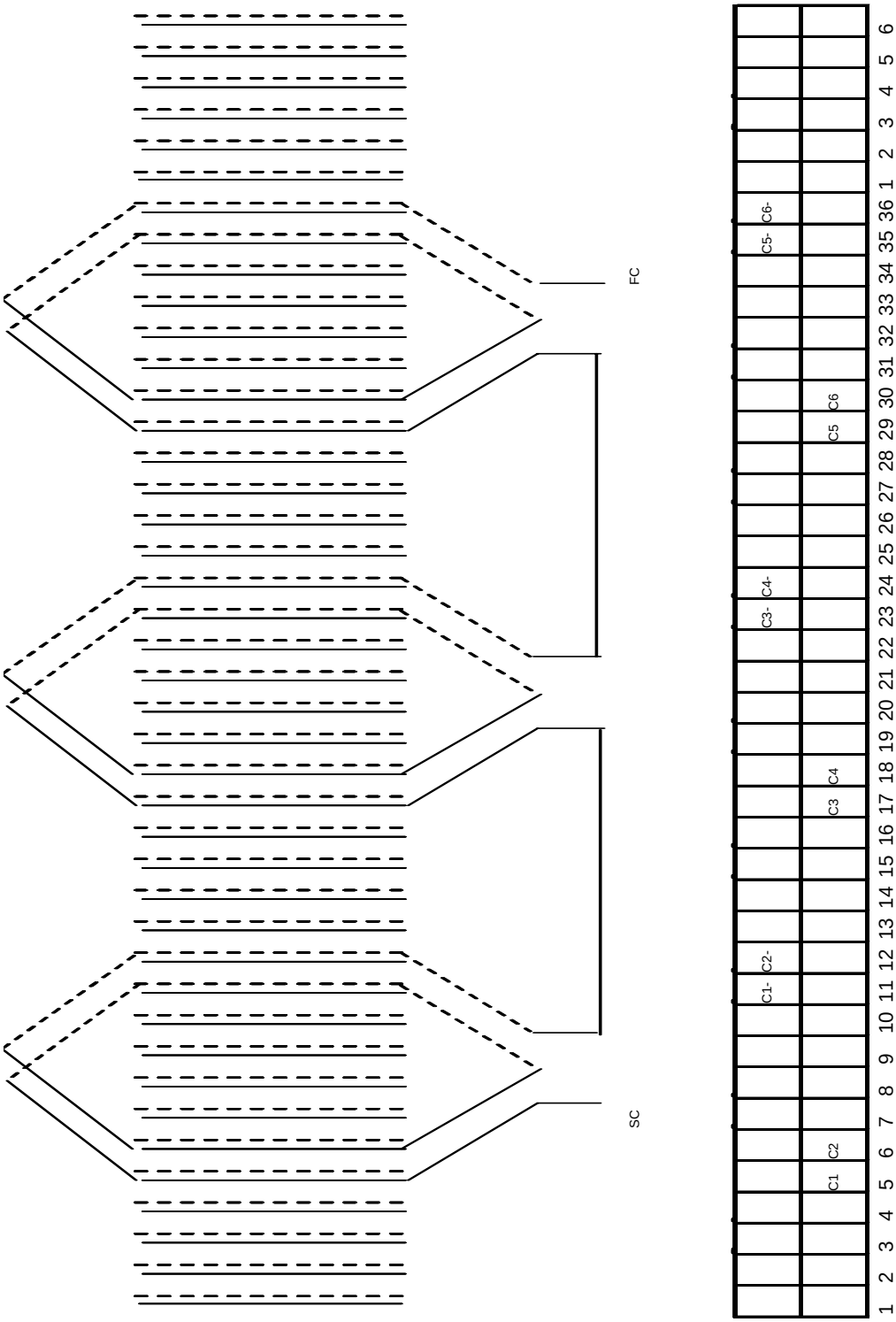

Figure 4-10. Connection of coils of Group III constituting Phase C of the three-phase machine.

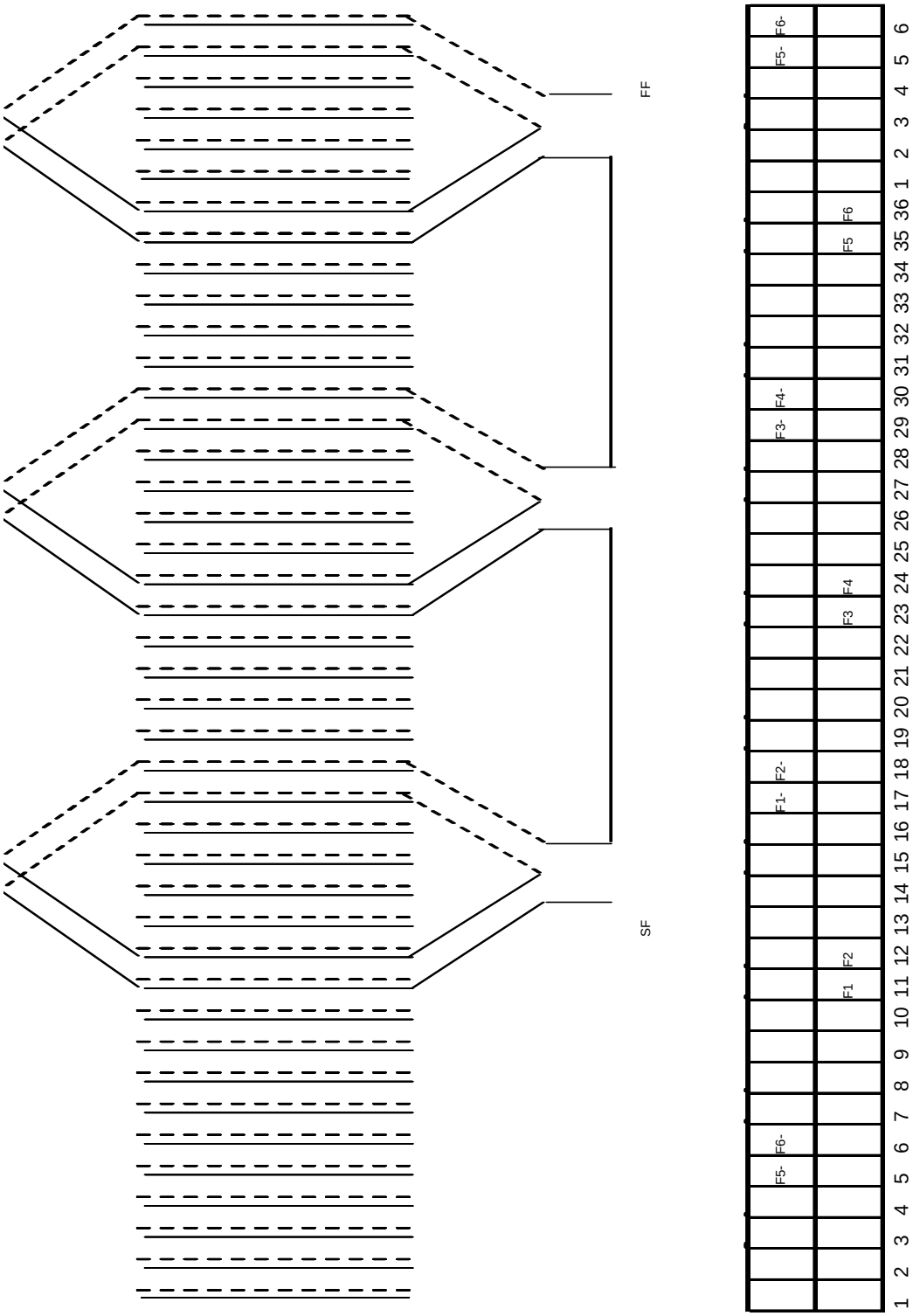

Figure 4-11. Connection of coils of Group IV constituting Phase F of the six-phase machine.

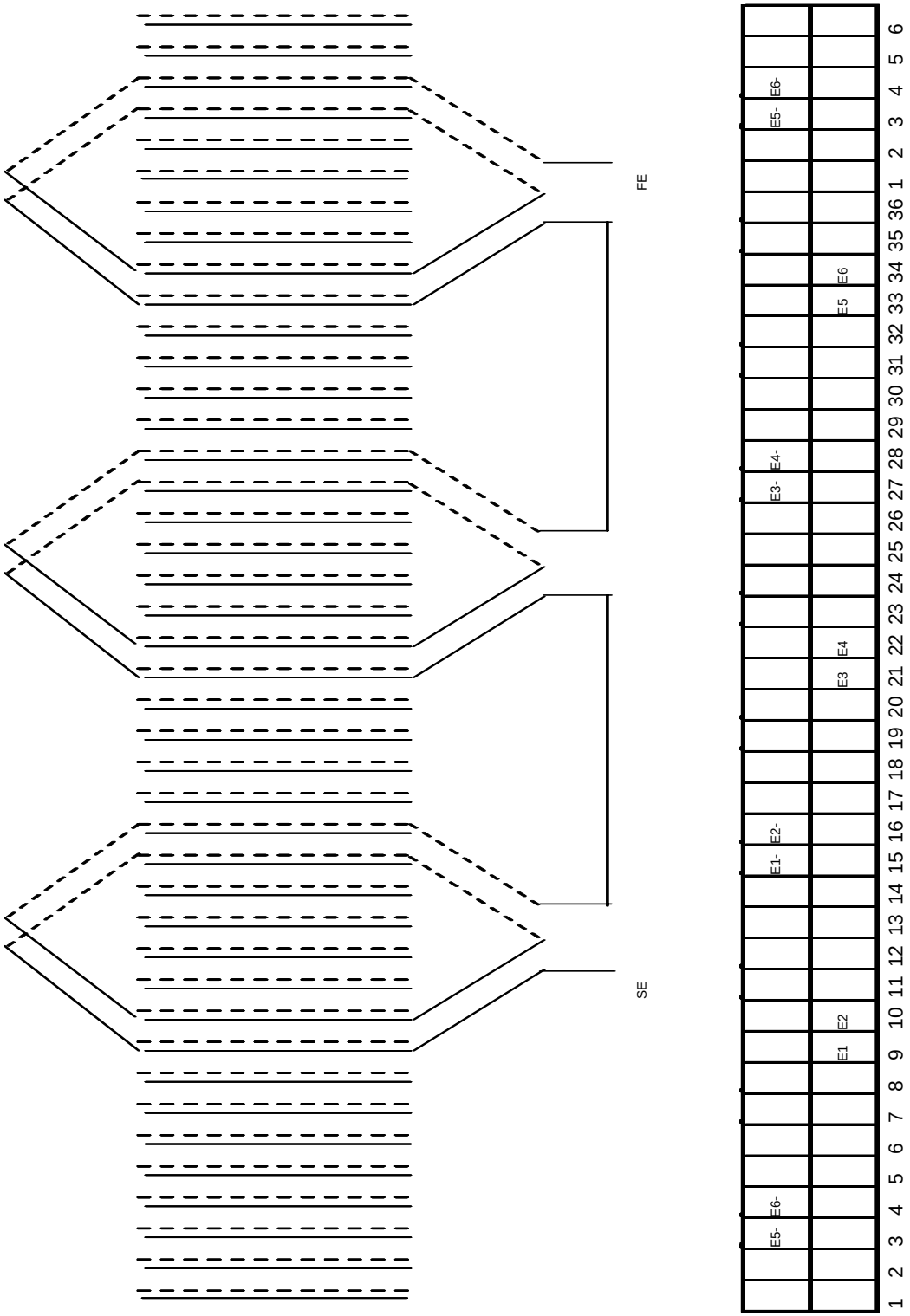

Figure 4-12. Connection of coils of Group V constituting Phase E of the six-phase machine.

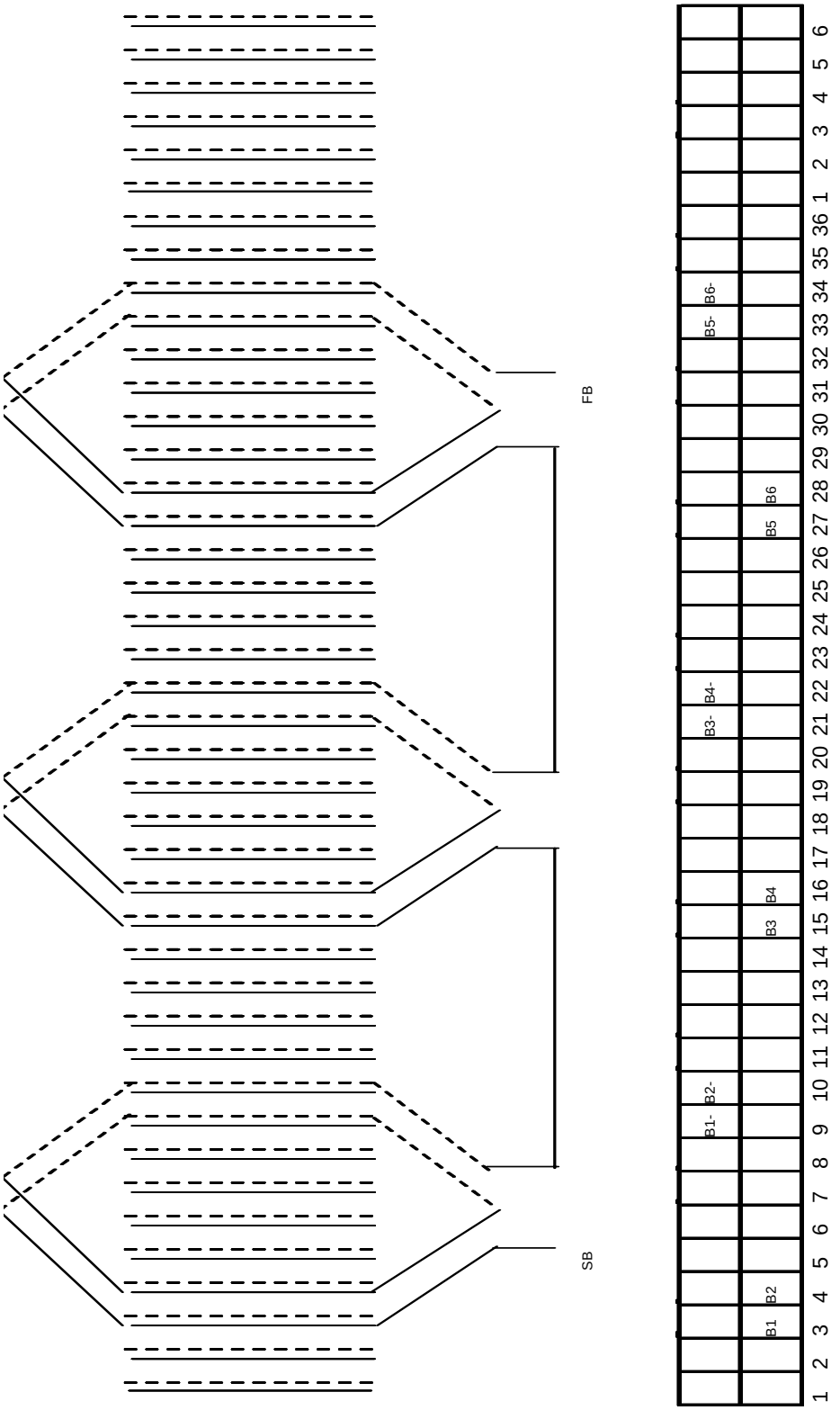

Figure 4-13. Connection of coils of Group VI constituting Phase B of the six-phase machine.

The Winding layout/phase distributions for the six-phase induction machine with 36 slots and a full-pitched coil span of 6 is shown in Figure 4-14. The complete winding layout of the reconfigured six-phase induction machine is shown in Figure 4-15

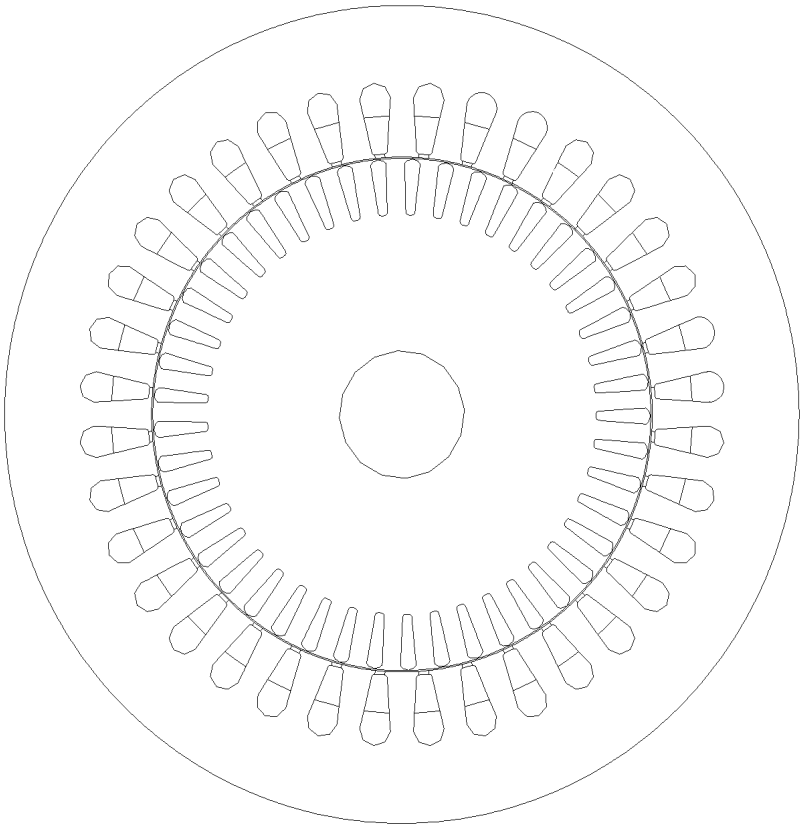

	1	2	3	4	5	6	7	8	9	10	11	12	13	14	15	16	17	18
Top	D5-	D6-	E5-	E6-	F5-	F6-	A1-	A2-	B1-	B2-	C1-	C2-	D1-	D2-	E1-	E2-	F1-	F2-
Bottom	A1	A2	B1	B2	C1	C2	D1	D2	E1	E2	F1	F2	A3	A4	B3	B4	C3	C4
	19	20	21	22	23	24	25	26	27	28	29	30	31	32	33	34	35	36
Top	A3-	A4-	B3-	B4-	C3-	C4-	D3-	D4-	E3-	E4-	F3-	F4-	A5-	A6-	B5-	B6-	C5-	C6-
Bottom	D3	D4	E3	E4	F3	F4	A5	A6	B5	B6	C5	C6	D5	D6	E5	E6	F5	F6

Figure 4-14:Cross-sectional view of the stator slots showing the winding distributions of the Six Phases.

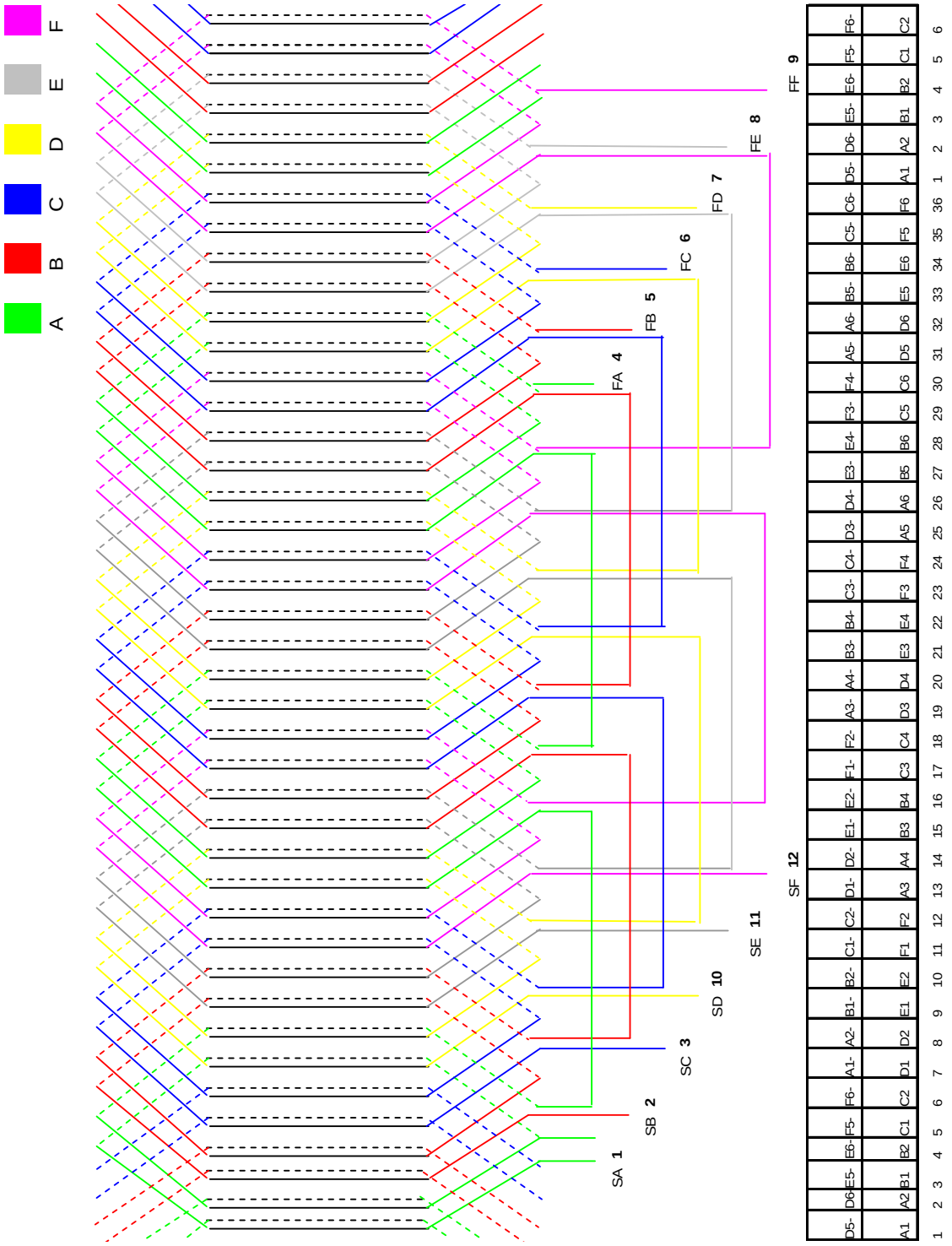

Figure 4-15:Complete Winding layout Of The Reconfigured Six-Phase induction machine Showing connections of all the coils

4.4.1 MMF DISTRIBUTION

From Equation 2-33 , for a six-phase armature winding the MMFs of phases A, B, C, D, E and F can be represented as follows:

$$F_a(\theta,t) = F_{\max} \times \sum_{h=1}^{k} \frac{1}{h}[K_{wh} \times \cos(h \cdot \theta) \times \cos(h \cdot \omega \cdot t)] \quad (4\text{-}21)$$

$$F_b(\theta,t) = F_{\max} \times \sum_{h=1}^{k} \frac{1}{h}[K_{wh} \times \cos(h \cdot \theta - \frac{\pi}{3}) \times \cos(h \cdot \omega \cdot t - \frac{\pi}{3})] \quad (4\text{-}22)$$

$$F_c(\theta,t) = F_{\max} \times \sum_{h=1}^{k} \frac{1}{h}[K_{wh} \times \cos(h \cdot \theta - \frac{2\pi}{3}) \times \cos(h \cdot \omega \cdot t - \frac{2\pi}{3})] \quad (4\text{-}23)$$

$$F_d(\theta,t) = F_{\max} \times \sum_{h=1}^{k} \frac{1}{h}[K_{wh} \times \cos(h \cdot \theta - \pi) \times \cos(h \cdot \omega \cdot t - \pi)] \quad (4\text{-}24)$$

$$F_e(\theta,t) = F_{\max} \times \sum_{h=1}^{k} \frac{1}{h}[K_{wh} \times \cos(h \cdot \theta - \frac{4\pi}{3}) \times \cos(h \cdot \omega \cdot t - \frac{4\pi}{3})] \quad (4\text{-}25)$$

$$F_f(\theta,t) = F_{\max} \times \sum_{h=1}^{k} \frac{1}{h}[K_{wh} \times \cos(h \cdot \theta - \frac{5\pi}{3}) \times \cos(h \cdot \omega \cdot t - \frac{5\pi}{3})] \quad (4\text{-}26)$$

Therefore, the resultant / total fundamental stator MMF , $F_s(\theta,t)$, can be expressed by adding by adding all the first harmonic / fundamental terms in Equations (4-21) through (4-26) , which yield the following upon proper trignometric / algebraic reductions:

$$F_s = F_a(\theta,t) + F_b(\theta,t) + F_c(\theta,t) + F_d(\theta,t) + F_e(\theta,t) + F_f(\theta,t) = 6/2 \times F_{\max} \times \cos(\theta - \omega t)$$

where, $F_{\max} = \frac{4}{\pi} \times \frac{N_{ph}}{P} \times \frac{I_{ph}}{m} \times \sqrt{2}\ AT/Pole$, N_{ph} is the Number of turns per phase, P is the Number of poles, m is the Number of phases , h is the harmonic order, for the fundamental h = 1 , and K_{wh} is the winding factor for the harmonic order , h

The MMF distribution produced by the six-phase winding layout given earlier in Figure 4-15 is shown in here in Figure 4-16, including a developed diagram of the layout of the six-phases.

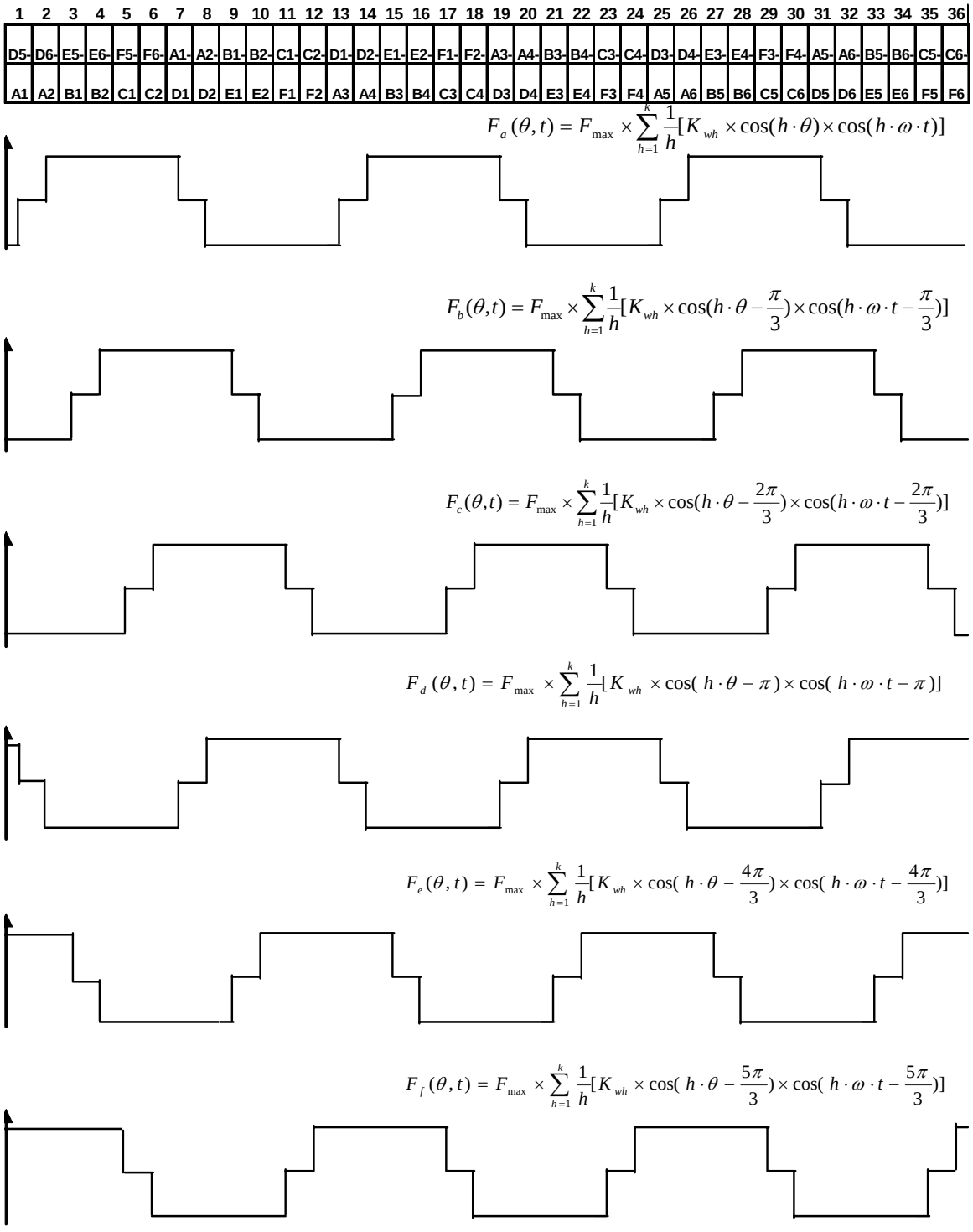

Figure 4-16. The mmf distribution produced by the currents in the six windings of the six-phase machine.

4.5 CONNECTION SCHEME FOR THE REVERSIBLE THREE-PHASE TO SIX-PHASE OPERATION

- FOR SIX-PHASE OPERATION

The twelve (12) terminals of the individual phase windings referring to starts (S) and finishes (F) of all the phases A, B, C, D, E and F are symbolized here by, SA,SB,SC,SD,SE,SF,FA,FB,FC,FD,FE and FF as shown in Figure 4-17 of the reconfigured 6 – phase machine. For the six-phase operation , line-to-line voltage phasors are separated by 60^0 *e,* and are connected to terminals 1 , 2 , 3 , 10, 11 and 12 , respectively as shown in Figure 4-17. The neutral point is formed by connecting terminals 4 , 5 , 6 , 7 , 8 , and 9 together. Thus terminals 1 , 2 , 3 , 10 , 11 and 12 are the outer / input leads.

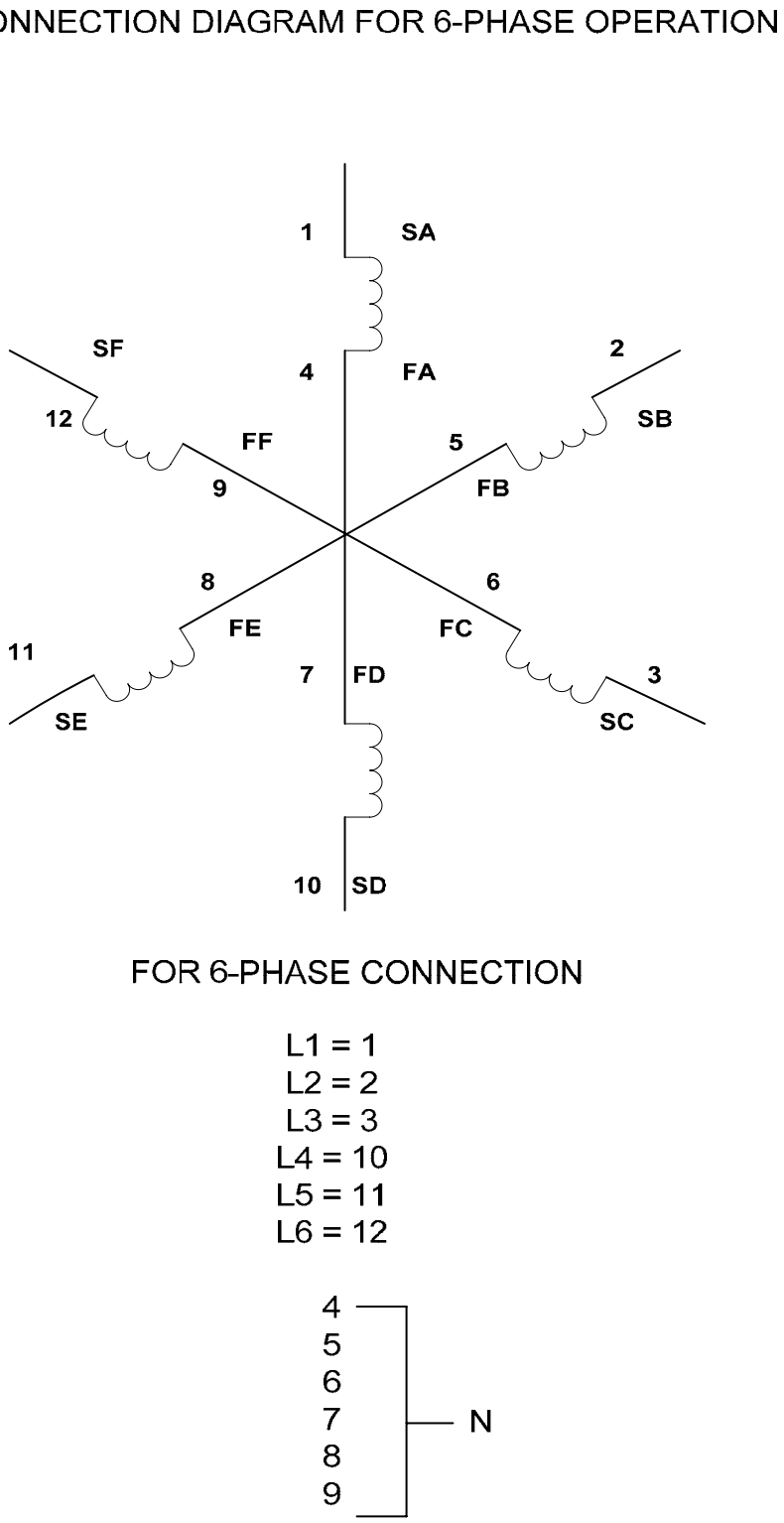

Figure 4-17:Connection Scheme For Six-Phase Operation

- FOR THREE-PHASE OPERATION

The twelve terminals of the individual coils referring to the starts and finishes of the reconfigured six-phase machine connection of Figure 4-17 , are connected as shown in Figure 4-18 for three-phase operation, line-to-line voltages here are separated by 120^0 *e* and connected to terminals 1 , 3 and 11. It is important to note that for three-phase operation

terminal 4 is connected to terminal 7,

terminal 6 is connected to terminal 9,

and terminal 8 is connected to terminal 5. Here,

terminals 2, 10 and 12 are connected together to form the neutral.

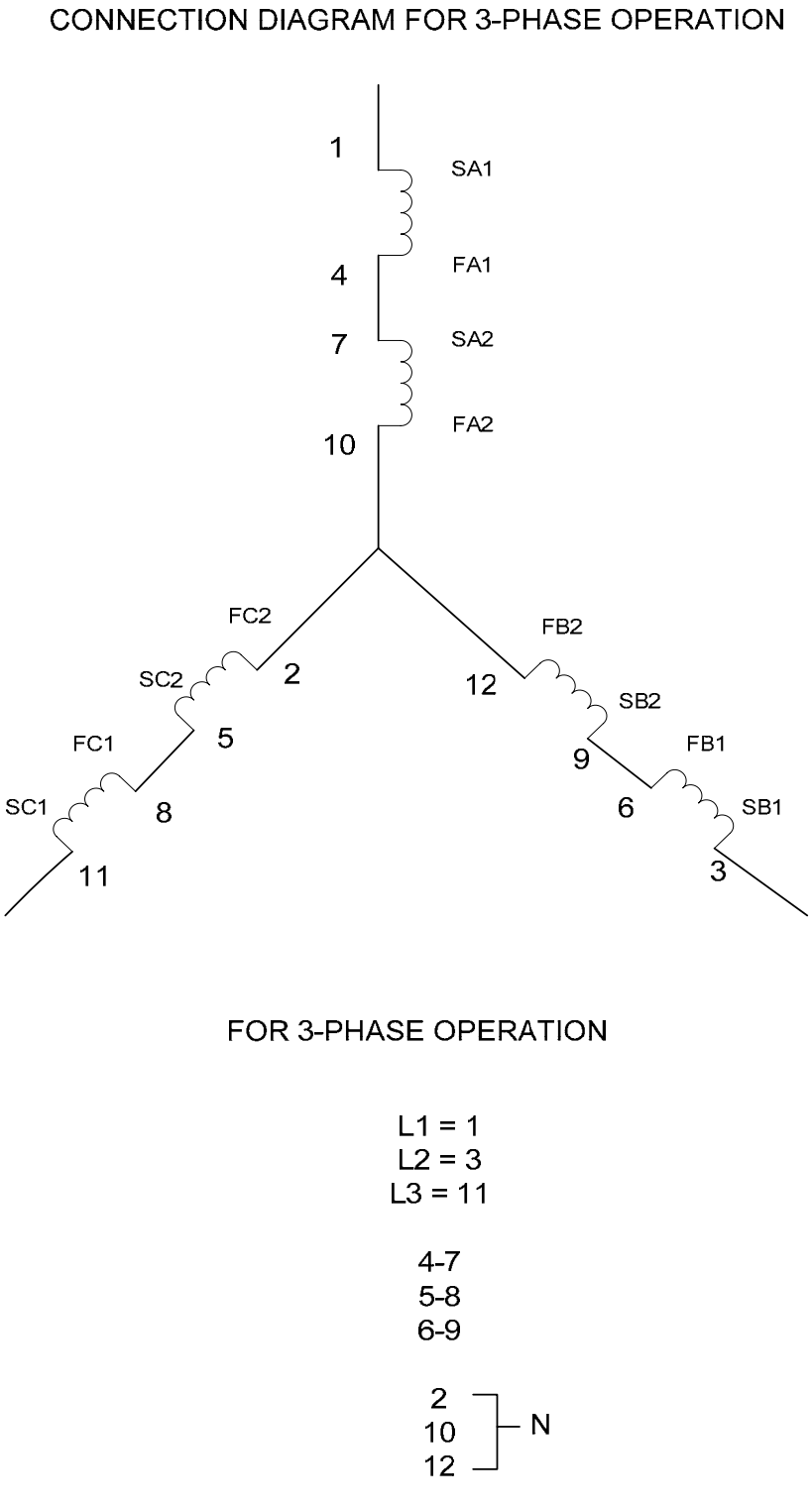

Figure 4-18:Connection Scheme For Three-Phase Operation

CHAPTER 5: FUNDAMENTALS OF THE TIME-STEPPING FINITE ELEMENT METHOD

5.1 INTRODUCTION

In this chapter the development of the Time-Stepping Finite Element (TSFE) model will be discussed. It should be noted that the TSFE model used in this thesis has been implemented in the commercially available software package, namely MAGSOFT (Flux 2D). This chapter will present some basic principles of the TSFE modeling approach .

5.2 DEVELOPMENT OF THE FINITE ELEMENT METHOD

Earlier the magnetic circuit or permeance (magnetic Ohms-law) method was used for calculating approximate magnetic fields in devices of simple geometry [28,29]. For more accurate calculations , however, finite element computer algorithms programs are necessary.

The key limitation of the magnetic circuit method is that it requires assumption of the magnetic flux paths. The lengths and cross-sectional areas of all the paths must be known. Usually the paths are assumed to consist of straight lines, which is erroneous to some extent. To calculate the effects of flux fringing, saturation, and leakage flux one usually uses empirical correction factors. If a motor or other magnetic device has had essentially the same type of design for many years, then the empirical factors may be fairly well known.

Today's motor designer is often involved with new motor design concepts for which the flux paths and empirical factors are unknown. Even if the design is a well-understood older design configuration or concept, there is a great need today for accurately determining the effects

of geometric changes and saturation on motor efficiency and other performance parameters related to the magnetic field.

The Finite Element (FE) method is readily available in the laboratory in the form of a commercial computer software with the trade name " MAGSOFT ". The software requires no assumption of flux paths or related empirical factors. This FE software accurately calculates magnetic fields and the related motor design parameters for motors of complicated geometry, with saturation , with significant armature reaction ,and with or without eddy currents.

5.3 BASIC PRINCIPLES

The finite element method is based on energy conservation. It is well known that the flux density , $\overline{B}$, field intensity , $\overline{H}$, the current density , $\overline{J}$, and the electric field , $\overline{E}$, are related to each other by the constitutive Equations 5-1 through 5-3 , as follows [30]:

$$\overline{B} = \mu \cdot \overline{H} \qquad (5\text{-}1)$$

$$\overline{H} = \nu \cdot \overline{B} \qquad (5\text{-}2)$$

$$\overline{J} = \sigma \overline{E} \qquad (5\text{-}3)$$

where μ is the magnetic permeability of the material

ν is the magnetic reluctivity of the material and

σ is the electrical conductivity in conductive regions of a given device.

The law of conservation of energy in electric motors may be derived from Maxwell's equations which are as follows [30]:

$$\nabla \times \overline{H} = \overline{J} + \frac{\partial \overline{D}}{\partial t} \quad \text{(Ampere's law)} \qquad (5\text{-}4)$$

$$\nabla \times \overline{E} = -\frac{\partial \overline{B}}{\partial t} \qquad \text{(Faraday's law)} \qquad (5\text{-}5) \text{ and}$$

$$\nabla \cdot \overline{B} = 0 \qquad (5\text{-}6)$$

where , $\overline{D}$ is the electric flux density / displacement vector.

Applying the null identity , equation 5-6 can be rewritten as $\nabla \cdot (\nabla \times \overline{A}) = 0$, where , $\overline{A}$ is defined here as the magnetic vector potential . Thus , the flux density in terms of magnetic vector potential can be defined as follows:

$$\overline{B} = \nabla \times \overline{A} \qquad (5\text{-}7)$$

From equations 5-7 , 5-4 and 5-2 , the differential equation describing a field distribution can be can be expressed as follows [30]:

$$\nabla \times (\nu(\nabla \times \overline{A})) = \overline{J} \qquad (5\text{-}8)$$

Also from Faraday's law i.e. equation 5-5 and 5-7 , one can write the following:

$$\nabla \times (\overline{E} + \nabla \phi) = -\nabla \times (\frac{\partial \overline{A}}{\partial t}) \qquad (5\text{-}9)$$

where ϕ is an arbitrary differentiable scalar potential function.Hence, from (5-9) it follows that:

$$(\overline{E} + \nabla \phi) = -(\frac{\partial \overline{A}}{\partial t}) \qquad (5\text{-}10)$$

Thus ,

$$\overline{E} = -\nabla \phi - (\frac{\partial \overline{A}}{\partial t}) \qquad (5\text{-}11)$$

Finally from equation 5-3 and 5-11 , the current density , $\overline{J}$, can be expressed as ,

$$\overline{J} = -\sigma (\nabla \phi + \frac{\partial \overline{A}}{\partial t}) \qquad (5\text{-}12)$$

Substituting equation 5-12 in 5-8 , one can obtain the following key partial differential equation (pde):

$$\nabla \times (\nu(\nabla \times \bar{A})) = -\sigma(\nabla \phi) - \sigma \frac{\partial \bar{A}}{\partial t} \qquad (5\text{-}13)$$

Equation 5-13 is the principle equation solved in time-stepping finite-element models of time-domain electromagnetic events in electromechanical energy conversion devices or systems [30].

If time-domain events are not of concern , and the emphasis is on static magnetic field computation in electromechanical devices , Equation 5-13 can be simplified to the static form in which a current density , $\bar{J} = -\sigma(\nabla \phi)$, and hence one can write the following governing pde:

$$\nabla \times (\nu(\nabla \times \bar{A})) = \bar{J} \qquad (5\text{-}14)$$

Variational techniques such as the finite element method obtain solutions to field problems by mimimizing a functional whose minimization satisfies either Equation 5-13 or 5-14, and the associated boundary conditions simultaneously [31]. This energy functional [31] expresses the difference between the stored magnetic energy and the input energy in the volume of the device under study.

5.4 FINITE ELEMENT FORMULATION

Minimization of the magnetic energy functional [32] over a set of finite elements (called a mesh) leads to a matrix equation that can be solved for the magnetic vector potential , (mvp) $\bar{A}$, throughout the mesh.This is essentially a numerical solution of Equation 5-14 governing magnetostatic fields. Figure 5-1 shows a typical finite element belonging to a finite element mesh.

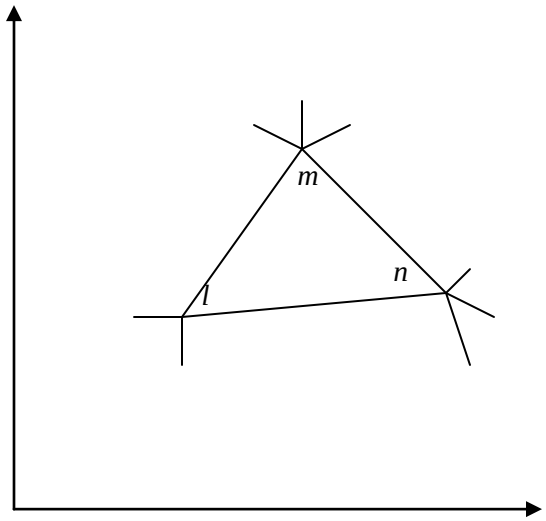

Figure 5-1: Typical triangular finite element connected to other finite elements

In this case, the device analyzed must be subdivided into triangles or quadrilaterals called finite elements , each of which has three or four vertices called grid points. Given the motor geometry , MAGSOFT software automatically generates the finite element mesh for best solution accuracy.Within each triangular finite element, the mvp, A, is assumed to vary linearly according to a polynomial such as follows [33]:

$$A = \sum_{k=l,m,n} \frac{A_k}{2\Delta}(d_k + e_k X + f_k Y) \qquad (5\text{-}14)$$

Where, Δ is the triangle area

An $N \times N$ global finite element $\underline{S} \cdot \underline{A} = \underline{I}$ is obtained , which matrix equation that is obtained is solved for the vector , $\underline{A}$, at the grid point potentials using Newton-Raphson based sparse matrix techniques. Generally , all the interior grid points are unconstrained, while grid points on the exterior of the mesh are constrained in a manner dependent on the boundary conditions at the exterior of the region analysed. In two-dimensional planar problems a flux line is a line of

constant magnetic vector potential , *A*. For most electrical machines with steel exterior surfaces, the flux is assumed to be confined to the steel outer boundary. By using the boundary condition, *A=0* , flux lines are constrained to follow the boundary. Many electrical machines have identical poles, or even identical half-poles. The matrix equation with size $N \times N$ can be greatly reduced if the mesh contains only one-pole or one-half pole. Absence of any constraint on an exterior grid point can be shown to cause the flux lines to be perpendicular to the finite element mesh boundary. This perpendicularity is called the natural boundary condition.

5.5 SOLUTION TECHNIQUES

Once the matrix equation , $\underline{S} \cdot \underline{A} = \underline{I}$, has been assembled and the mvp constraints have been enforced, solution for the mvp vector , $\underline{A}$, at the unconstrained grid points may proceed. The advantage of using the mvp stems from the fact that all parameters used to characterize magnetic fields, such as, the magnetic field intensity, $\vec{H}$, and the magnetic flux density, $\vec{B}$, are readily obtainable from the knowledge of magnetic vector potential vector , $\underline{A}$, at the grid nodes , and hence the need of using multiple physical quantities to characterize the field is eliminated.

If the permeability μ is known throughout the region , then the flux density can be solved directly by Gauss-Jordan elimination. If the permeability μ is not constant, then the matrix equations depends on the magnitude of *B* (and *J*). In this case an iterative procedure is developed. The matrix is first estimated from an initial solution using approximate material permeabilities. Then the equations are solved repeatedly (iteratively) using a Newton-raphson based approach, which depends on the latest values of $\underline{A}$, enabling rapid convergence to the correct saturable condition mvps, $\underline{A}$.

In the algorithm of MAGSOFT, the parameters are automatically computed from the *B-H* curves applied as input data.While the distribution of the resulting mvp , $\underline{A}$, has little meaning to

design engineers , many useful performance parameters can be calculated from $\underline{A}$ .The MAGSOFT postprocesses $\underline{A}$ to obtain parameters of significant interest such as the flux density $\overline{B}$, is calculated in each finite element using the curl of the mvp , $\underline{A}$, as in equation 5-7.From the mvps , $\underline{A}$, the flux flowing between any two points (nodes) is easily obtained by using the equation:

$$\phi = \int \overline{A} \cdot d\overline{l} \qquad (5\text{-}15)$$

For two-dimensional problems the flux between two grid points 1 and 2 is simply:

$\phi_{12} = (A_1 - A_2)d$ (5-16) where d is the axial depth or stack length in a motor or a machine.Also calculable from the *A* distribution are the various flux linkages and the inductances.

5.6 THE TIME-STEPPING FINITE ELEMENT METHOD

The time-stepping finite element method is one in which 5-13 is solved , hich is a solution of a time-varying electromagnetic field throughout the cross-section of a device. Such solution enables one to directly predict essentially all the performance parameters of a device whether it is a motor, generator, or a transformer. The Time-stepping finite element software [34] provides more thorough and accurate prediction of a motor performance than the state-space-finite element approach in which a series of state field solutions are utilized [34-39]. All motor performance parameters, such as torque, induced or eddy currents, and winding currents are predicted as functions of time. Thus cogging torques and harmonic currents are predicted as well as average torque and fundamental current. The time-stepping finite element software must allow the rotor to move, either at constant speed or in response to motor torque and mechanical load.

The theory of time-stepping finite element computation of motor performance is best summarized as given next.

The power source driving the motor , the motor's electromagnetic fields , and the motor-mechanical load dynamic equations are all time-dependent subject to the appropriate initial conditions. Kirchoff's electric circuits voltage law is used to describe the connection between the power source and the windings of the motor. Two types of conductors are considered :solid conductors in which eddy currents can be induced, and stranded conductors without eddy currents.

Because motion occurs in motors, the field equations for the stator and the rotor can be written in their own coordinate systems to avoid the rotational speed appearing explicitly in the formulation. Conductors are normally connected to produce multiturn windings. To represent voltage-fed windings in motors , circuit equations are coupled with field equations.

The equation of motion of the rotor of any motor is typically expressable as follows:

$$J\alpha + \lambda\Omega = T_{em} + T_{app} \qquad (5\text{-}17)$$

Where $\alpha = angular\,acceleration$

$\Omega = rotational\,angular\,velocity$

$J = moment\,of\ inertia$

$\lambda = coefficient\,of\ \ friction$

$T_{em} = developed\,electromagnetic\,torque$

$T_{app} = externally\,applied\,mechanical\,torque$

At each time step,the electromagnetic torque is computed from the time-stepping finite-element magnetic field solution using the method of virtual work involved. This is followed by solving the equation of motion, which allows computation of a new rotor angular acceleration versus time and thus the rotor speed and angular position versus time.

To allow the rotor to move in the finite element mesh, the MAGSOFT software uses the moving surface method [34]. The idea is to share a common slip surface between the rotor mesh and the stator mesh, One side of the surface is attached to the stator and the other moves with the rotor. After any computed angular motion during the time step, the two independent meshes are automatically coupled together within the finite element functions. Thus the rotor mesh is free to move to any specified angle without remeshing.

In this work , finite element analysis method was used to model the case-study 5-hp induction machine.The generated meshes for the case-study 5-hp motor resulted in a total of 13563 nodes and 6622 elements. A parital view of the motor cross-section subdivided into finite elements is shown in Figure 5-2. Notice the high density of meshing in the rotor slots and sirgap as well as at the tips of the stator slots. The FE grid is much coarser in the cores, where flux density variations are less severe than near the airgap.

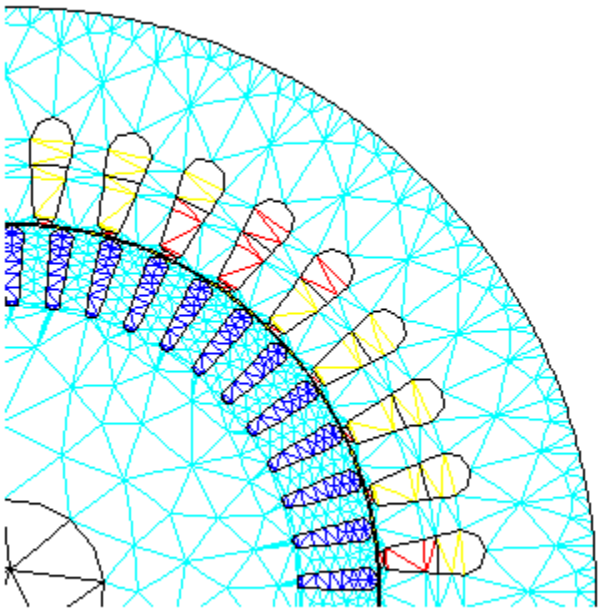

Figure 5.2 Finite-element mesh of a portion of the case-study 5HP induction motor

The results of simulations using the commercially available MAGSOFT time-stepping finite element software package are given in the next chapter.

CHAPTER 6: EXPERIMENTAL AND SIMULATION RESULTS

6.1 INTRODUCTION

In this chapter, the experimental and simulation results of the case-study 5HP squirrel cage induction motor used in this thesis will be presented in detail for various operating conditions.In the first section the experimental and simulation results of the 3-phase operation will be considered. Following this , a comparitive analysis of the simulation results of the 3-phase versus the simulation results of the 6-phase operations will be studied. It should be mentiond that the experimental and simulation results for the 3-phase operation will be presented whereas for the 6-phase operation , only the simulation results are presented, because of the lack of availability of a rewound machine. It should also be mentioned that the experimental and simulation results presented here were obtained at rated operating conditions, with the machine developing a torque of 30Nm under rated conditions at a corresponding speed of 1165 rpm. This was accomplished while the machine was supplied from a balanced 3-phase 460-V (line-to-line),60hz voltage source.The results include both laboratory obtained performance data and Time-stepping-finite-element (TSFE) simulation obtained performance data . Furthermore , for the 6-phase induction machine supplied from a balanced 6-phase , 132.5-V(line-to-line), 60hz source ,only TSFE simulation obtained performance results are presented.

Most importantly, the operation of the 6-phase machine was studied through TSFE simulation results obtained under different types of phase loss scenarios to predict the 5-phase , 4-

phase and 3-phase operations. A flow-chart of the various cases considered is presented in Figure 6-1

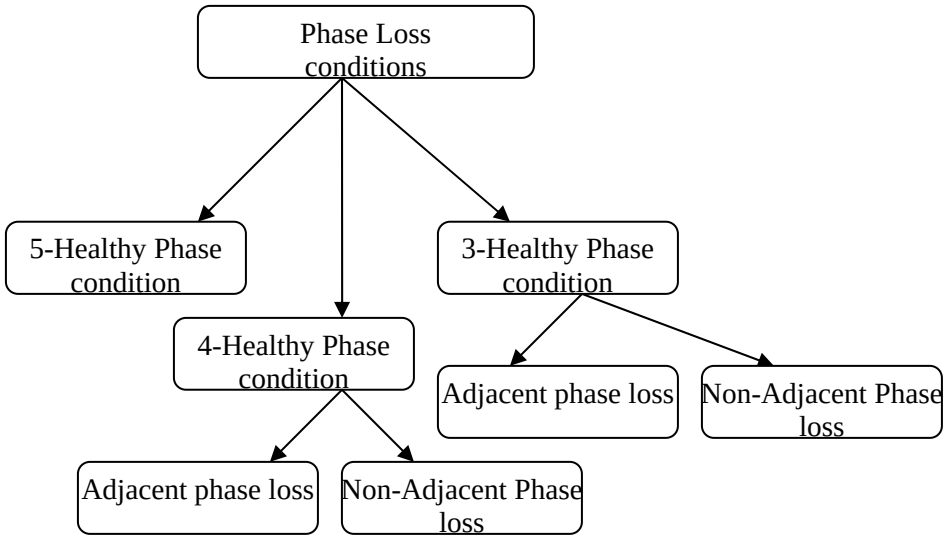

Figure 6-1: Flow-Chart of types of phase-loss scenarios studied.

6.2 Comparison Of Experimental And Simulation Results Of The 3-Phase Operation

In this section , the experimental results are obtained for the 3-phase machine with a short-pitched winding, the cross-section of which is shown in Figure (2-18), and the design details of which were given earlier in Chapter 2 . These results were compared with the Time-Stepping Finite-Element (TSFE) simulation results for the 3-phase machine with the same short-pithced and the full-pitched winding whose cross-section is shown in Figure (2-19). It turned out that the current and voltage waveforms, as well as the torque profiles of the short-pitched and full-pitched windings are identical.

Depicted in Figure 6-2 and Figure 6-3 are the line voltages , V_{ab},V_{bc} and V_{ca} obtained from experimental test and the TSFE simulation respectively. In Figures 6-4 and 6-5 , the rated

currents i_a , i_b and i_c obtained from experimental test and TSFE are shown. Futhermore, in Figures 6-6 and 6-7 , the rated torque from experimental test and TSFE simulation are compared. It should be mentioned that the experimental results were obtained at a sampling frequency rate of *50khz*

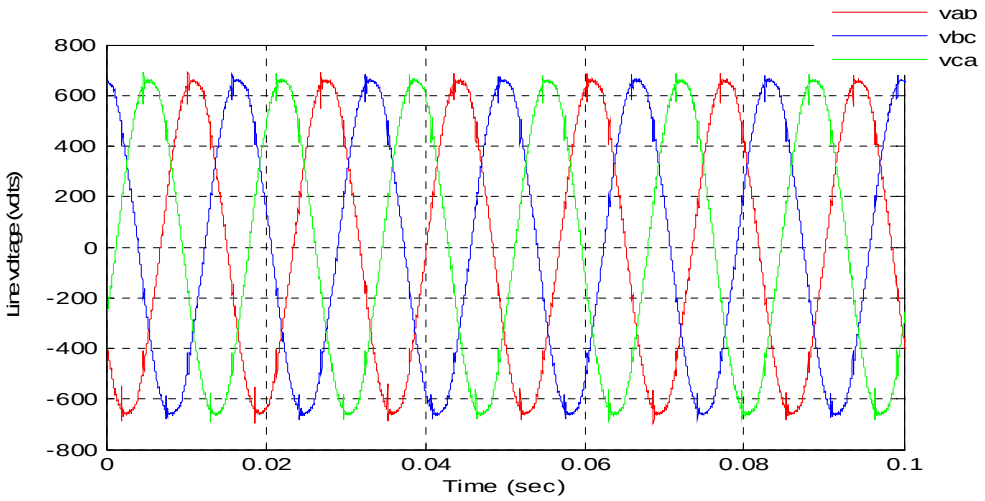

Figure 6-2 : Line voltages obtained from experimental test for the case study 5HP , 3-phase induction

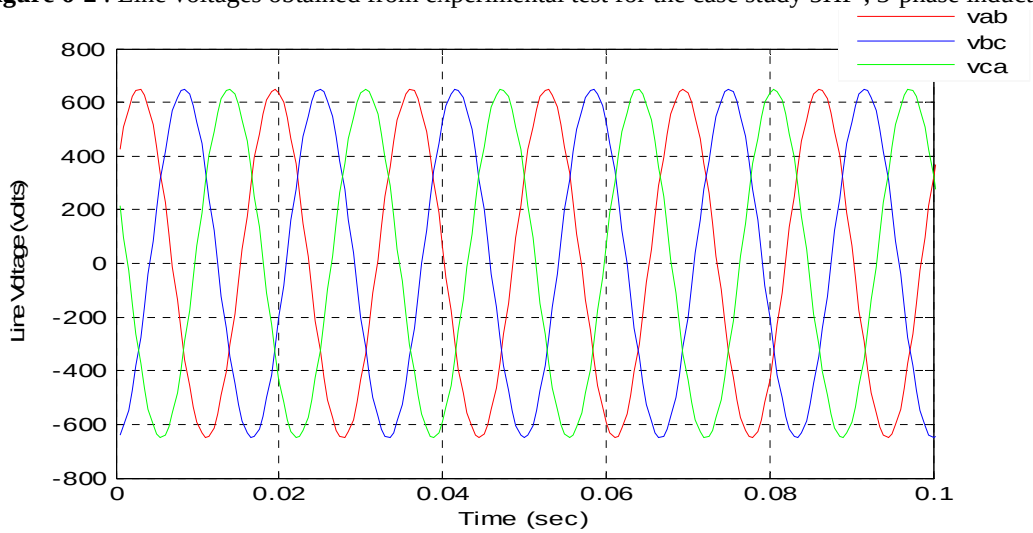

Figure 6-3:Line voltages obtained from the TSFE simulation for the 5HP, 3-phase induction motor .

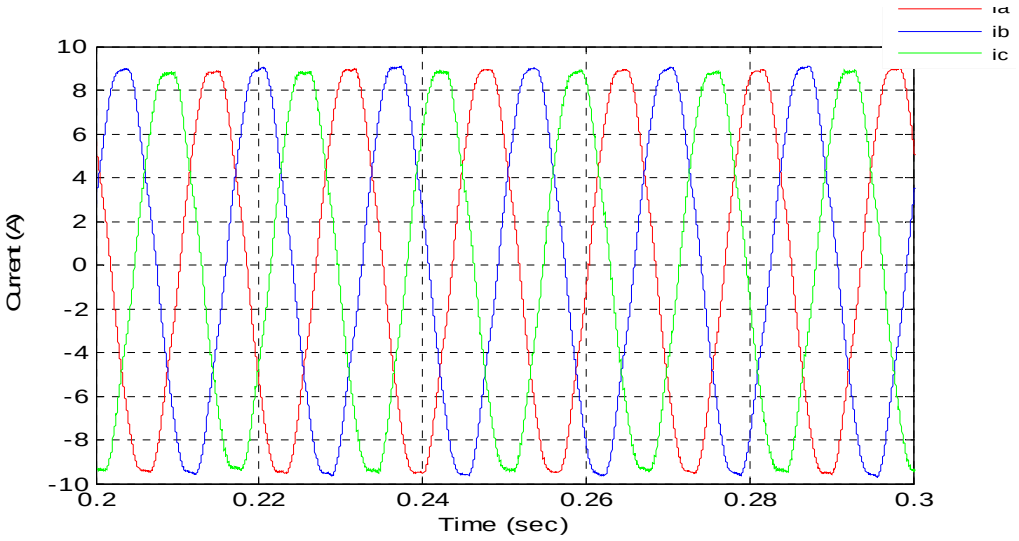

Figure 6-4: Phase Currents obtained from experimental test for the 5HP, 3-phase induction motor.

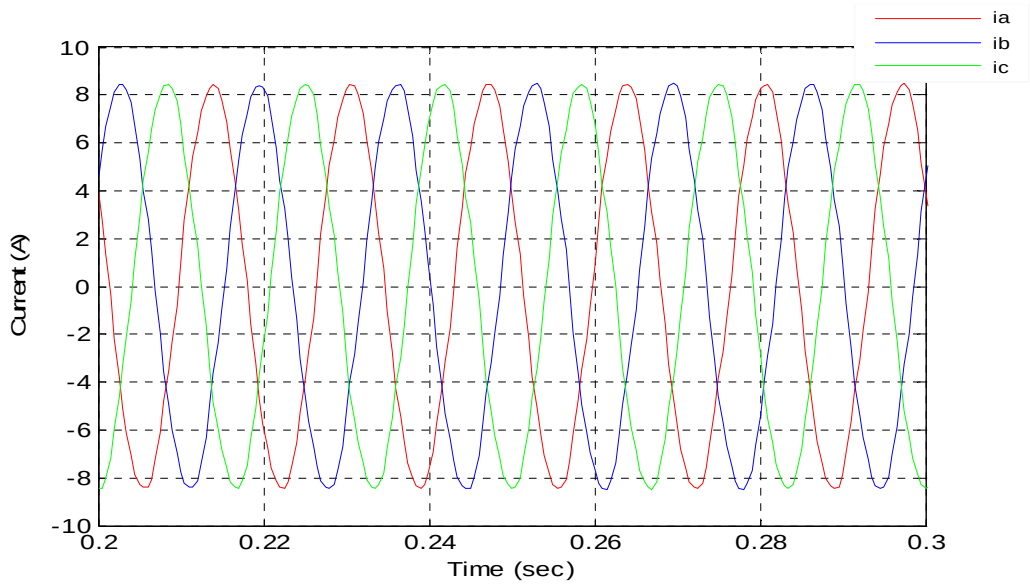

Figure 6-5: Phase Currents obtained from the TSFE simulation for the 5HP, 3-phase induction motor.

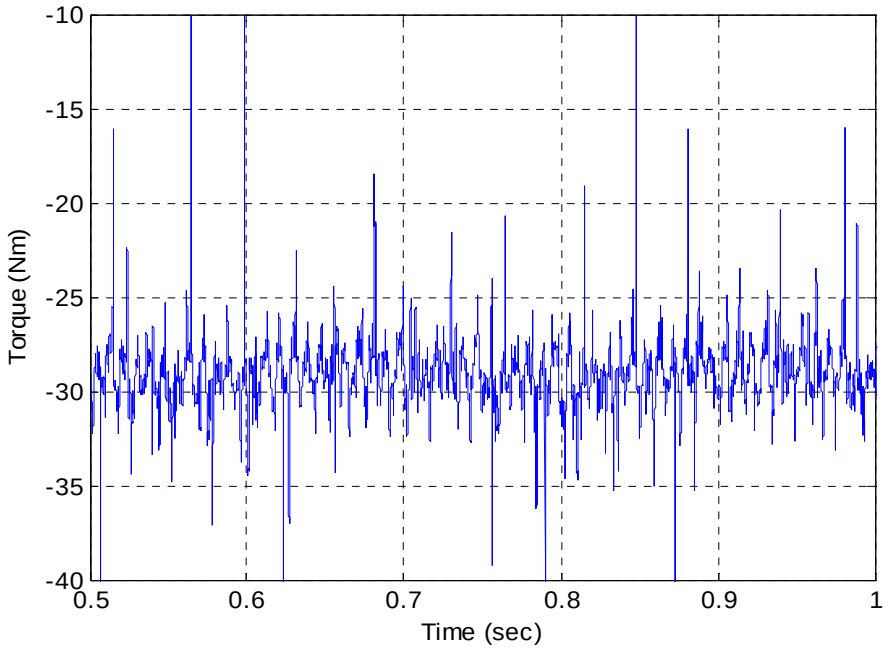

Figure 6-6: steady state torque profile from experimental test for the 5HP , 3-phase induction motor

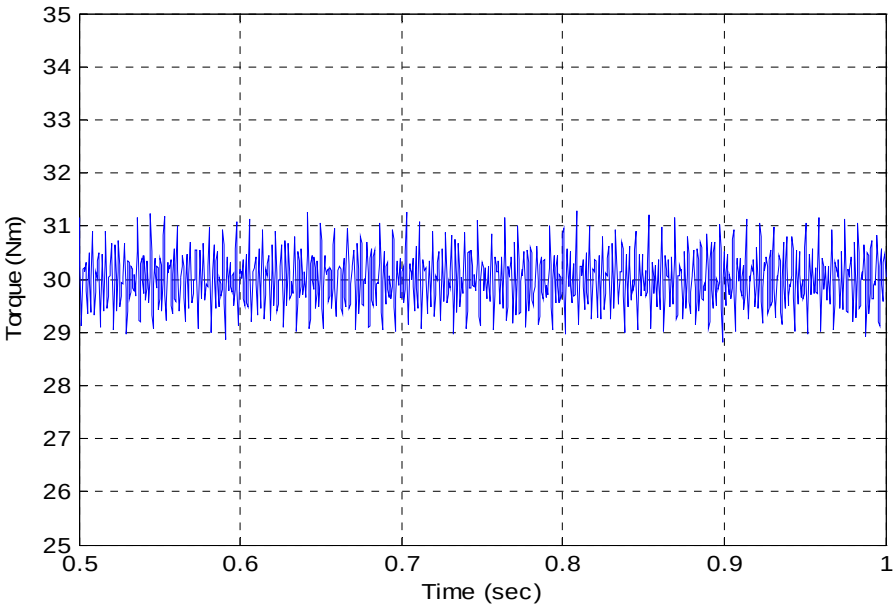

Figure 6-7: steady state torque profile from the TSFE simulation for the 5HP , 3-phase induction motor

Upon careful examination of the above results , it can be noticed that the experimental results are very similar to the results obtained from the TSFE simulation . The rms value of the rated current obtained in both the cases is about 6.8 A and the average value of steady state torque is about 30 Nm.

The harmonic breakdowns of both the experimental voltage, current and torque data are compared with their respective TSFE simulation data in Tables 6-1 through 6-3. Again regarding the fundamental and major low-order harmonic components , there exists a reasonable engineering correlation.

Harmonic order	Magnitude (V)	
	Experimental	TSFE Simulation
Fundamental component 1	649.5	650
2	1.955	0
4	2.238	0
6	2.013	0
8	1.2	0
10	0.67	0
12	0.65	0
14	0.6531	0

Table 6-1: Harmonic breakdown of the experimental versus the TSFE simulation results of the line-to-line voltage for the case study 5hp Induction motor

Harmonic order	Magnitude (A)	
	Experimental	TSFE Simulation
Fundamental component 1	9.3	8.9
2	0.0002504	0
4	0.0001117	0
6	0.0006211	0
8	0.0002762	0
10	0.00000105	0
12	0.0000256	0
14	0.00000002	0

Table 6-2: Harmonic breakdown of the experimental versus the TSFE simulation results of the phase current for the case study 5hp Induction motor.

Harmonic order	Magnitude (Nm)	
	Experimental	TSFE Simulation
Fundamental component 0	30	30
2	0.02	0
4	0.007	0
6	0.1	0
8	0.00036	0
10	0.00253	0
12	0.00087	0
14	0.00006	0

Table 6-3: Harmonic breakdown of the experimental versus the TSFE simulation results of the torque for the case study 5hp Induction motor.

6.3 Comparison Of The Time-Stepping Finite-Element Simulation Results Of The 3-Phase Operation And 6-Phase Opeartion

Here , a comparative analysis between the TSFE simulation results of the operation performance of the 3-phase and 6-phase winding configuration are presented. In Figures 6-8 and 6-9 , the flux plots generated by the TSFE technique are shown for the 3-phase and 6-phase machine designs, respectively.These flux plots were obtained at a time instant t=0.9 sec in the TSFE simulation, at which time the machine has reached steady state operation. It can be observed that these flux plots demonstrate the fact that both the machines have a six-pole arrangement, and the field distribution are almost indistinguishable from each other.

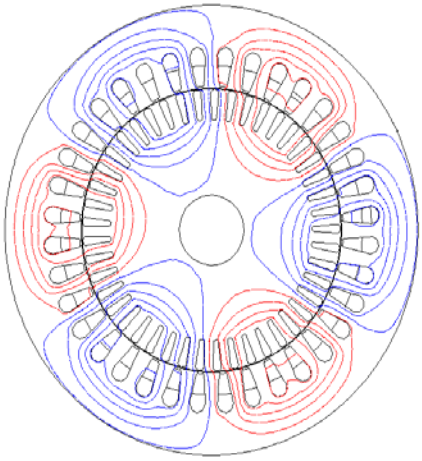

Figure 6-8: Flux plot of the 3-phase machine

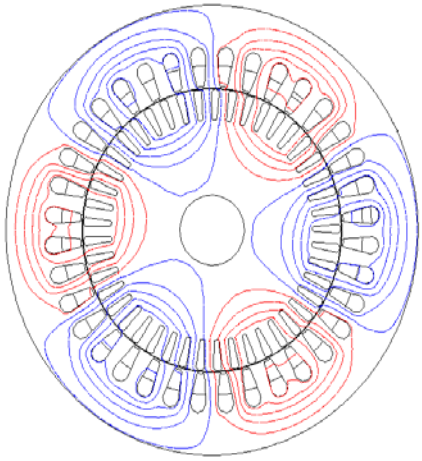

Figure 6-9: Flux plot of the 6-phase machine

Depicted in Figures 6-10 and 6-11 are the comparison of phase voltages under rated conditions of the 3-phase and 6-phase machines, respectively. In Figures 6-12 and 6-13 , the flux-density waveform (profile) at the mid-airgap, are given for the 3-phase and 6-phase machines , respectively .These waveforms were plotted against the mid-airgap circumference of the machine in mm at a time instant t= 0.85 sec. , at which time the machine has reached steady state operation. Further , In Figures 6-14 and 6-15 , the phase currents i_a , i_b and i_c for the 3-phase machine and the phase currents i_a , i_b , i_c , i_d , i_e and i_f for the 6-phase machine are shown. It can be observed that the phase currents in the 3-phase case are phase shifted by 120^0 *e* whereas the phase currents in the 6-phase machine are phase shifted by 60^0 *e* , respectively. The steady-state torque profiles of the 3-phase and 6-phase machines are shown in Figures 6-16 and 6-17, and the steady-state profile of the angular velocity versus time for the 3-phase and 6-phase machines are shown in Figures 6-18 and 6-19 , respectively. Notice that in both the torque and speed profiles of Figures 6-16 through 6-19, the initial transients appearing in these profiles are not natural but numerical in nature , arising from the mismatch between the given initial conditions and the natural steady state forced response of the electromagnetic /electromechanical energy motor-load system.

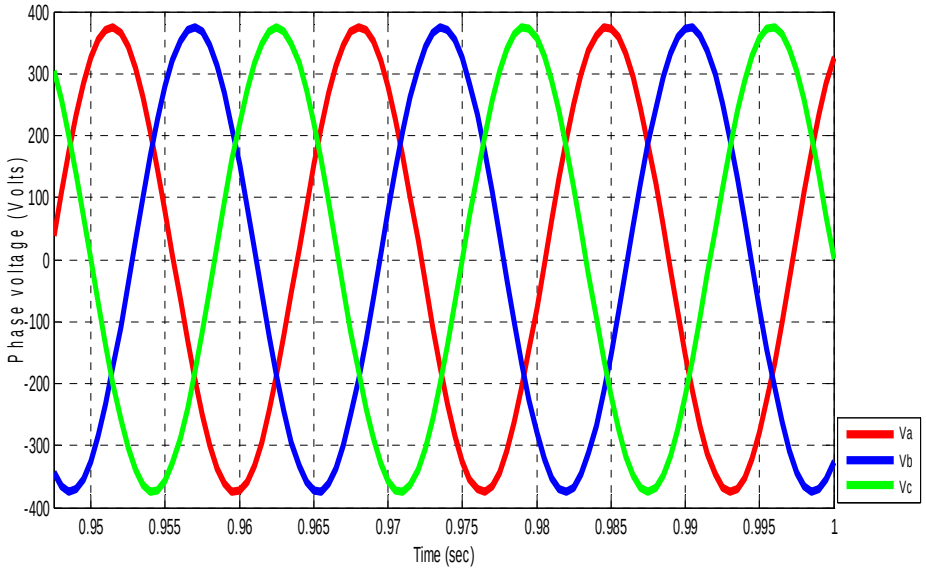

Figure 6-10 : plot of phase voltages in the 3-phase machine

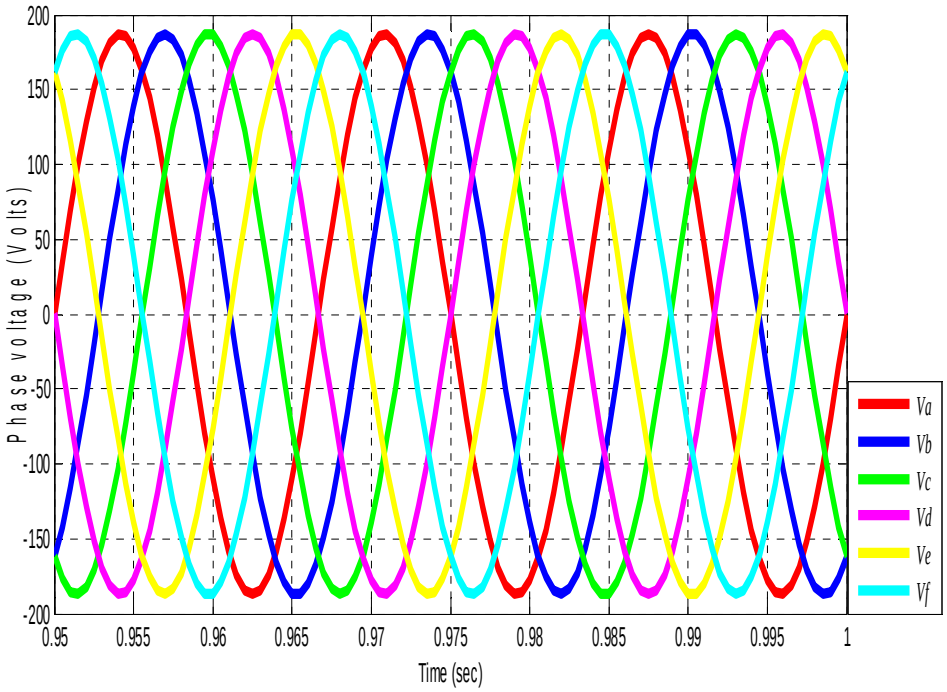

Figure 6-11 : plot of phase voltages in the 6-phase machine

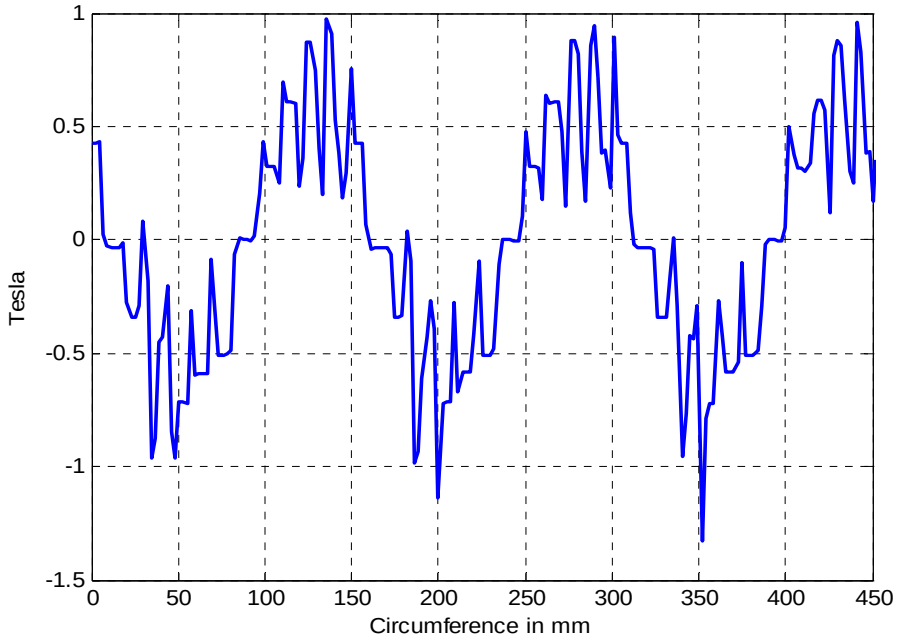

Figure 6-12: Plot of flux-density in the mid-airgap of the 3-phase induction machine from TSFE simulation

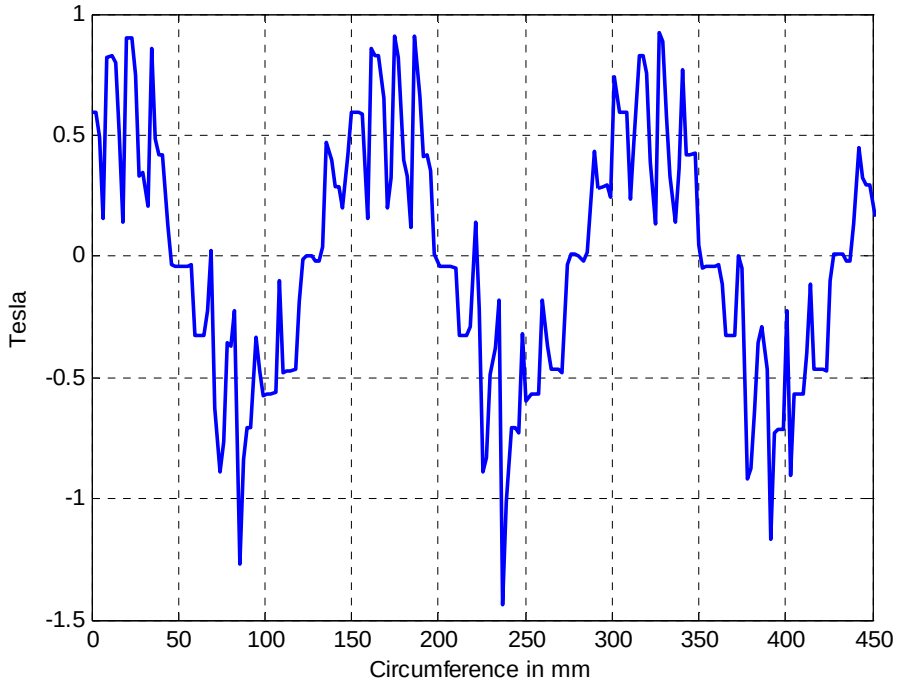

Figure 6-13: Plot of flux-density in the mid-airgap of the 6-phase induction machine from TSFE simulation

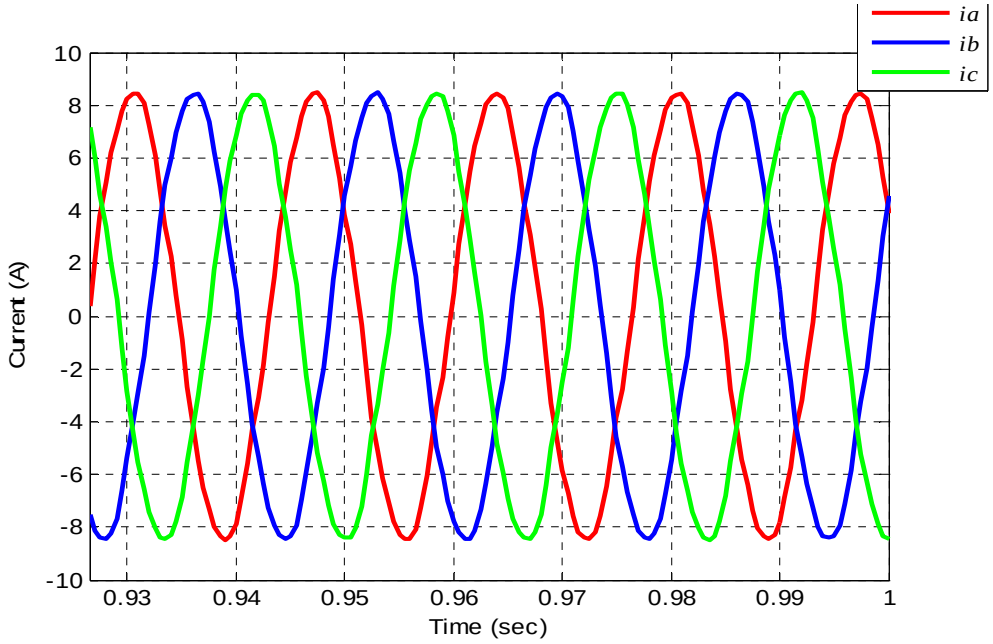

Figure 6-14: Phase currents i_a , i_b and i_c of the 3-phase induction machine from TSFE simulation.

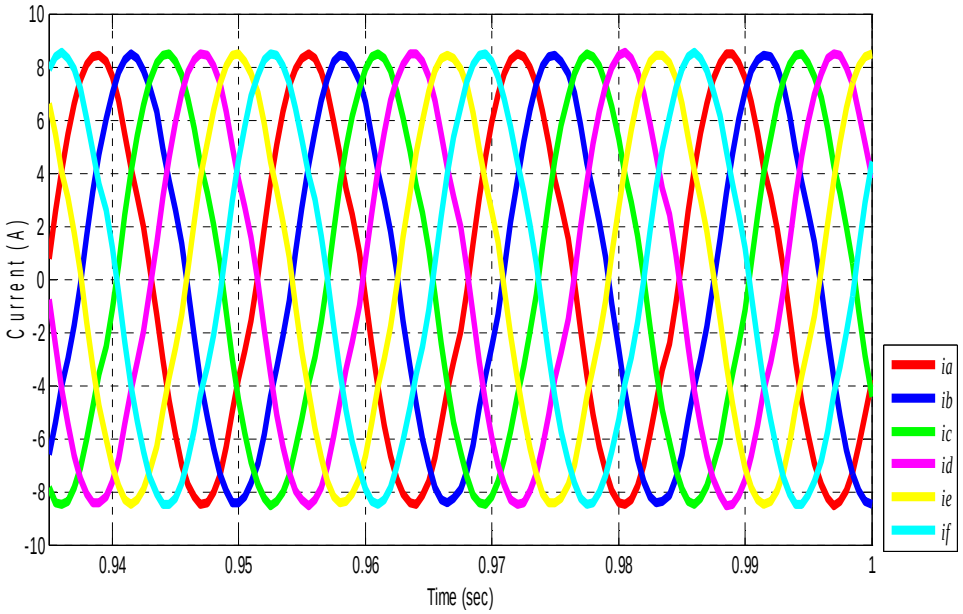

Figure 6-15: Phase currents i_a , i_b , i_c , i_d , i_e and i_f of the 6-phase induction machine from TSFE simulation.

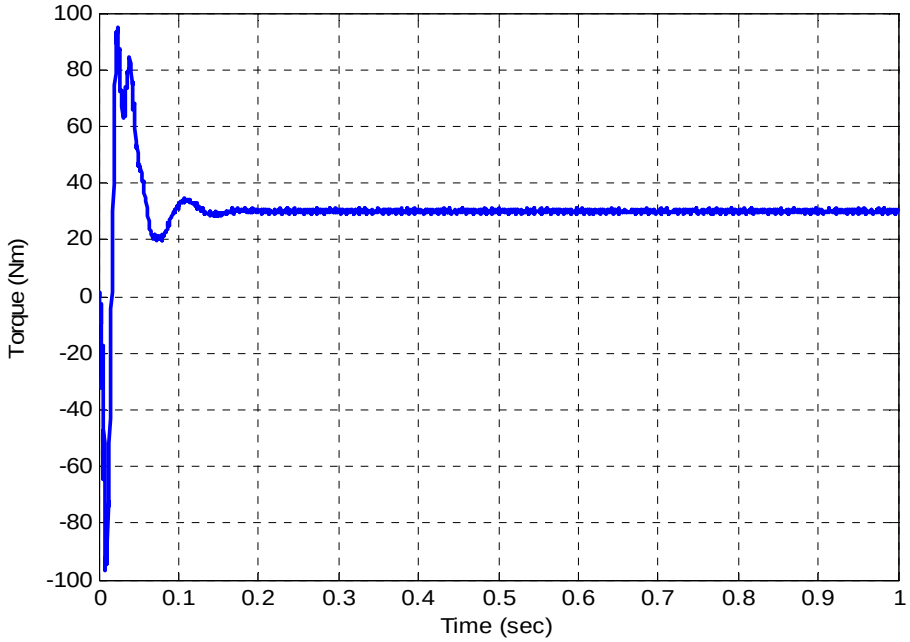

Figure 6-16: Torque profile of 3-phase induction motor under rated conditions from TSFE simulation.

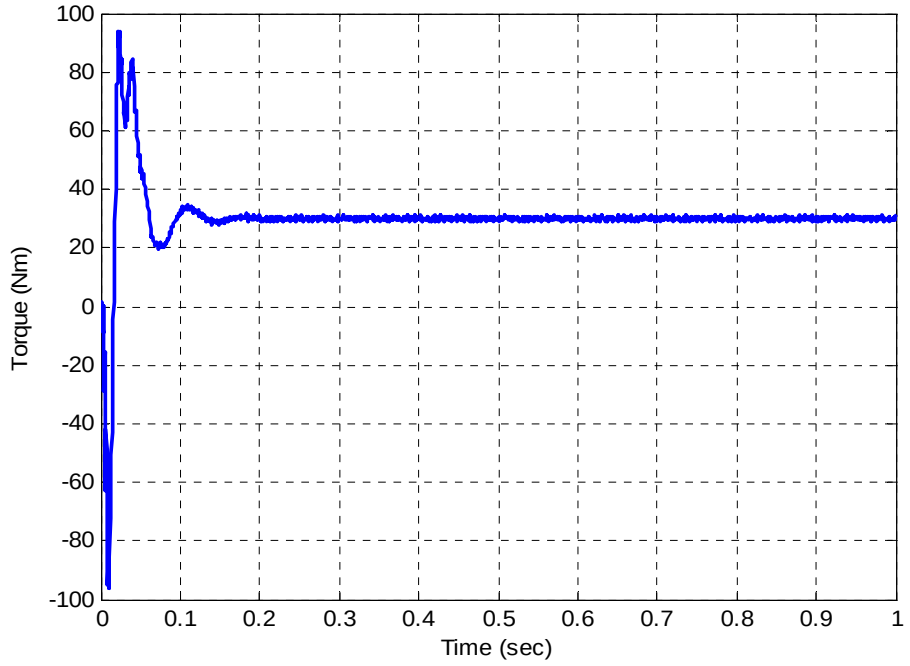

Figure 6-17: Torque profile of 6-phase induction motor under rated conditions from TSFE simulation.

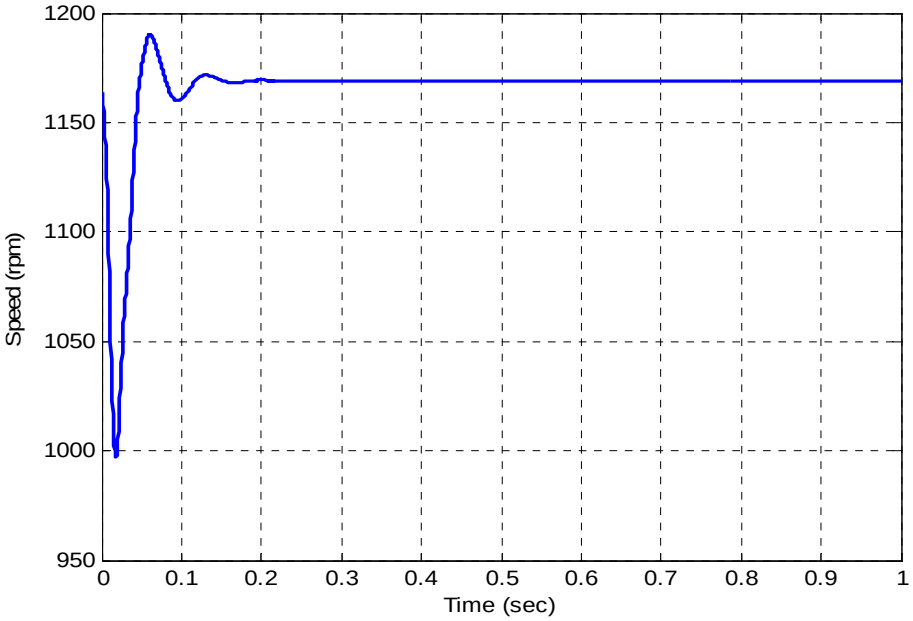

Figure 6-18: Speed profile of 3-phase induction motor under rated conditions from TSFE simulation.

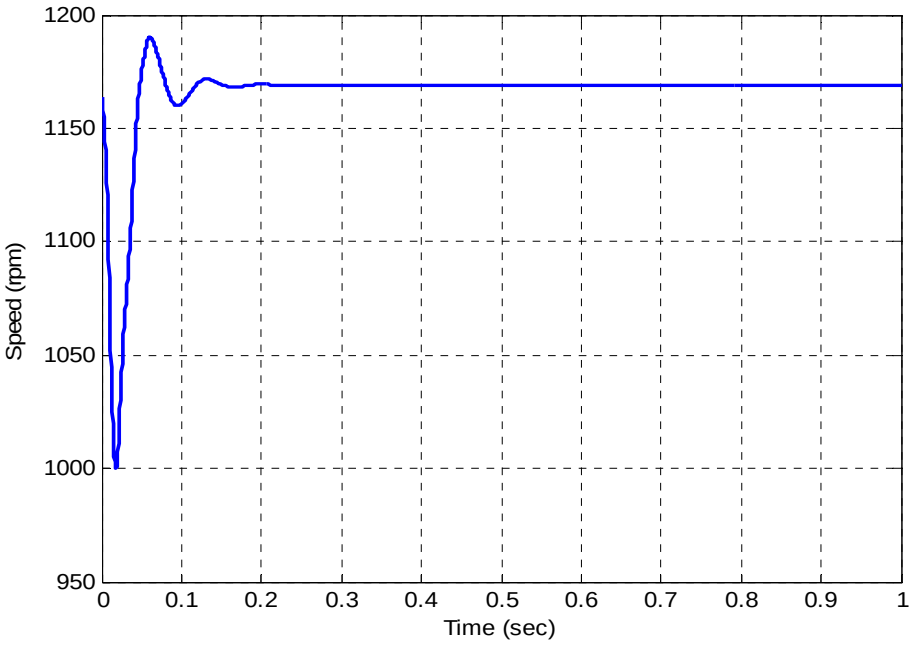

Figure 6-19: Speed profile of 6-phase induction motor under rated conditions from TSFE simulation.

6.4 SIMULATION OF THE SIX-PHASE INDUCTION MOTOR UNDER VARIOUS PHASE LOSS SCENARIOS

As depicted in Figure 6-1 , the phase loss scenarios studied in this work are , 5-phase operation where there is a loss of one phase , 4-phase operation where there is a loss of two phases and 3-phase operation where there is a loss of three phases. Furthermore, the 4-phase and 3-phase operations, in which two or three phases have been taken out of service, were studied under conditions where there is a loss of adjacent phases that is a loss of phases which are located adjacent to each other or alternately a loss of two or more phases which are non-adjacent to each other, that is the loss of phases separated by one or two other healthy phases were also studied in this work.

6.4.1 5-HEALTHY PHASE AND ONE FAULTY PHASE OPERATION

Here ,the six-phase motor is TSFE- simulated with the loss of phase A .Figures 6-20 and 6-21 show the phasor representation of voltages in the six-phase healthy case and the five-phase healthy and one faulty phase case, under the loss of phase A. In Figures 6-22 and 6-23 , the torque profiles of the faulty case with 5 healthy phases should be compared with the 6-phase healthy case. These figures are accompanied by a magnified (zoom) , portion of the steady-state torque profiles, in order to obtain a better sense of the consequences of the loss of one phase on the torque-ripple content in the resulting time-domain torque profile. In Figures 6-24 and 6-25 , the Harmonic breakdown of the steady state torque profile for the 6-phase healthy case and the faulty case with 5 healthy phases are shown. Notice that the 2^{nd} order harmonic is more pronounced in the faulty case with 5 healthy phases with a magnitude of 2.776 Nm when compared to the healthy case for which the 2^{nd} order harmonic has a magnitude of 0.1345 Nm .

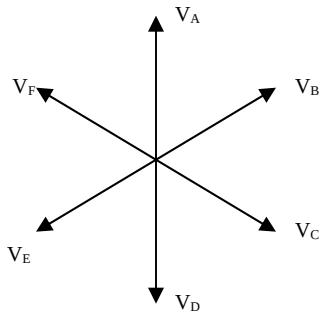

Figure 6-20 : Phasor representation of the voltages in six-phase healthy operation

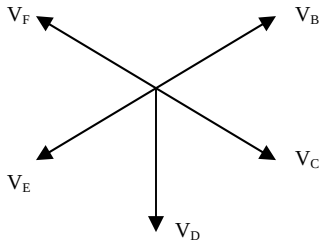

Figure 6-21 : Phasor representation of the voltages in the five-phase operation with loss of Phase A

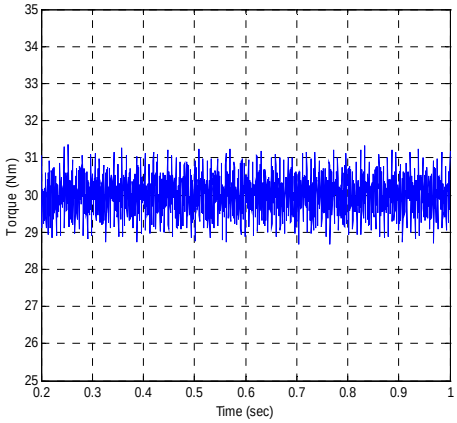

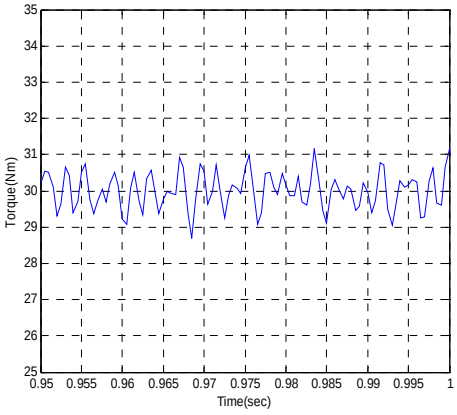

Figure 6.22 : Torque profile of the healthy 6-phase case under full-load

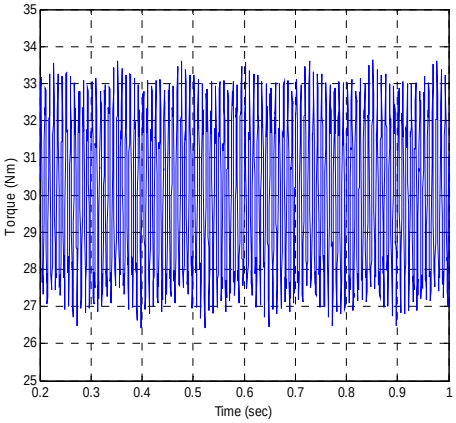

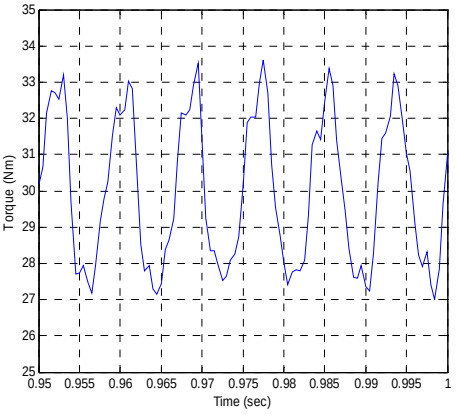

Figure 6.23:Torque profile of the 5-healthy phase case with loss of phase A

RIPPLE CONTENT: 6.67 %

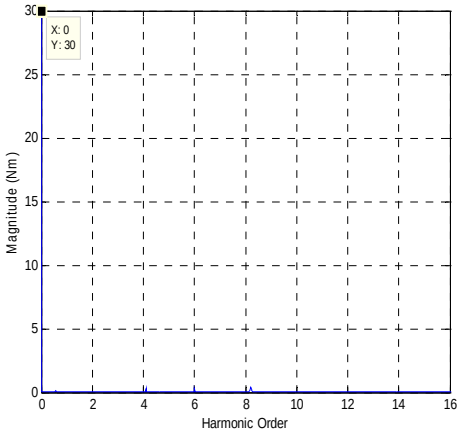

Figure 6.24:Harmonic spectrum of the torque profile of the healthy 6-phase case

RIPPLE CONTENT: 18.33 %

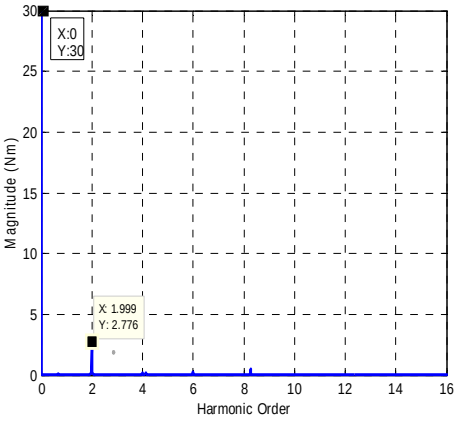

Figure 6.25:Harmonic spectrum of the torque profile of the 5-healthy phase case with loss of phase A

Figure 6-26 and 6-27 shows the phase currents in the 5-healthy phase and one faulty phase with loss of phases A and the healthy six-phase operations.

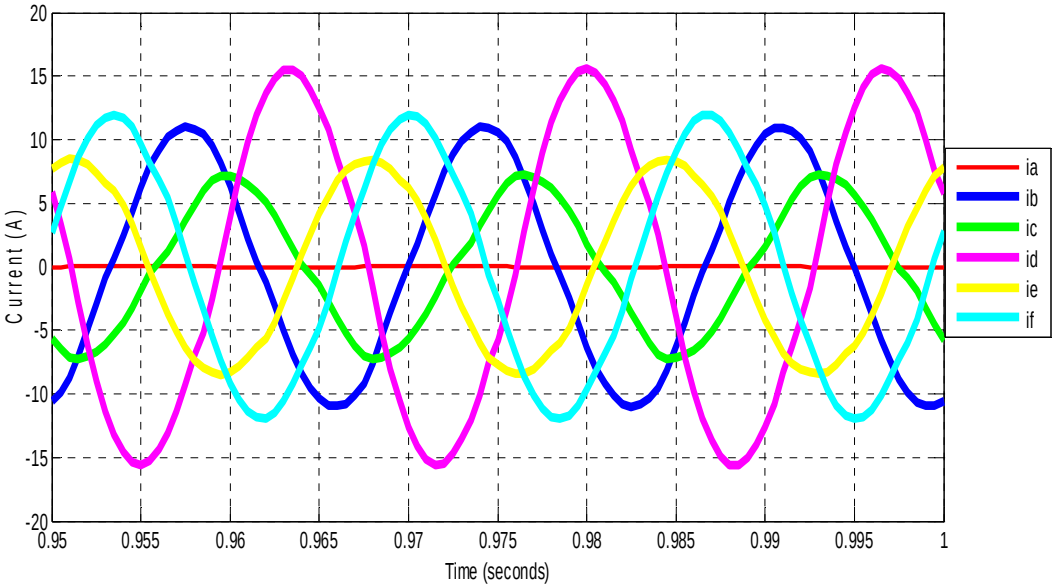

Figure 6-26 : Phase currents i_a , i_b , i_c , i_d , i_e and i_f of the 5-healthy and one faulty phase operation of the six-phase induction motor.

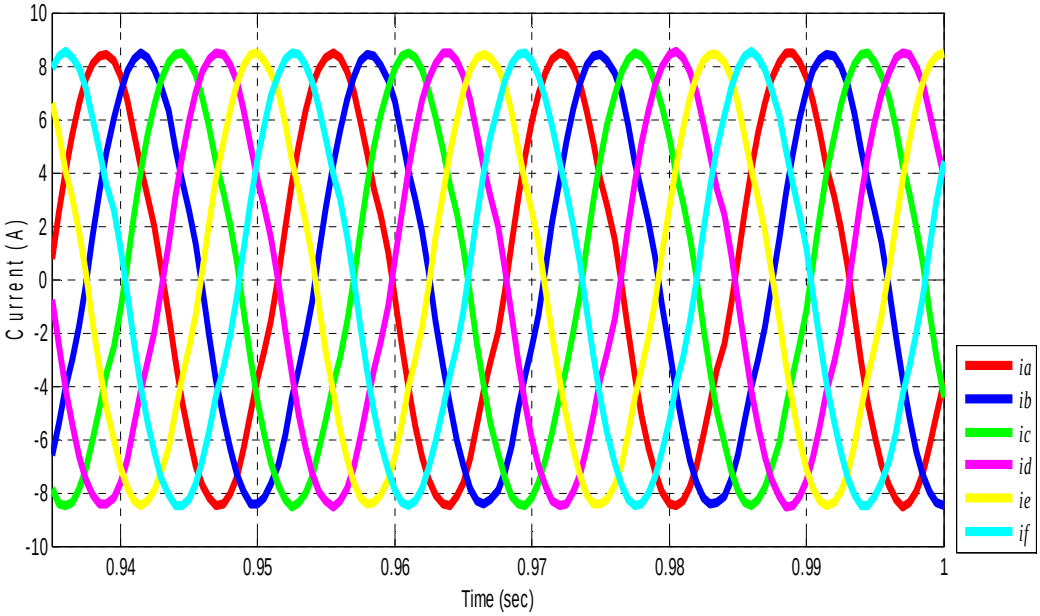

Figure 6-27 : Phase currents i_a , i_b , i_c , i_d , i_e and i_f of the healthy six-phase induction motor.

From the above analysis , the torque ripple content in the resulting torque is 18.33% with the 5-healthy phases and one faulty phase case, in comparison with 6.67% torque ripple content in the healthy six-phase case.

6.4.2 THE FOUR HEALTHY PHASE – TWO FAULTY PHASE OPERATION

As mentioned earlier , here two cases are considered ,One case is the loss of two adjacent phases and the other case is the loss of two non-adjacent phases. Figure 6-28 summarizes the four-healthy phase and two faulty phase operations which are considered in this thesis.

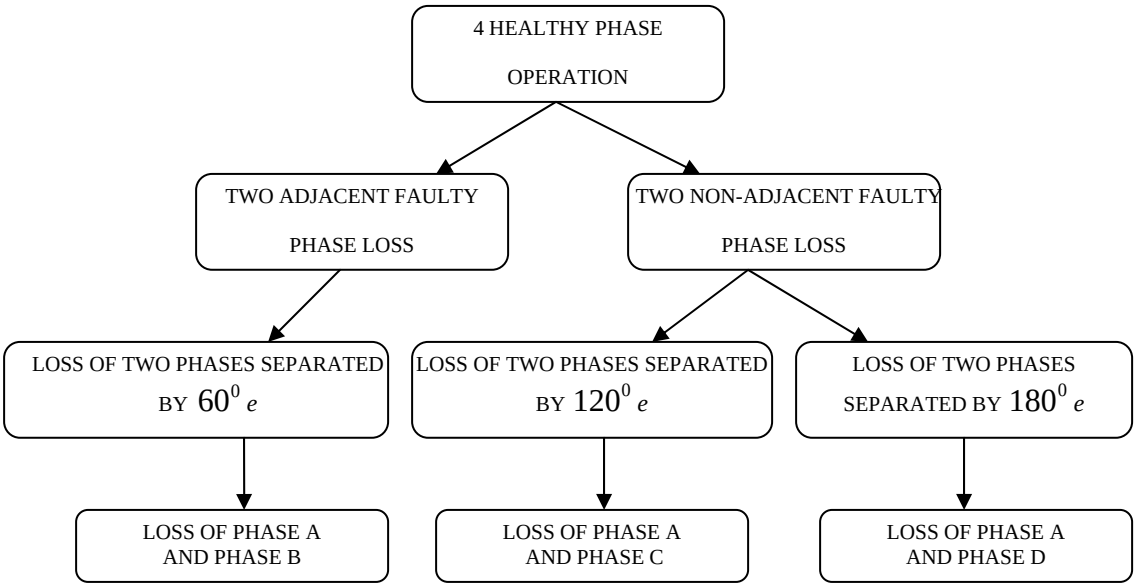

Figure 6-28: Flow chart summarizing the various cases of 4-phase operations studied.

6.4.2.1 LOSS OF TWO ADJACENT PHASES

In this case , the six-phase motor is simulated under loss of two adjacent phases ,namely Phase A and Phase B . Figures 6-29 and 6-30 show the phasor representation of voltages in the six-phase healthy case and the four-healthy phase faulty two-phase case under loss of phase

A and phase B. In Figures 6-31 and 6-32 , the torque profiles of the 4-healthy phase and two-faulty phase case is compared with the six-healthy phase case. These figures are accompanied by a magnified (zoom) portion of the steady-state torque profile. In Figures 6-33 and 6-34 , the Harmonic breakdown of the steady state torque profile for the 6-phase healthy case and the faulty case with 4 healthy phases are two faulty phases which are adjacent to each other are shown. Notice that the 2^{nd} order harmonic is more pronounced in the faulty case with 4 healthy phases and two faulty phases adjacent to each other with a magnitude of 6.984 Nm when compared to the healthy case for which the 2^{nd} order harmonic has a magnitude of 0.1345 Nm .

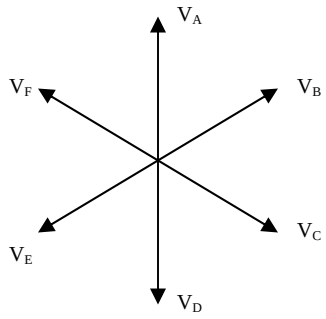

Figure 6-29 : Phasor representation of the voltages in six-phase healthy operation

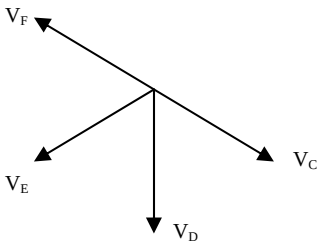

Figure 6-30 : Phasor representation of the voltages in the four-healthy phase operation with loss of adjacent phases A and B

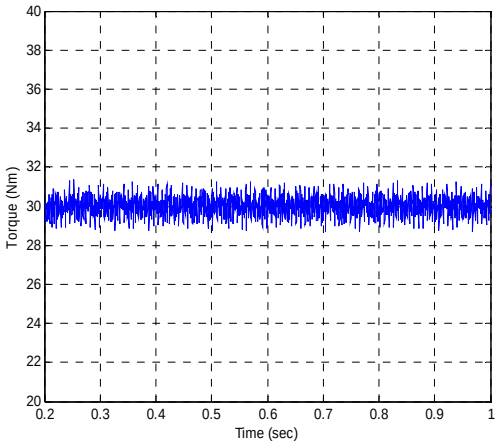

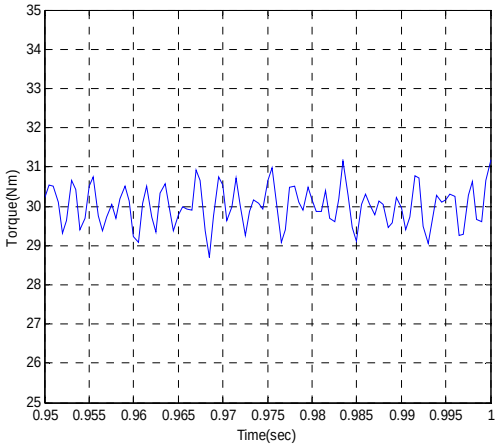

Figure 6.31 : Torque profile of the healthy 6-phase case under full-load
RIPPLE CONTENT: 6.67%

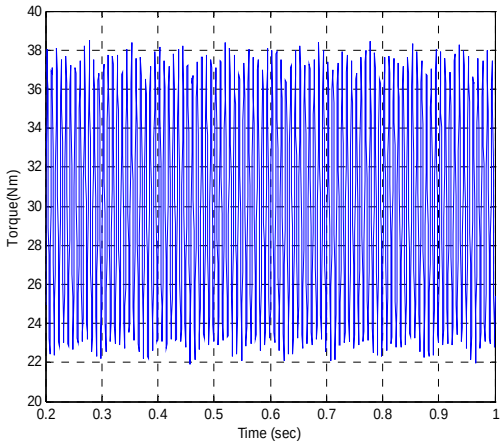

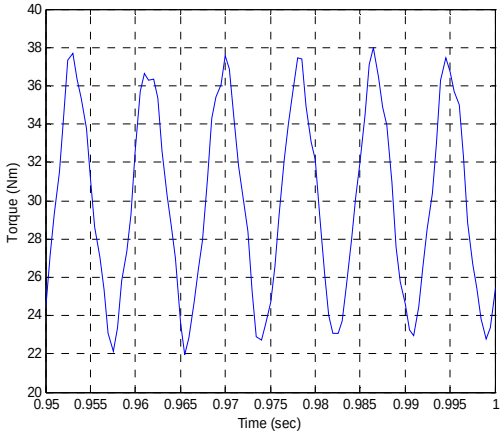

Figure 6.32:Torque profile of the 4-healthy phase case with loss two adjacent phases A and B
RIPPLE CONTENT: 49.667 %

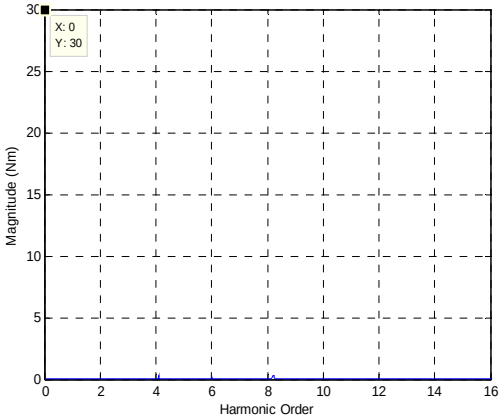

Figure 6.33:Harmonic spectrum of the torque profile of the healthy 6-phase case

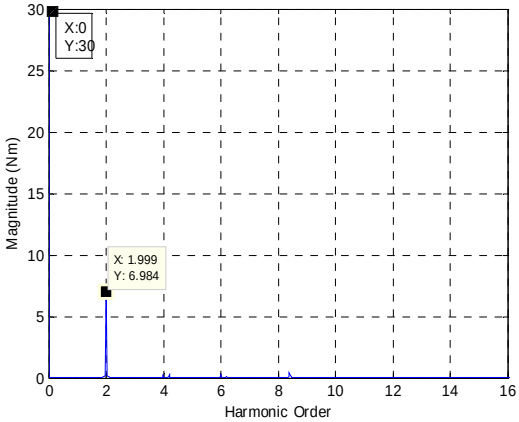

Figure 6.34::Harmonic spectrum of the torque profile of the 4-healthy phase case with loss of adjacent phases A and B

Figure 6-35 and 6-36 shows the phase currents in the 4-healthy phase and two faulty phase with loss of phases A and B and the healthy six-phase operations.

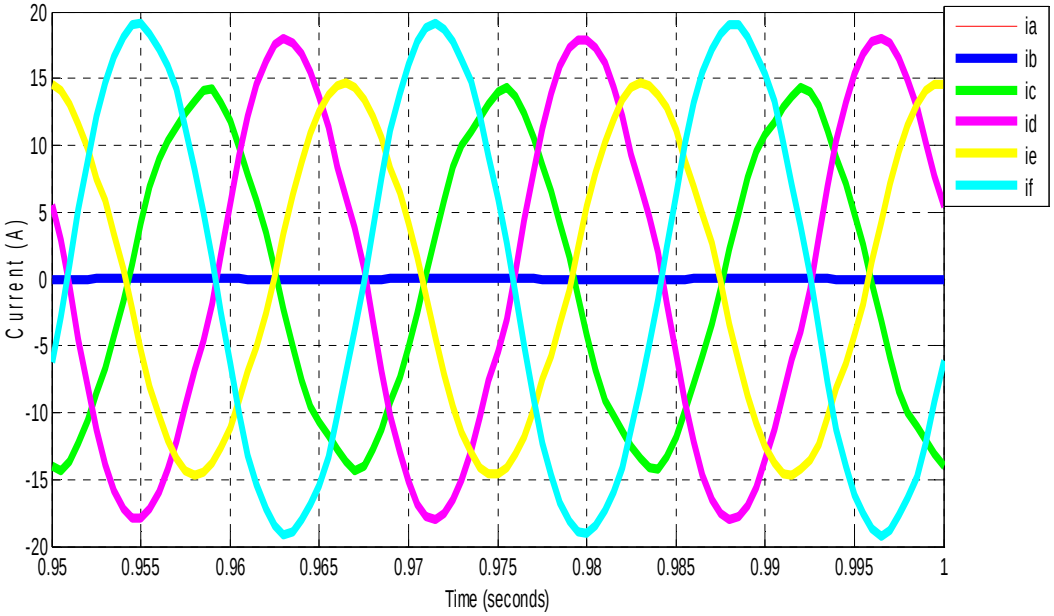

Figure 6-35 : Phase currents i_a , i_b , i_c , i_d , i_e and i_f of the 4-healthy and two faulty phase operation of the six-phase induction motor with loss of adjacent phases A and B

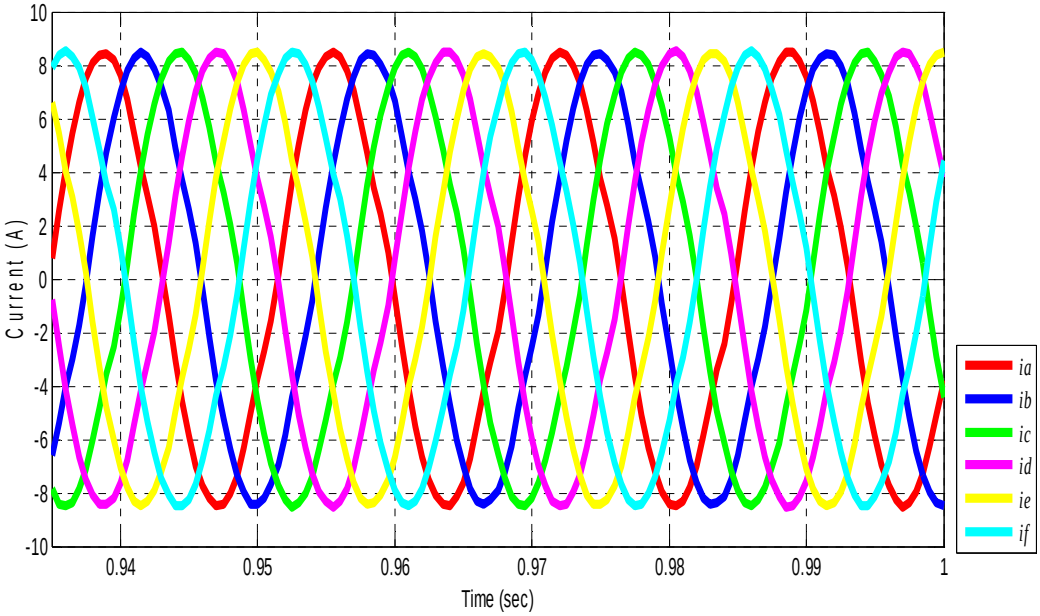

Figure 6-36: Phase currents i_a , i_b , i_c , i_d , i_e and i_f of the healthy six-phase induction motor.

From the above analysis , the torque ripple content in the resulting torque is 49.667 % with the 4-healthy phases and two faulty phase adjacent to each other , in comparison with 6.67% torque ripple content in the healthy six-phase case. This is significant , and some applications may constitute an unacceptable performance.

6.4.2.2 LOSS OF TWO NON-ADJACENT PHASES

Here , the two non-adjacent faulty phase cases shown in Figure 6-28 are considered , In the first case , the six-phase motor is simulated under loss of two non-adjacent phases separated by 120^0 e , i.e. , loss of phase A and phase C are considered. Figures 6-37 and 6-38 show the phasor representation of the voltages in the six-phase healthy case and the four-healthy phase faulty two-phase case such as under loss of phase A and phase C. In Figures 6-39 and 6-40 , the torque profile of the 4-healthy phase with two faulty phases separated by 120^0 should be compared with the 6-phase healthy case. These figures are accompanied by a magnified (zoom) portion of the steady-state torque profile. In Figures 6-41 and 6-42 , the Harmonic breakdown of the steady state torque profile for the 6-phase healthy case and the faulty case with 4 healthy phases are two faulty phases separated by 120^0 are shown. Notice that the 2^{nd} order harmonic is in the faulty case with 4 healthy phases and two non-adjacent faulty phases separated by 120^0 has a magnitude of 0.8318 when compared to the healthy case for which the 2^{nd} order harmonic has a magnitude of 0.1345 . Here the magnitudes of the 2^{nd} order harmonics in both the cases are almost equal to each other.

In the second case, the six-phase motor is simulated under loss of two non-adjacent phases separated by 180^0 e , i.e. , the loss of phase A and phase D are considered. Figures 6-45 and 6-46 show the phasor representation of voltages in the six-phase healthy case and the four-phase healthy case with two non-adjacent faulty phases separated by 180^0 e under loss of phase A and phase D. In Figures 6-47 and 6-48 , the torque profile of the four-phase healthy case with two

non-adjacent faulty phases separated by 180^0 *e* should be compared with the 6-phase healthy case. Again, these figures are accompanied by a magnified (zoom) portion of the steady-state torque profile. In Figures 6-49 and 6-50 , the Harmonic breakdown of the steady state torque profile for the 6-phase healthy case and the faulty case with 4 healthy phases are two faulty phases separated by 180^0 are shown.Notice that the 2^{nd} order harmonic is more pronounced in the faulty case with 4 healthy phases and two non-adjacent faulty phases separated by 180^0 *e* than in the case with 4 healthy phases and two non-adjacent faulty phases separated by 120^0 *e* with a magnitude of 16.06 Nm when compared to the healthy case for which the 2^{nd} order harmonic has a magnitude of 0.1345 Nm .

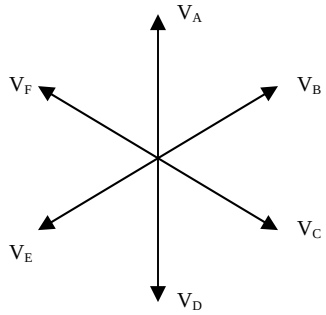

Figure 6-37 : Phasor representation of the voltages in six-phase healthy operation

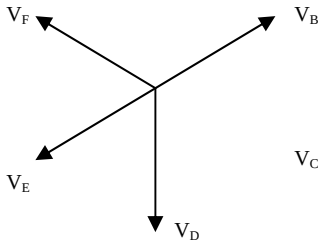

Figure 6-38 : Phasor representation of the voltages in the four-healthy phases with two non-adjacent faulty phase separated by 120^0 *e* operation with loss of phases A and C

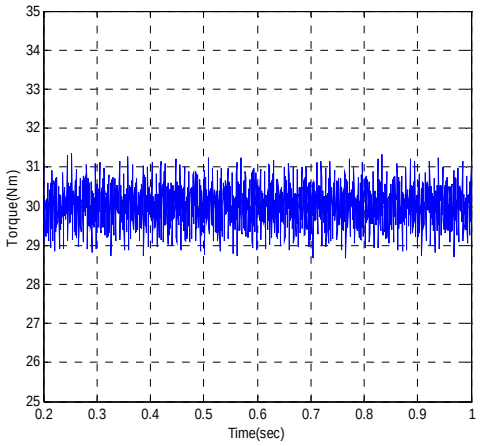

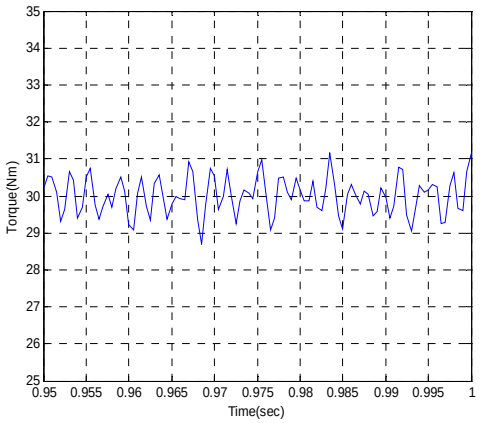

Figure 6.39 : Torque profile of the healthy 6-phase case under full-load
RIPPLE CONTENT: 6.67 %

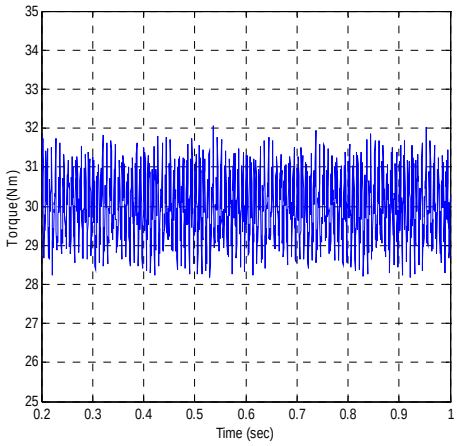

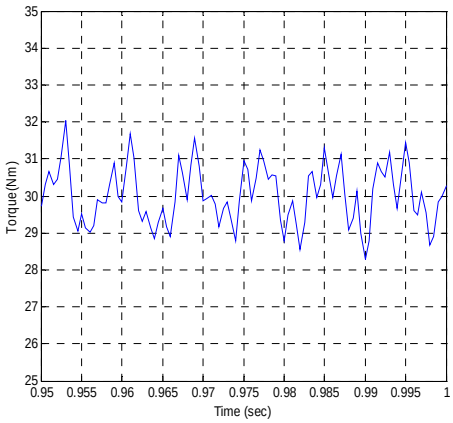

Figure 6.40: Torque profile of the 4-healthy phase case with loss two non-adjacent phases separated by 120^0 *e* i.e. phases A and C
RIPPLE CONTENT: 10.33%

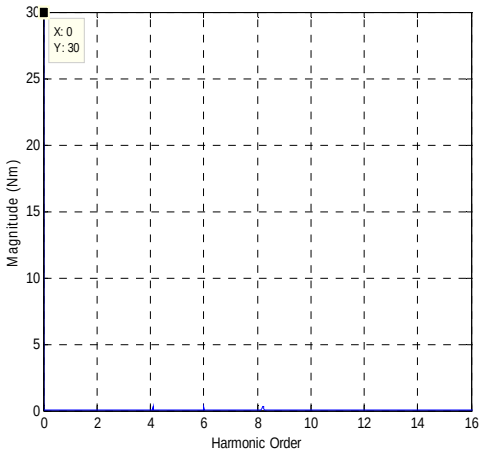

Figure 6.41:Harmonic spectrum of the torque profile of the healthy 6-phase case

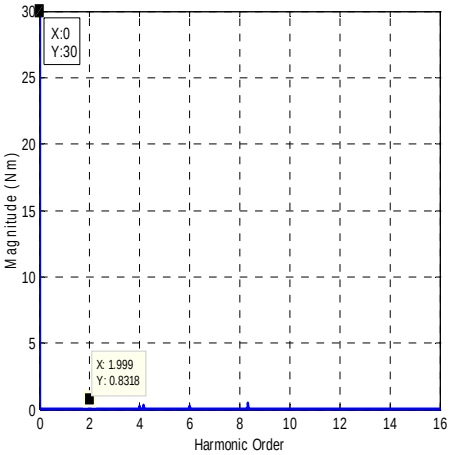

Figure 6.42::Harmonic spectrum of the torque profile of the 4-healthy phase case with loss of non-adjacent phases A and C

Figure 6-43 and 6-44 shows the phase currents in the 4-healthy phase and two faulty phase with loss of phases A and C and the healthy six-phase operations.

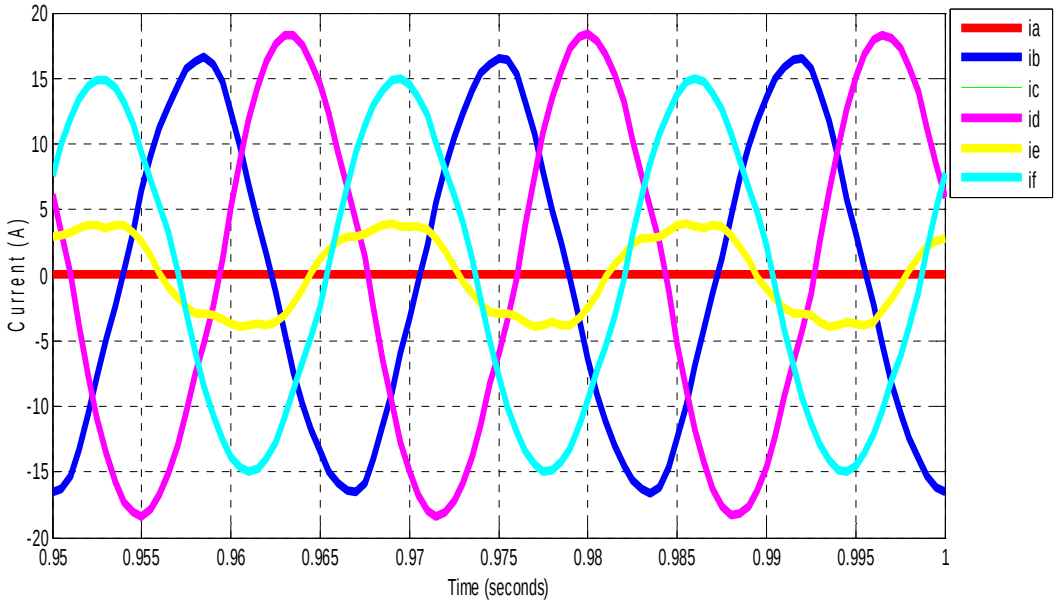

Figure 6-43: Phase currents i_a , i_b , i_c , i_d , i_e and i_f of the 4-healthy and two faulty phase operation of the six-phase induction motor with loss of non-adjacent phases A and C

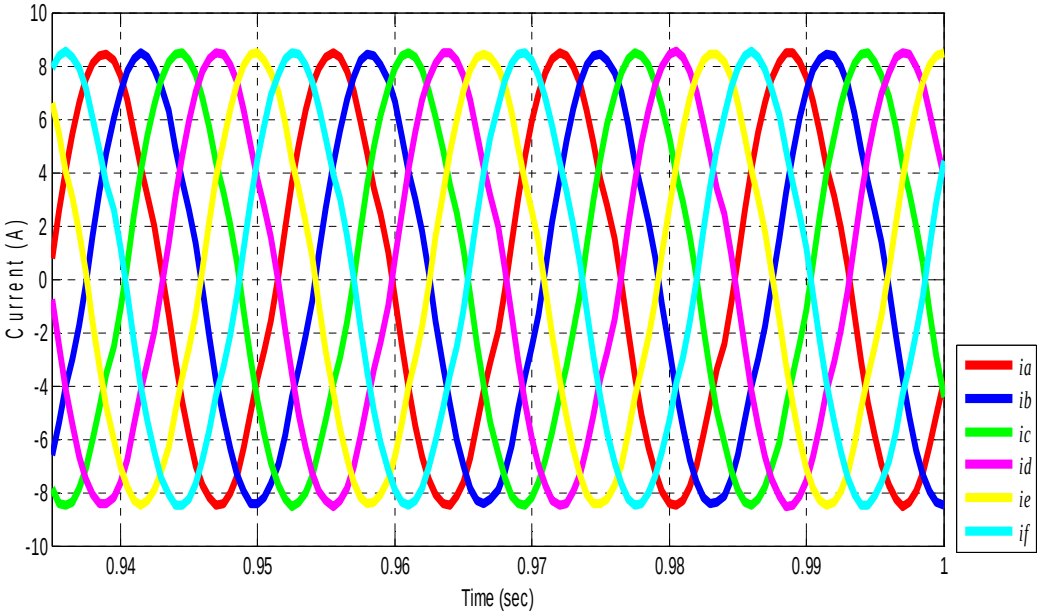

Figure 6-44 : Phase currents i_a , i_b , i_c , i_d , i_e and i_f of the healthy six-phase induction motor.

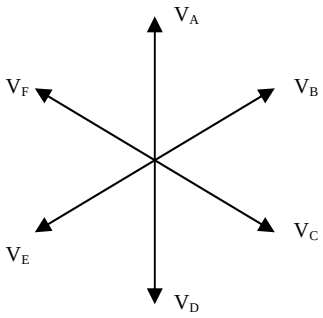

Figure 6-45 : Phasor representation of the voltages in six-phase healthy operation

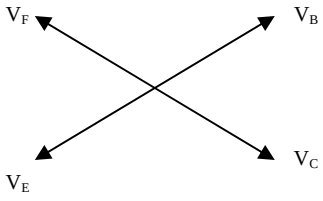

Figure 6-46 : Phasor representation of the voltages in the four-healthy phase with two non-adjacent faulty phase separated by $180^0\ e$ operation with loss of phases A and D

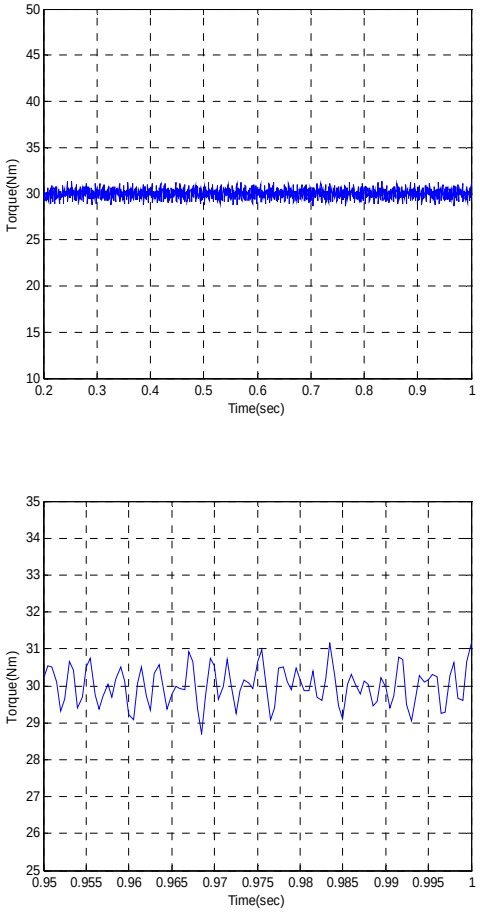

Figure 6.47 : Torque profile of the healthy 6-phase case under full-load

RIPPLE CONTENT: 6.67%

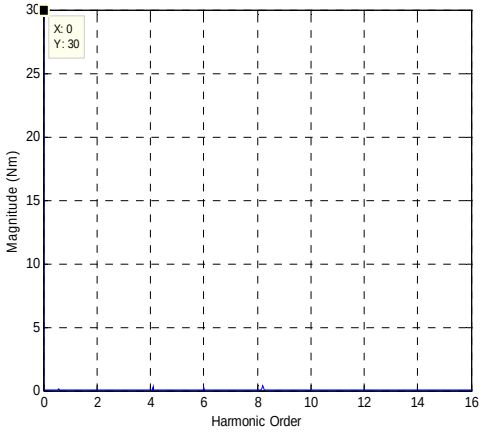

Figure 6.49:Harmonic spectrum of the torque profile of the healthy 6-phase case

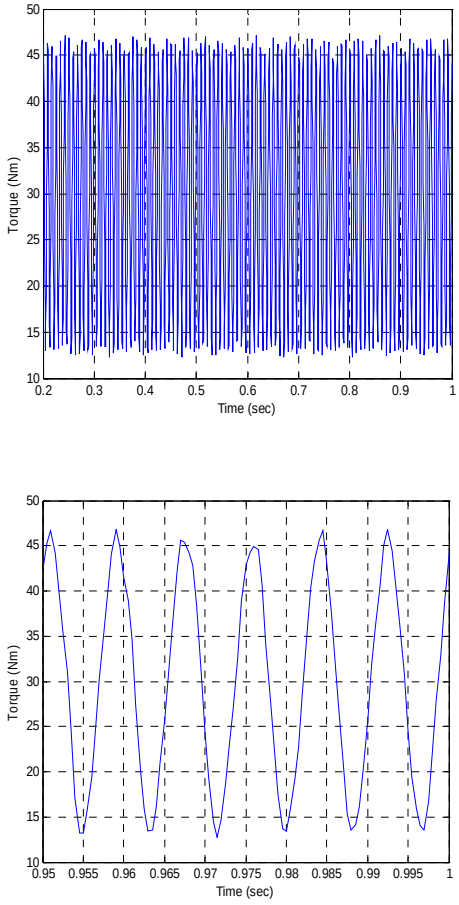

Figure 6.48:Torque profile of the 4-healthy phase case with loss two non-adjacent phases separated by 180^0 *e* i.e. phases A and D

RIPPLE CONTENT: 111%

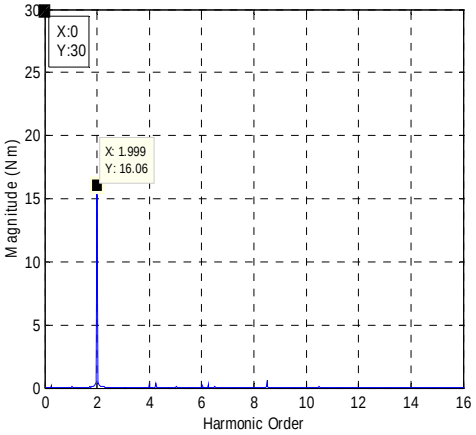

Figure 6.50::Harmonic spectrum of the torque profile of the 4-healthy phase case with loss of non-adjacent phases A and D

Figure 6-51 and 6-52 shows the phase currents in the 4-healthy phase and two faulty phase with loss of phases A and D and the healthy six-phase operations.

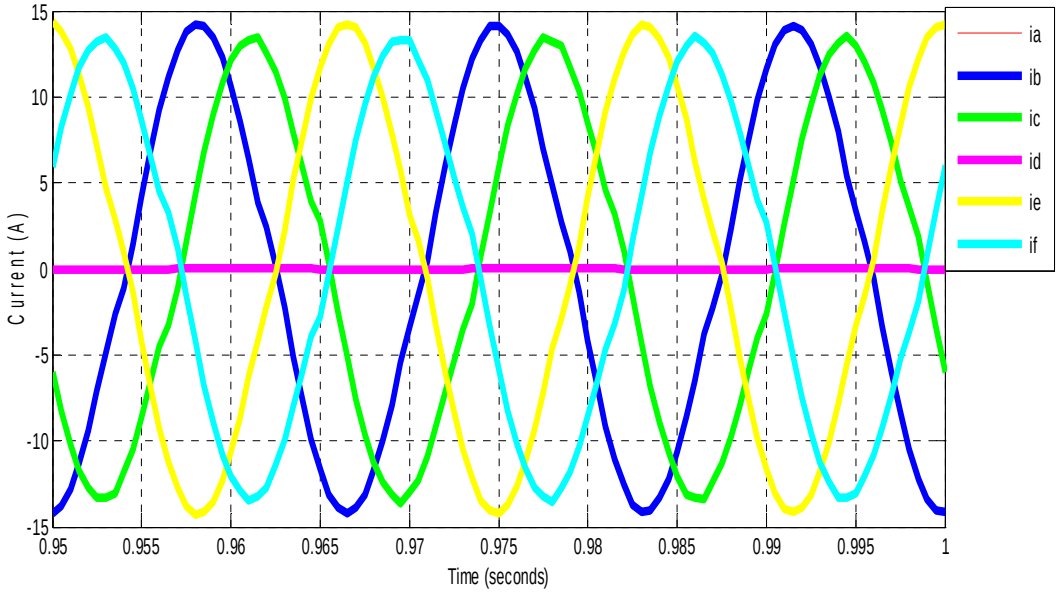

Figure 6-51: Phase currents i_a , i_b , i_c , i_d , i_e and i_f of the 4-healthy and two faulty phase operation of the six-phase induction motor with loss of non-adjacent phases A and D

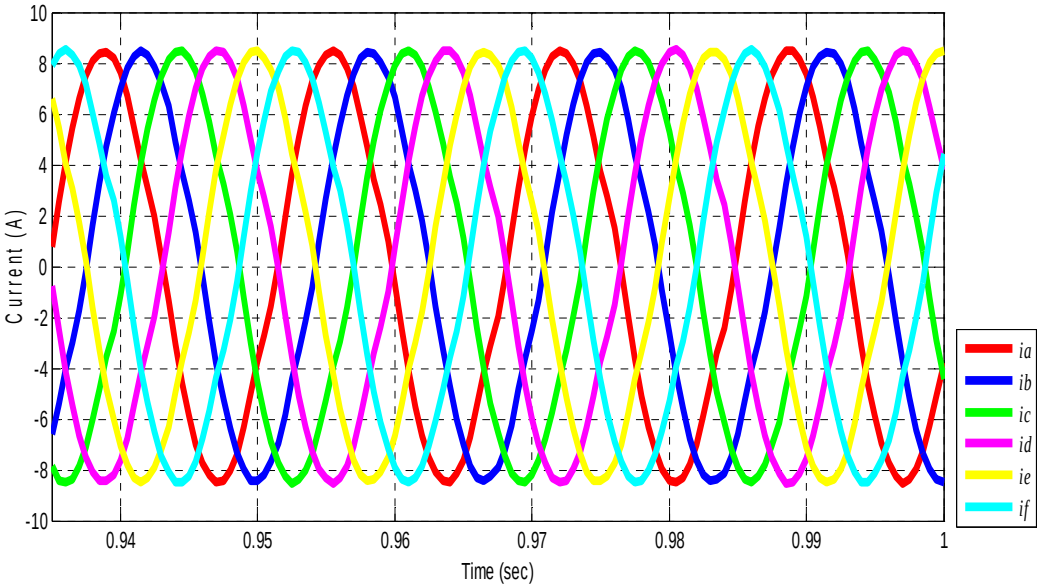

Figure 6-52 : Phase currents i_a , i_b , i_c , i_d , i_e and i_f of the healthy six-phase induction motor.

From the above analysis , the torque ripple content in the resulting torque is 10.33 % with the 4-healthy phases and two non-adjacent faulty phase separated by 120^0 e, in comparison with 6.67% torque ripple content in the healthy six-phase case whereas , the torque ripple content in the 4-healthy phases and two non-adjacent faulty phase separated by 180^0 e is 111% in comparison with 6.67% torque ripple content in the healthy six-phase case. It should be observed that for the two non-adjacent faulty phase cases there is a marked difference between the 120^0 e separation and the 180^0 e separation cases in so far as the adverse effect on the ripple content in the time-domain torque profile. The 120^0 e separation is far less severe.

A quasi-quantitative explanation of the deterioration of the quality of the torque profile using current space vector concepts is presented later-on in this chapter.

6.4.3 THE THREE-HEALTHY PHASE AND THREE FAULTY PHASE OPERATION

As in the 4-healthy phase and two faulty phase operation , here also , there are two possible cases , Namely this is when there is loss of three adjacent phases each separated by 60^0 e , and when there is loss of three non-adjacent phases each separated by 120^0 e . Figure 6-53 summarizes the phase loss scenarios of the three-healthy phase and three faulty phase operations studied in this thesis.

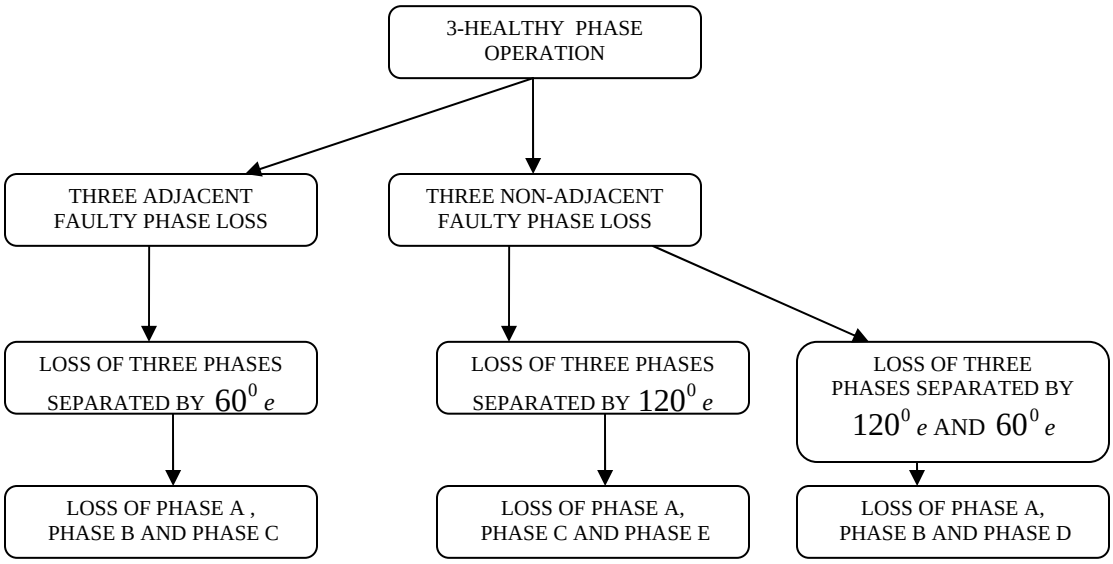

Figure 6-53: Flow chart summarizing the various cases of 3-phase operations studied.

6.4.3.1 LOSS OF THREE ADJACENT PHASES

Here , the six-phase motor is simulated under loss of three phases adjacent to each other such as when phase A , phase B and phase C become faulty and are taken out of operation. Figures 6-54 and 6-55 show the phasor representation of voltages in the six-phase healthy case and the three-healthy phase and three adjacent faulty phase case under loss of phase A , phase B and phase C. In Figures 6-56 and 6-57, the torque profile of the three-healthy phase and three adjacent faulty phase case should be compared with the 6-phase healthy case. These figures are accompanied by a magnified (zoom) portion of the steady-state torque profile. In Figures 6-58 and 6-59 , the Harmonic breakdown of the steady state torque profile for the 6-phase healthy case and the faulty case with three healthy phases are three faulty phases which are adjacent to each other are shown. Notice that the 2^{nd} order harmonic is more pronounced in the faulty case with 3 healthy phases and three faulty phases adjacent to each other with a magnitude of 26.45 Nm when compared to the healthy case for which the 2^{nd} order harmonic has a magnitude of 0.1345 Nm .

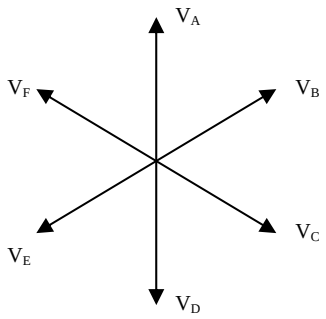

Figure 6-54 : Phasor representation of the voltages in six-phase healthy operation

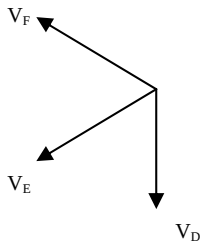

Figure 6-55 : Phasor representation of the voltages in the three healthy phase with three adjacent faulty phase loss operation with loss of phases A, B and C

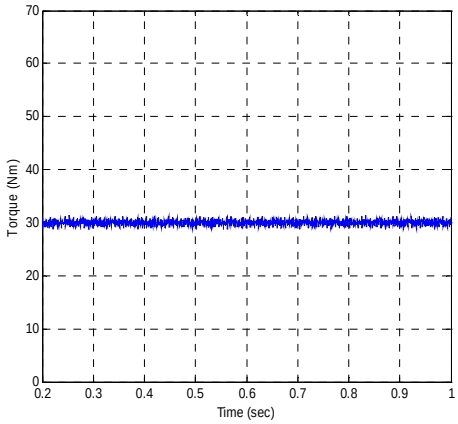

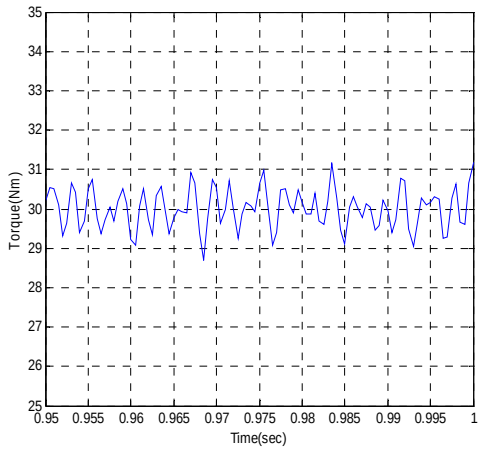

Figure 6.56 : Torque profile of the healthy 6-phase case under full-load
RIPPLE CONTENT: 6.67%

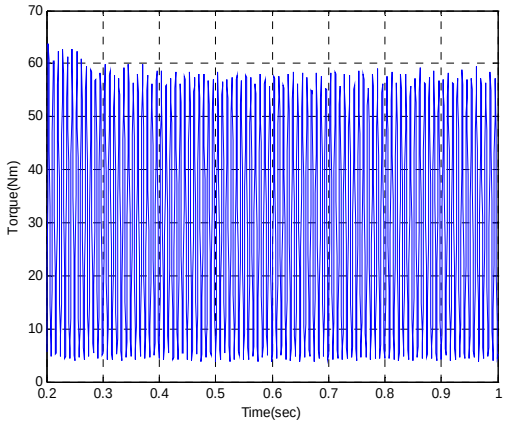

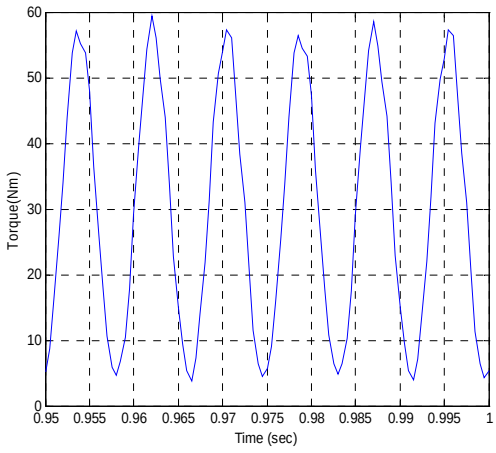

Figure 6.57:Torque profile of the 3-healthy phase case with loss three adjacent phases separated by 60^0 *e* i.e. phases A , B and C
RIPPLE CONTENT: 178%

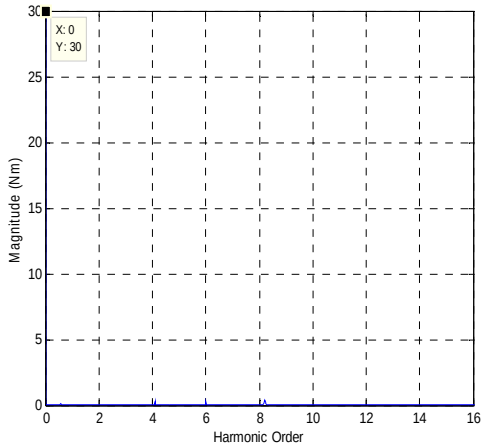

Figure 6.58::Harmonic spectrum of the torque profile of the healthy 6-phase case

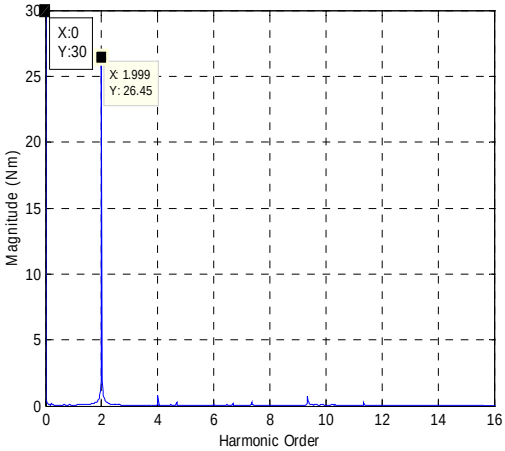

Figure 6.59::Harmonic spectrum of the torque profile of the 3-healthy phase case with loss of three djacent phases A,B and C

Figure 6-60 and 6-61 shows the phase currents in the 3-healthy phase and three faulty phase with loss of phases A,B and C and the healthy six-phase operations.

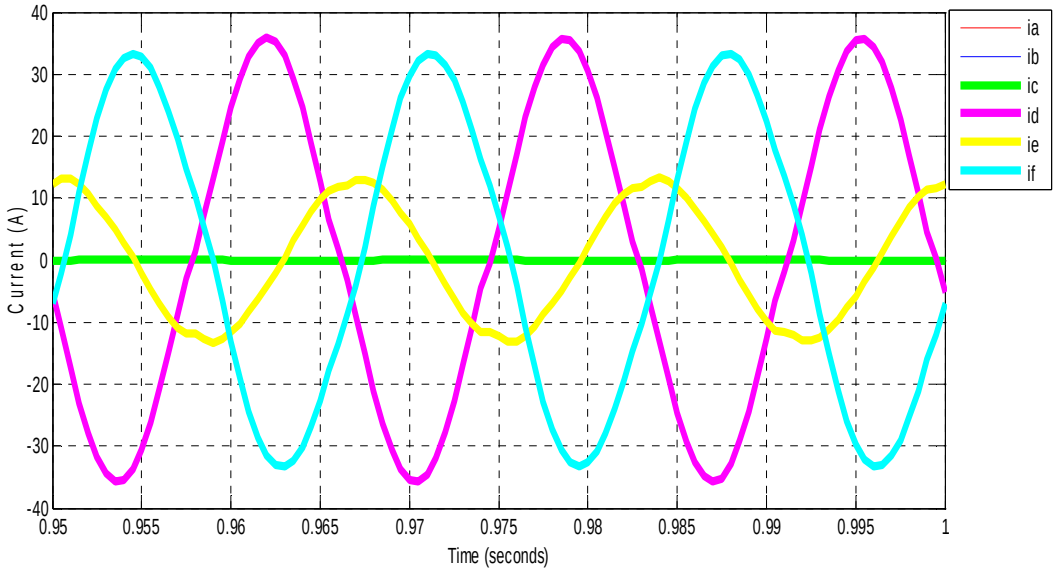

Figure 6-60: Phase currents i_a , i_b , i_c , i_d , i_e and i_f of the 3-healthy and three faulty phase operation of the six-phase induction motor with loss of adjacent phases A , B and C

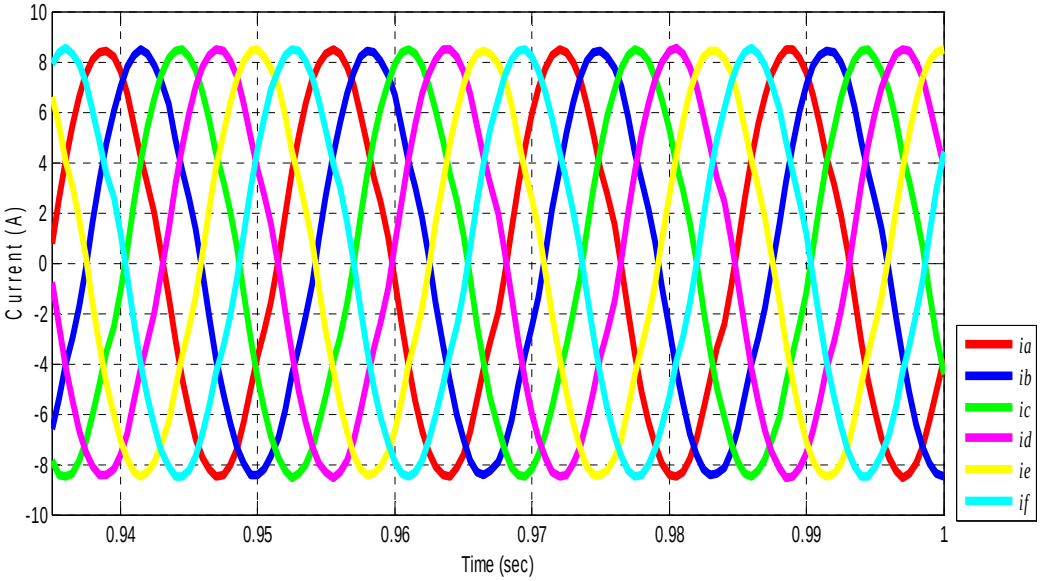

Figure 6-61: Phase currents i_a , i_b , i_c , i_d , i_e and i_f of the healthy six-phase induction motor.

From the above analysis , the torque ripple content in the resulting torque is 178 % with the 3-healthy phases and three adjacent faulty phase, in comparison with 6.67% torque ripple content in the healthy six-phase case. This is a very significant amount of torque ripple and is not suitable.

6.4.3.2 LOSS OF THREE NON-ADJACENT PHASES

Here , the two non-adjacent faulty phase cases shown in Figure 6-53 are considered , In the first case , the six-phase motor is simulated under loss of three non-adjacent phases each separated by 120^0 e , such as the loss of phase A and phase C and phase E. Figures 6-62 and 6-63 show the phasor representation of the voltages in the six-phase healthy case and the three-healthy phase and three non-adjacent faulty phase separated by 120^0 e case such as under loss of phase A , phase C and phase E. In Figures 6-64 and 6-65 , the torque profile of the 3-healthy phase with three faulty phases each separated by 120^0 should be compared with the 6-phase healthy case. These figures are accompanied by a magnified (zoom) portion of the steady-state torque profile. In Figures 6-66 and 6-67 , the Harmonic breakdown of the steady state torque profile for the 6-phase healthy case and the faulty case with 3 healthy phases are three faulty phases each separated by 120^0 are shown. Notice that the 2^{nd} order harmonic is in the faulty case with 3 healthy phases and three non-adjacent faulty phases separated by 120^0 has a magnitude of 0.1345 Nm when compared to the healthy case for which the 2^{nd} order harmonic has a magnitude of 0.1345 Nm . Here the magnitudes of the 2^{nd} order harmonics in both the cases are equal to each other.

In the second case, the six-phase motor is simulated under loss of three non-adjacent phases , two of which are separated by 60^0 e and the other is separated by 120^0 e , i.e. , the loss of phase A , phase B and phase D are considered. Figures 6-70 and 6-71 show the phasor representation of voltages in the six-phase healthy case and the three-phase healthy case with

three non-adjacent faulty phases separated by 60^0 *e* and 120^0 *e* under loss of phase A , phase B and phase D. In Figures 6-72 and 6-73 , the torque profile of the three-phase healthy case with three non-adjacent faulty phases separated by 60^0 *e* and 120^0 *e* should be compared with the 6-phase healthy case. Again, these figures are accompanied by a magnified (zoom) portion of the steady-state torque profile. In Figures 6-74 and 6-75 , the Harmonic breakdown of the steady state torque profile for the 6-phase healthy case and the faulty case with 3 healthy phases are three faulty phases separated by 60^0 *e* and 120^0 *e* are shown.Notice that the 2^{nd} order harmonic is more pronounced in the faulty case with 3 healthy phases and three non-adjacent faulty phases separated by 60^0 *e* and 120^0 *e* than in the case with 3 healthy phases and three non-adjacent faulty phases separated by 120^0 *e* with a magnitude of 12.66 Nm when compared to the healthy case for which the 2^{nd} order harmonic has a magnitude of 0.1345 Nm .

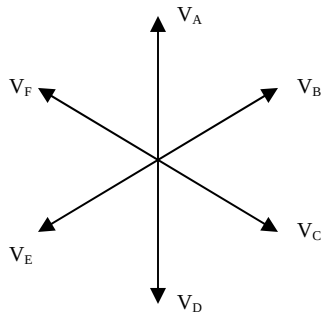

Figure 6-62 : Phasor representation of the voltages in six-phase healthy operation

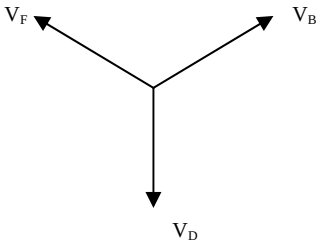

Figure 6-63 : Phasor representation of the voltages in the three healthy phase with three non-adjacent phase loss operation separated by120^0 *e* each i.e. with loss of phases A, C and E

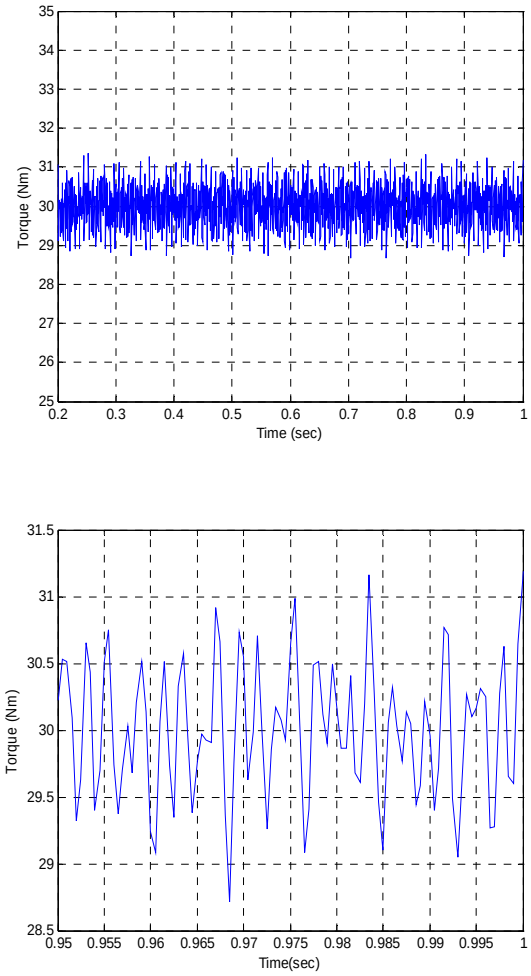

Figure 6.64 : Torque profile of the healthy 6-phase case under full-load

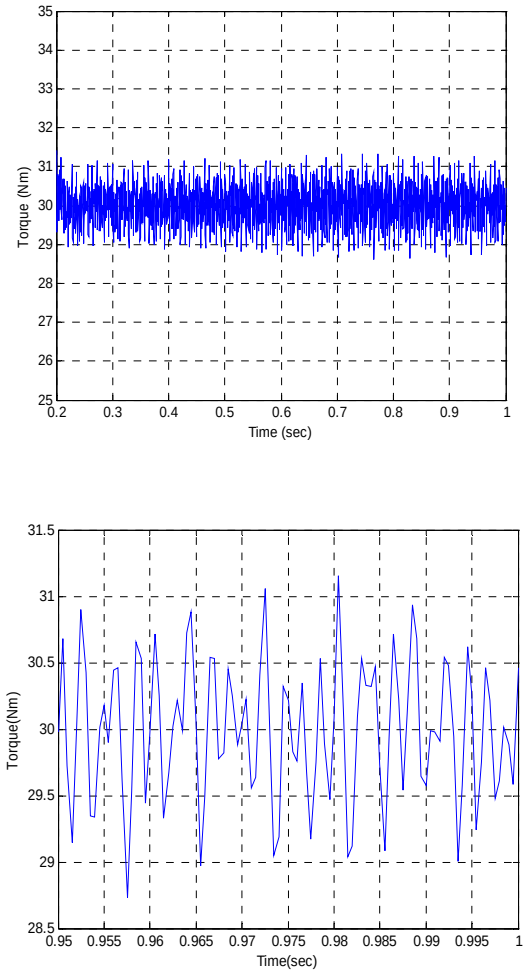

Figure 6.65:Torque profile of the 3-healthy phase case with loss three non- adjacent phases separated by 120^0 *e* i.e. phases A , C & E

RIPPLE CONTENT: 6.67%

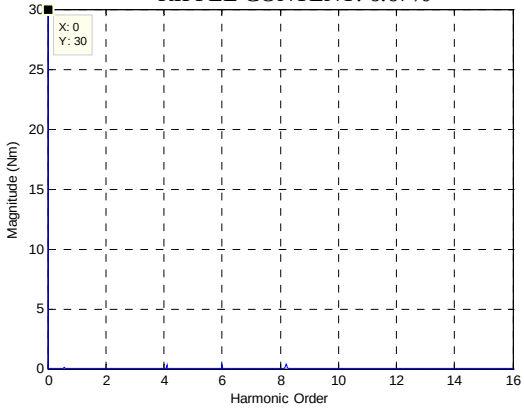

Figure 6.66::Harmonic spectrum of the torque profile of the healthy 6-phase case

RIPPLE CONTENT: 7.13%

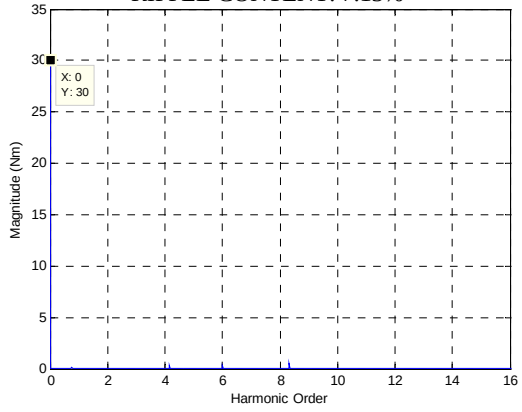

Figure 6.67::Harmonic spectrum of the torque profile of the 3-healthy phase case with loss of three non-adjacent phases A,C & E

Figure 6-68 and 6-69 shows the phase currents in the 3-healthy phase and three faulty phase with loss of phases A,C and E and the healthy six-phase operations.

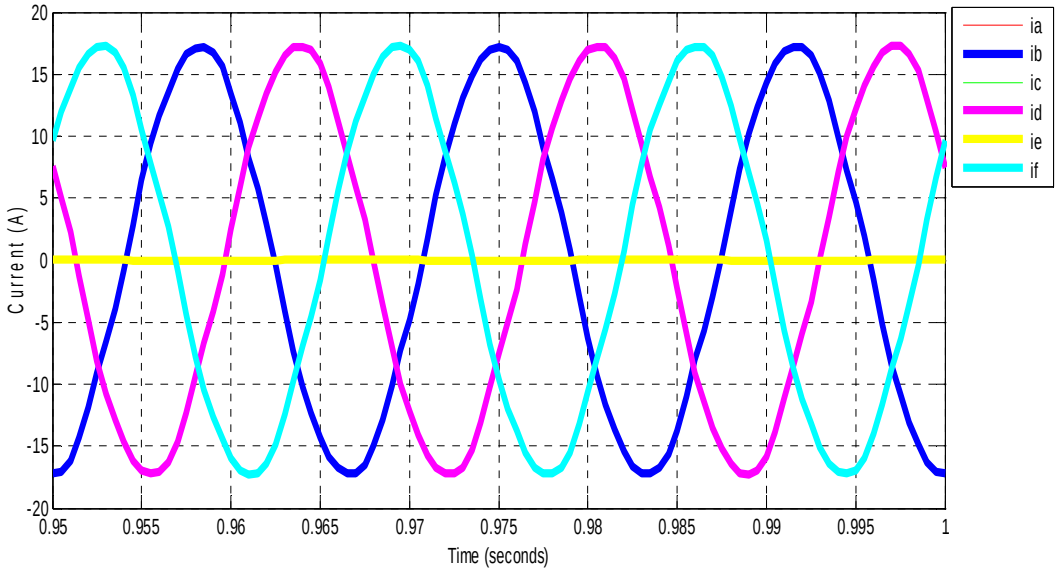

Figure 6-68: Phase currents i_a , i_b , i_c , i_d , i_e and i_f of the 3-healthy and three faulty phase operation of the six-phase induction motor with loss of non-adjacent phases A , C and E

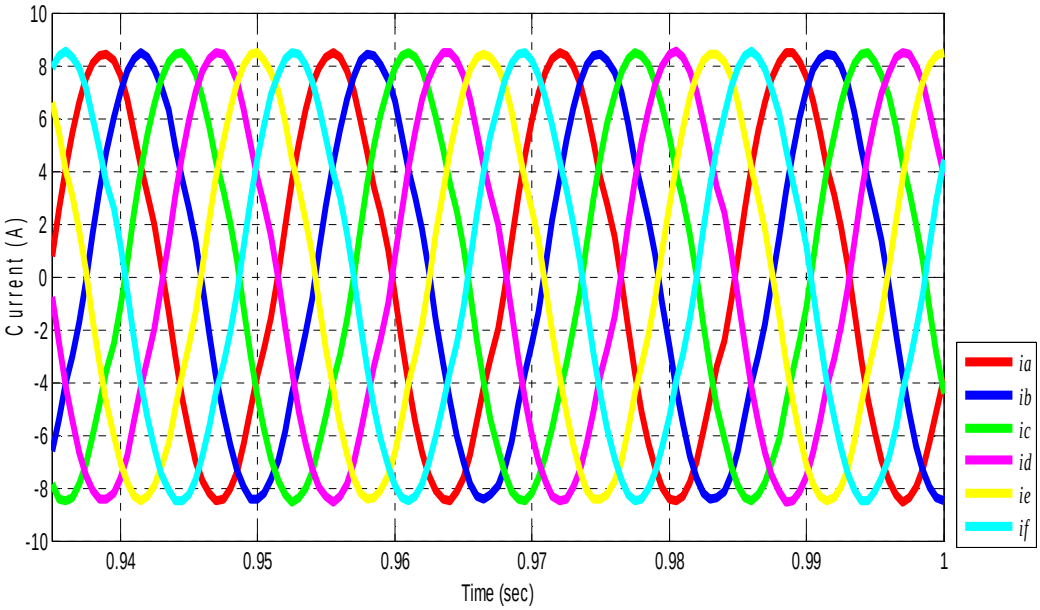

Figure 6-69 : Phase currents i_a , i_b , i_c , i_d , i_e and i_f of the healthy six-phase induction motor.

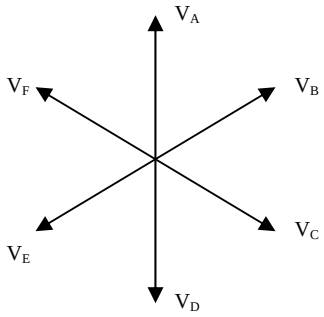

Figure 6-70 : Phasor representation of the voltages in six-phase healthy operation

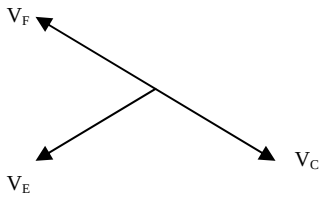

Figure 6-71: Phasor representation of the voltages in the three healthy phase with three non-adjacent faulty phase loss operation with loss of phases A, B and D

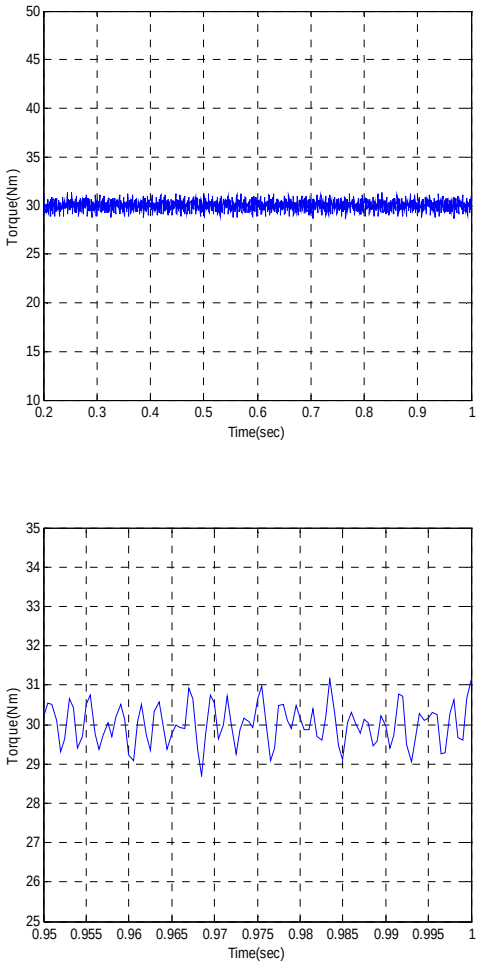

Figure 6.72: Torque profile of the healthy 6-phase case under full-load

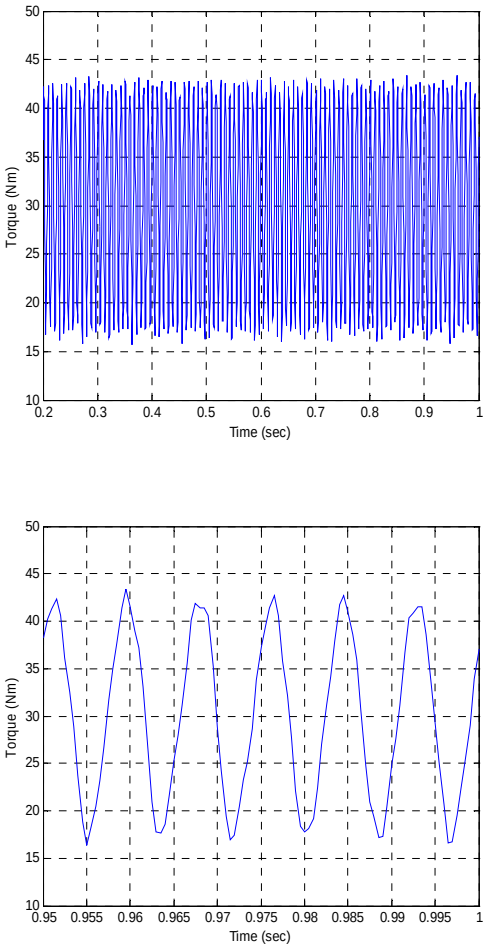

Figure 6.73:Torque profile of the 3-healthy phase case with loss three non- adjacent phases separated by 120^0 *e* and 60^0 *e* i.e. phases A , B and D

RIPPLE CONTENT: 6.67%

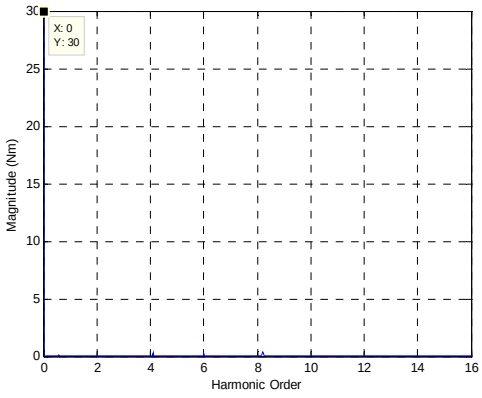

Figure 6.74::Harmonic spectrum of the torque profile of the healthy 6-phase case

RIPPLE CONTENT: 83.6%

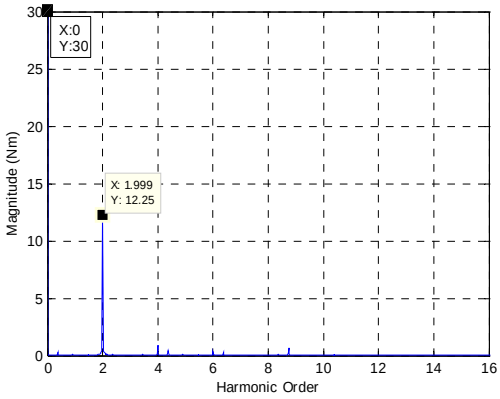

Figure 6.75::Harmonic spectrum of the torque profile of the 3-healthy phase case with loss of three non-adjacent phases A,B & D

Figure 6-76 and 6-77 shows the phase currents in the 3-healthy phase and three faulty phase with loss of phases A,B and D and the healthy six-phase operations.

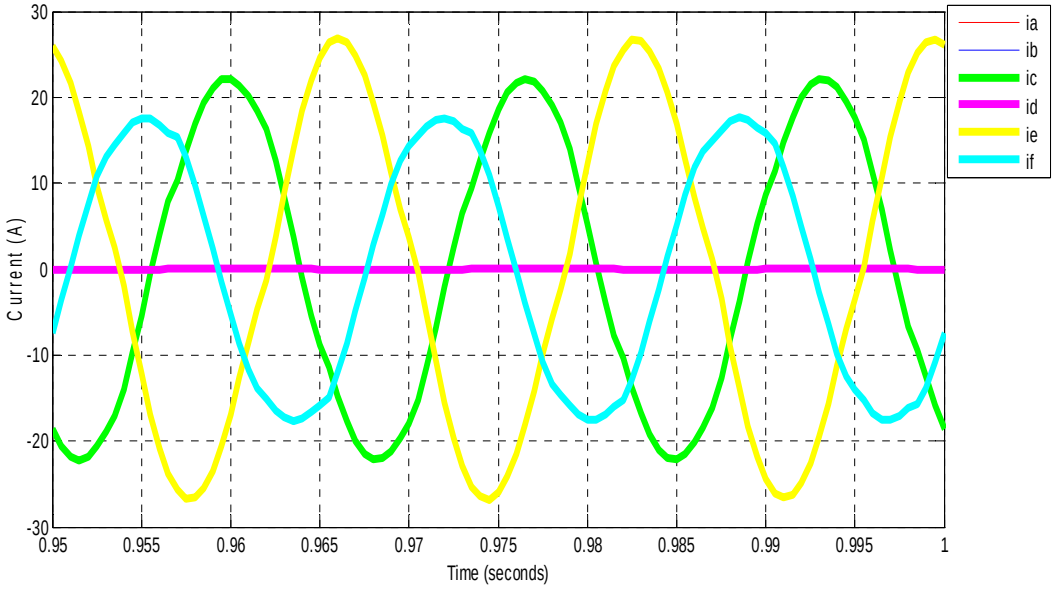

Figure 6-76: Phase currents i_a , i_b , i_c , i_d , i_e and i_f of the 3-healthy and three faulty phase operation of the six-phase induction motor with loss of non-adjacent phases A , B and D

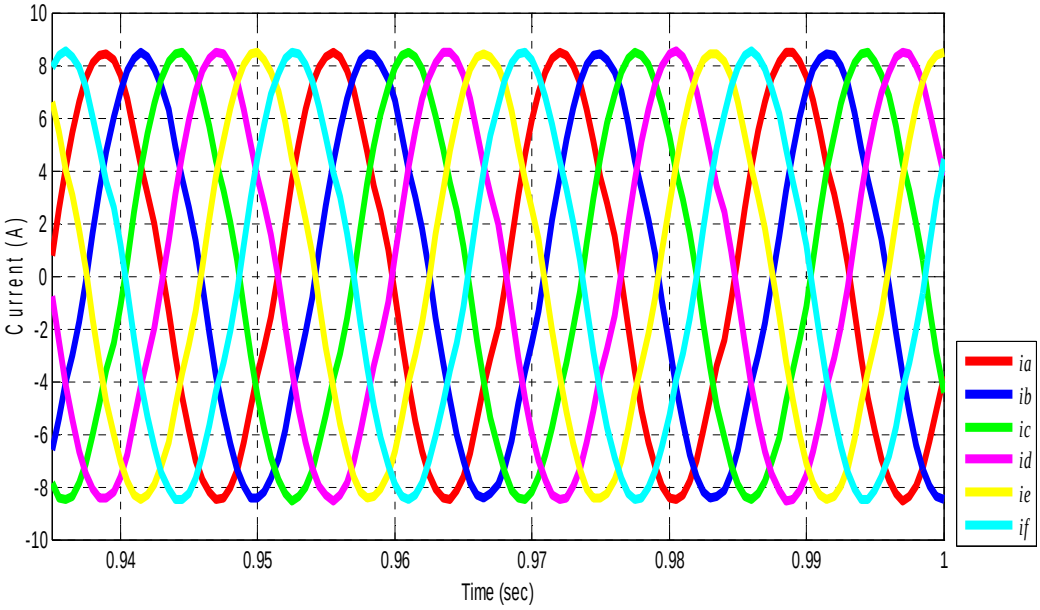

Figure 6-77 : Phase currents i_a , i_b , i_c , i_d , i_e and i_f of the healthy six-phase induction motor.

From the above analysis , the torque ripple content in the resulting torque is 7.13 % with the 3-healthy phases and three non-adjacent faulty phases each separated by 120^0 *e*, in comparison with 6.67% torque ripple content in the healthy six-phase case whereas , the torque ripple content in the 3-healthy phases and three non-adjacent faulty phase separated by 120^0 *e* and 60^0 *e* is 83.6 % in comparison with 6.67% torque ripple content in the healthy six-phase case. It should be observed that for the three non-adjacent faulty phase cases there is a marked difference between the 120^0 *e* separation and the phases separated by 120^0 *e* and 60^0 *e* cases in so far as the adverse effect on the ripple content in the time-domain torque profile. The 120^0 *e* separation is far less severe.It should also be observed that the ripple content in the three healthy phase and three non-adjacent faulty phase separated by 120^0 *e* and 60^0 *e* is far less when compared to the three phase healthy and three adjacent faulty phase operation. This would be acceptable in certain applications.

6.4.4 SIMULATION OF THE TWO-PHASE HEALTHY OPERATION WITH ONE FAULTY PHASE IN A THREE-PHASE MOTOR

Here , the case-study 5HP, 3-phase induction motor was simulated with the loss of one phase. Figures 6-78 and 6-79 show the phasor representation of voltages in the three-phase healthy case and the two-phase healthy and one-phase faulty case under the loss of phase A. In Figures 6-80 and 6-81, the torque profiles of the two-phase faulty operation and the healthy 3-phase operation should be compared. In Figures 6-82 and 6-83 , the Harmonic breakdown of the steady state torque profile for the 3-phase healthy case and the two-phase healthy operations are shown. Notice that the 2^{nd} harmonic is critical in the two-healthy phase case with a magnitude of 33.59 Nm when compared with the healthy 3-phase case which has a magnitude of 0.134 Nm.

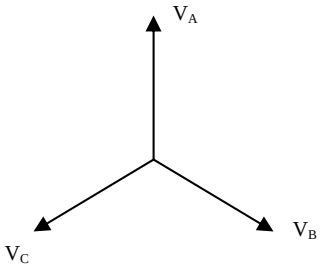

Figure 6-78 : Phasor representation of the voltages in three-phase healthy operation

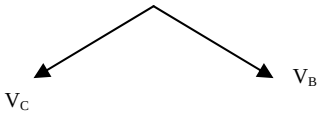

Figure 6-79: Phasor representation of the voltages in the two healthy phase with loss of phase A.

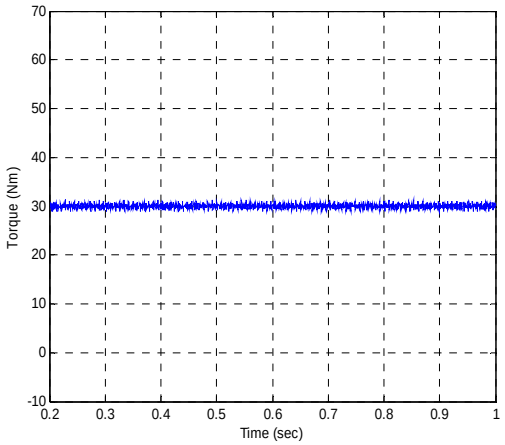

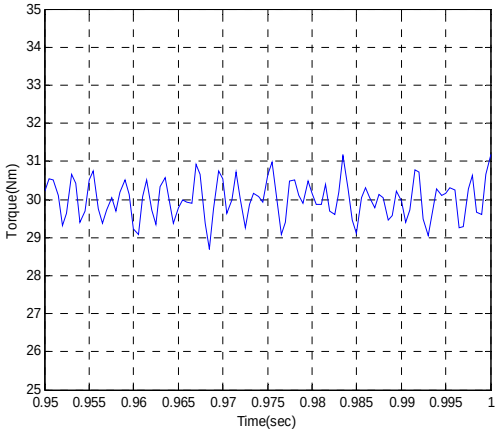

Figure 6.80 : Torque profile of the healthy 6-phase case under full-load

RIPPLE CONTENT: 6.67%

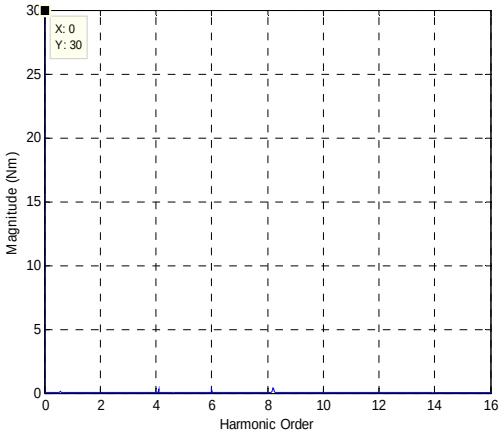

Figure 6.82::Harmonic breakdown of the torque profile of the healthy 6-phase case

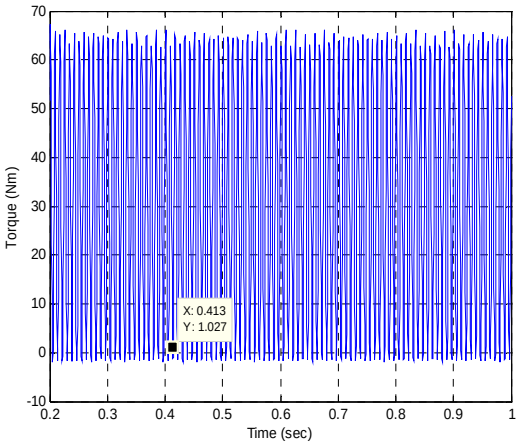

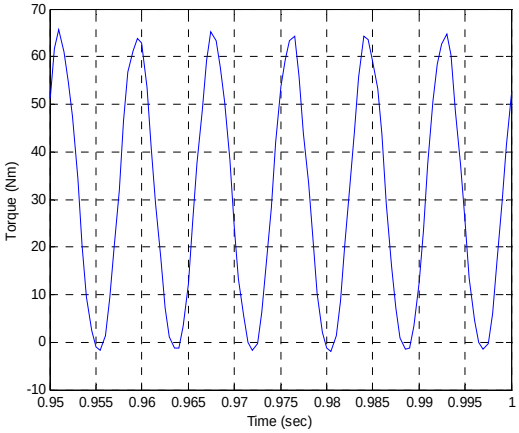

Figure 6.81:Torque profile of the 2-healthy phase case with loss of phase A

RIPPLE CONTENT: 213%

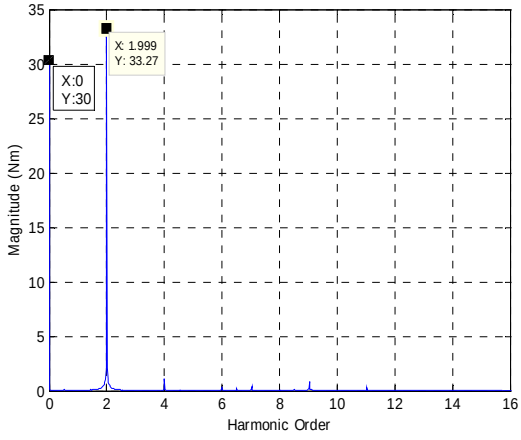

Figure 6.83::Harmonic breakdown of the torque profile of the 2-healthy phase case with loss of phase A

Figure 6-84 and 6-85 shows the phase currents in the 2-healthy phase and one faulty phase of a three-phase induction motor with loss of phase A and the healthy six-phase operations.

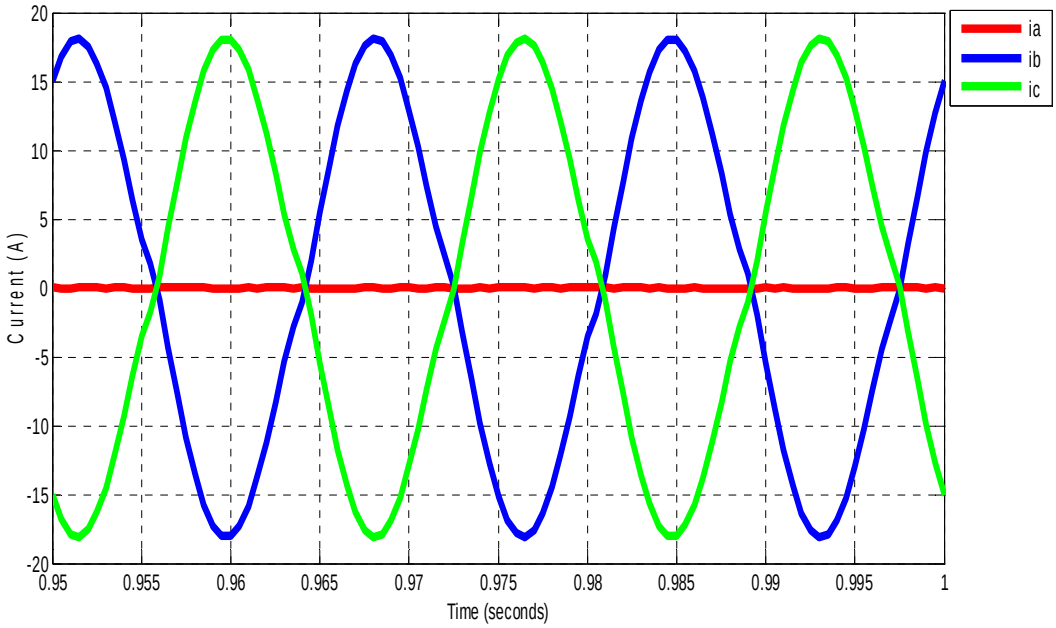

Figure 6-84: Phase currents i_a , i_b , i_c of the 2-healthy and one faulty phase operation of the three-phase induction motor with loss of phase A .

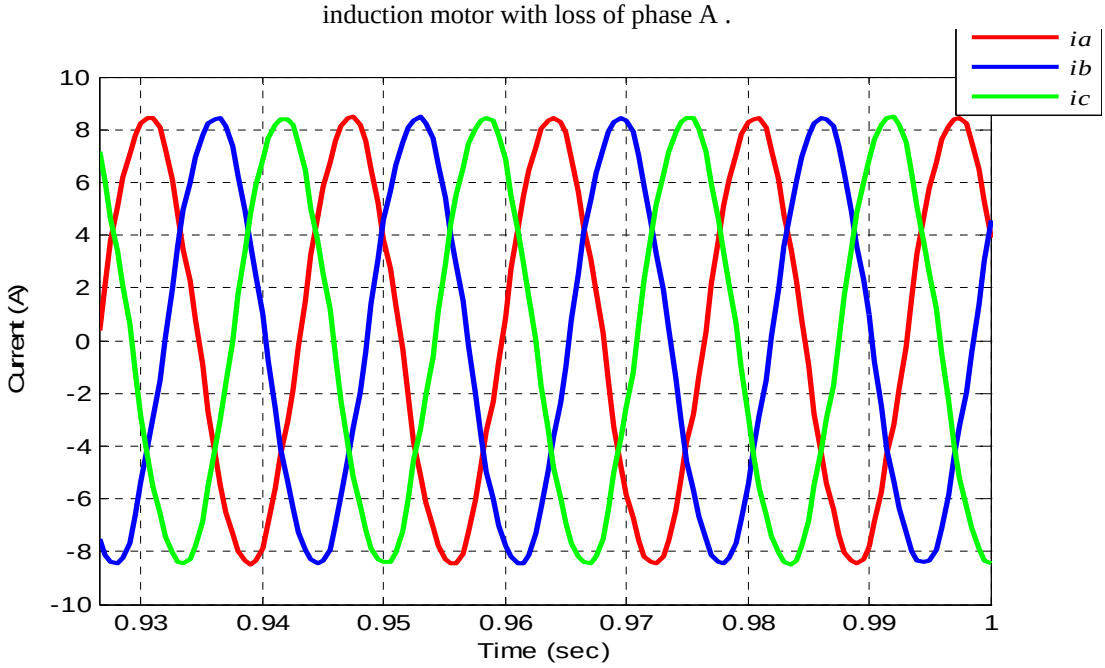

Figure 6-85: Phase currents i_a , i_b , i_c of the healthy three-phase induction motor.

From the above analysis , the torque ripple content in the resulting torque is 213 % with the 2-healthy phase operation , in comparison with 6.67% torque ripple content in the healthy three-phase case. This case yields the highest and has the most adverse effect on the torque ripple content when compared to any of the cases discussed earlier.

6.5 OBSEVATIONS AND DISCUSSIONS ON THE REASONS FOR TORQUE RIPPLES IN THE FAULTY PHASE OPERATIONS USING CURRENT SPACE VECTOR CONCEPTS

Now the results from the various unbalanced operations considered are used to obtain the locus of the stator current space vector , $\vec{i}_s$, for all the 3-phase and 6-phase healthy and faulty operation modes.

In the 3-phase motor case , the stator current space vector is defined as :

$$\vec{i}_s = \vec{i}_a + a \cdot \vec{i}_b + a^2 \cdot \vec{i}_c$$

where $a = e^{j2\pi/3} = 1\angle 2\pi/3 = 1\angle 120^0 e$

In the 6-phase motor case , the stator current space vector is defined as:

$$\vec{i}_s = \vec{i}_a + a \cdot \vec{i}_b + a^2 \cdot \vec{i}_c + a^3 \cdot \vec{i}_d + a^4 \cdot \vec{i}_e + a^5 \cdot \vec{i}_f$$

where $a = e^{j\pi/3} = 1\angle \pi/3 = 1\angle 60^0 e$

Figures 6-86 through 6-95 give a comparitive study of the locus of the current space vector , $\vec{i}_s$, distribution under all the various operating conditions studied in the previous sections of this chapter.

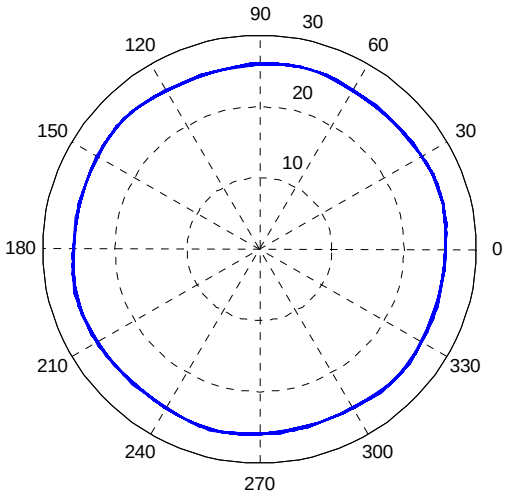

Figure 6.86: Locus of current space vector in the healthy 6-phase operation in a 6-phase motor.

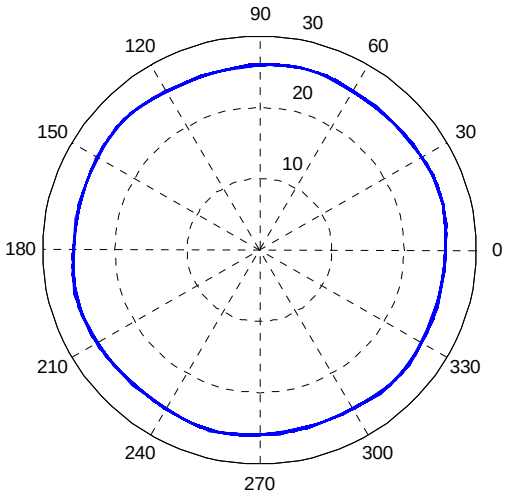

Figure 6.87: Locus of current space vector in the healthy 3-phase operation in a three-phase motor.

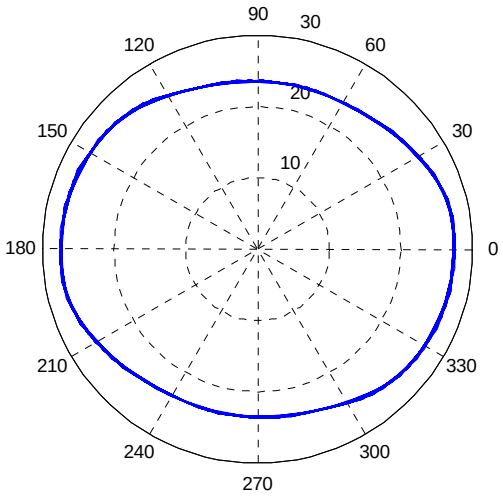

Figure 6.88: Locus of current space vector in the one faulty phase operation with loss of phase A in a 6-phase motor.

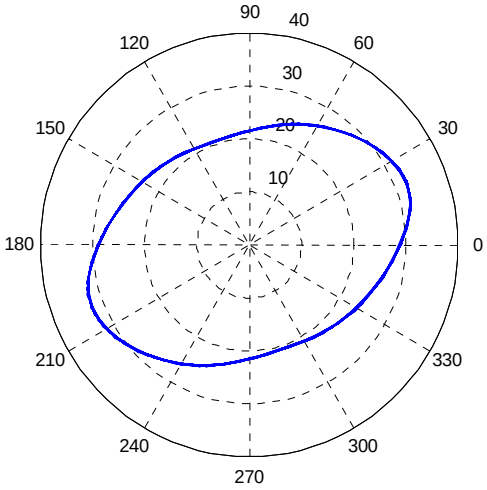

Figure 6.89: Locus of current space vector in two faulty phases operation with loss of adjacent phases A and B in a 6-phase motor.

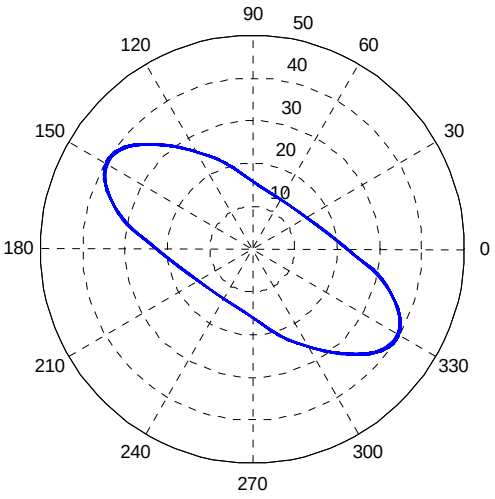

Figure 6.90:Locus of current space vector in the two faulty phases operation with loss of non-adjacent phases separated by 180^0 e i.e. phases A and D in a 6-phase motor.

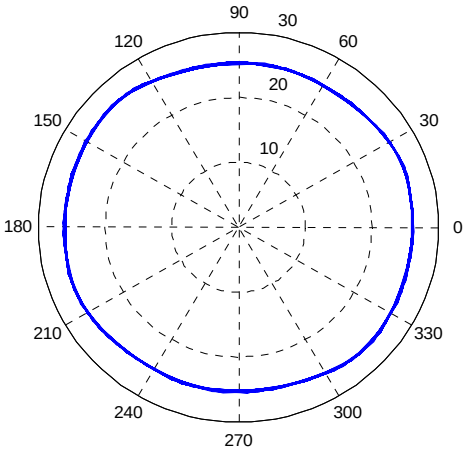

Figure 6.91 : Locus of the current space vector in the two faulty phases operation with loss of non-adjacent phases separated by 120^0 e i.e. phases A and C, in a 6-phase motor.

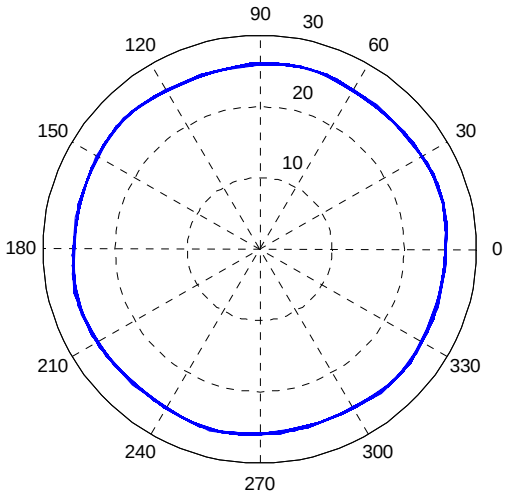

Figure 6.92:Locus of the current space vector in the three faulty phase operation with loss of non-adjacent phases separated by 120^0 e i.e. phases A , C and E, in a 6-phase motor.

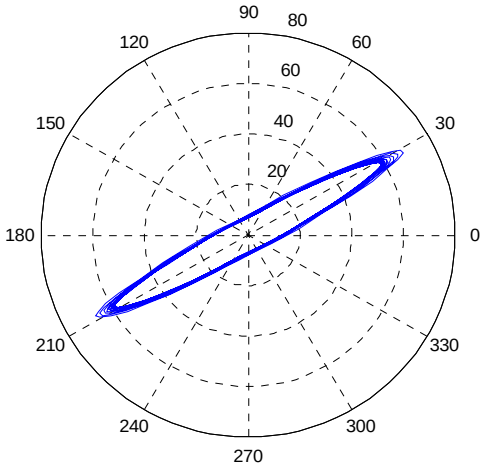

Figure 6.93:Locus of the current space vector in the three faulty phases operation with loss of adjacent phases separated by 60^0 e i.e. phases A , B and C, in a 6-phase motor.

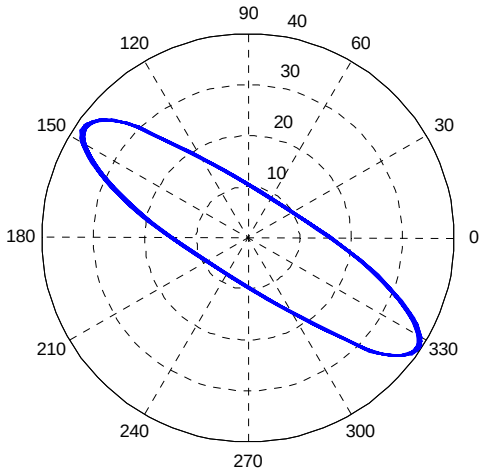

Figure 6.94:Locus of current space vector in the three-faulty phases operation with loss of non-adjacent phases separated by 120^0 e and 60^0 e i.e. phases A, B and D , in a 6-phase motor.

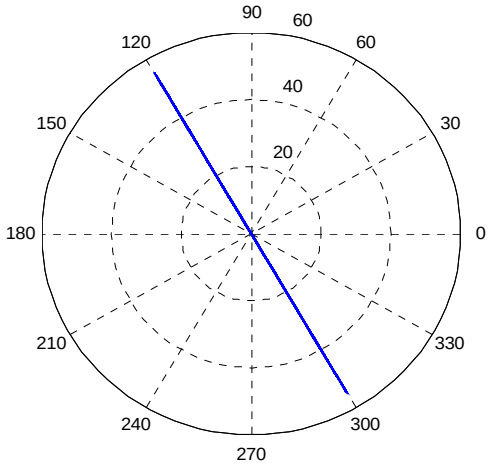

Figure 6.95:Locus of the current space vector in the one-faulty phase operation with loss of Phase A , in a three-phase motor.

6.5.1 HARMONIC ANALYSIS AND OBSERVATIONS

In Figures 6-97 through 6-105 , the harmonic spectrum of all the various operating modes studied in the previous sections are shown. Upon analyzing these results , it can be observed that the magnitude of the 2nd order harmonic bears a direct relationship to the ripple content in the torque profile which means that the magnitude of the 2nd harmonic increases with the increase in the ripple content in the time-domain torque profile. This is because of the negative sequence component induced in the unbalanced cases , which creates a field rotating in the backward direction. Therefore , the relative speed between the stator and rotor fields is 2ω which results in the dominant 2nd order harmonic. Figure 6-96 gives a comparative description of the various cases and the magnitude of the 2nd order harmonic .

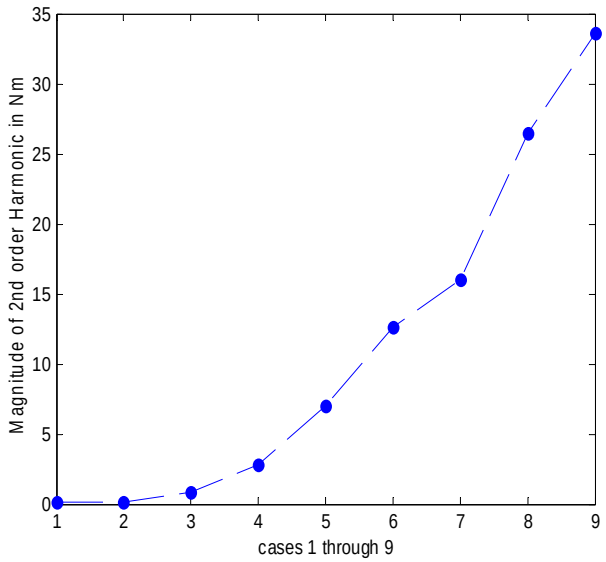

Case 1: Healthy 6-phase

Case 2: Three-Healthy Phases with loss of phases A, C and E

Case 3: Four-Healthy Phases with loss of phases A and C

Case 4: Five-Healthy Phases with loss of phase A

Case 5: Four-Healthy Phases with loss of phases A and B

Case 6: Three-Healthy phases with loss of phases A , B and D

Case 7: Four-Healthy Phases with loss of phases A and D

Case 8: Three-Healthy phases with loss of phases A , B and C

Case 9: Two-Healthy Phases of a three-phase motor

Figure 6-96: Variation of 2nd order harmonic in different cases

From Figure 6-96 , it is evident that the two-phase operation of a three-phase motor has the highest magnitude of 2nd order harmonic when compared to any of the other cases. Thus it can

be concluded any of the phase loss scenarios of the six-phase operation yields better performance than the two-phase operation of a three-phase motor. Also, in the six-phase motor case, Figure 6-80 gives at a quick glance the order of demerit of which loss of phase scenario is worst than which.

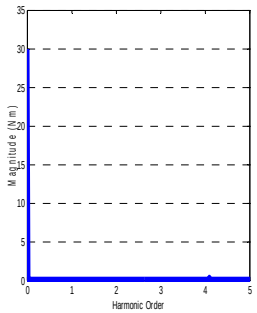

Figure 6-97:Harmonic spectrum of the 6-phase healthy case.

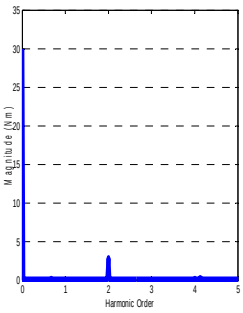

Figure 6-98:Harmonic spectrum of the 5-healthy phase and one faulty phase case

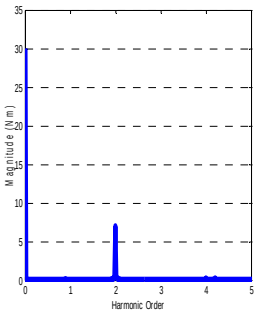

Figure 6-99:Harmonic Spectrum of the 4-healthy phase and two adjacent faulty phases A and B

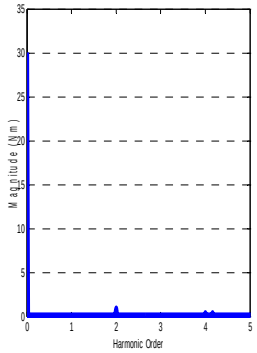

Figure 6-100:Harmonic Spectrum of the 4-healthy phase and two non-adjacent faulty phases A and C separated by 120^0 e

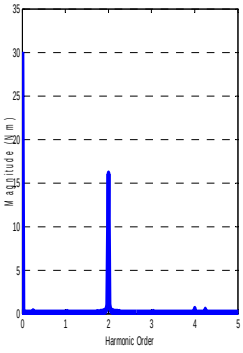

Figure 6-101:Harmonic Spectrum of the 4-healthy phase and two non-adjacent faulty phases A and D separated by 180^0 e

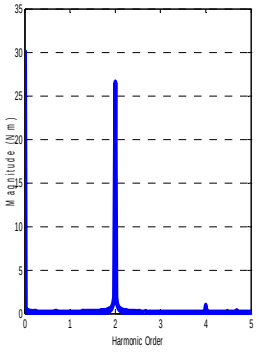

Figure 6-102:Harmonic Spectrum of the 3-healthy phase and 3 adjacent faulty phases A ,B and C separated by

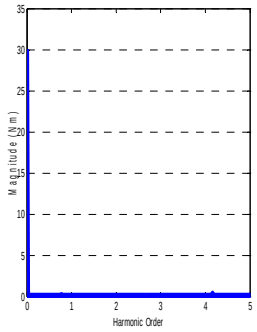

Figure 6-103:Harmonic Spectrum of the 3-healthy phase and 3 non- adjacent faulty phases A ,C and E separated by 120^0 e

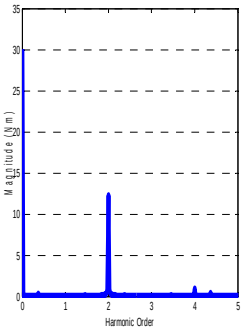

Figure 6-104:Harmonic Spectrum of the 3-healthy phase and 3 non- adjacent faulty phases A ,B and D separated by 120^0 e and 60^0 e

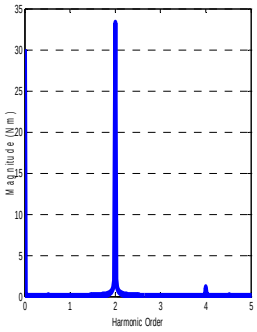

Figure 6-105:Harmonic Spectrum of the 2-healthy phase and one faulty phase of a three phase motor

Upon close examination of Figures 6-86 through 6-95 , it can be observed that the locus (trace) of the stator current space vector becomes closer to the elliptical / oval shape in unbalanced cases, whereas it is closer to a circle in the healthy case. From the detailed analysis of the results obtained , it can be observed that the 6-phase machine exhibits better performance under phase-loss conditions when compared to the 3-phase machine. A summary chart representing the percentage torque ripple content for various faults considered in percent of the developed average torque is shown in Figure 6-106

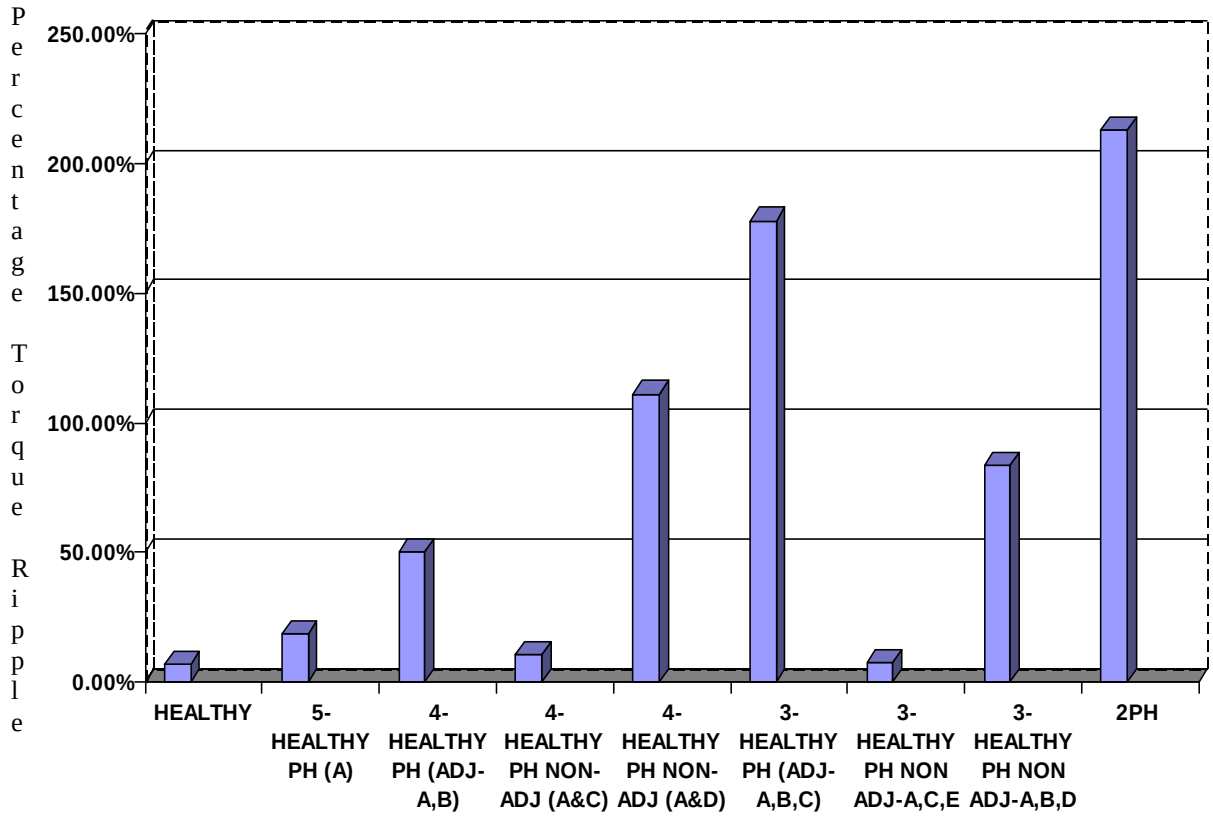

Figure 6-106. Summarized chart showing the torque ripple content under different cases.

Figure 6-106 clearly indicates that the 5-healthy phase operation with one faulty phase , 3-healthy phase and three non-adjacent faulty phase operation and 4-healthy phase and two non-adjacent faulty phase operation considering loss of phases separated by 120^0 *e* yields the least amount of torque ripple and are almost equal in ripple content , to the healthy case. The current space vector locus diagrams affirm these results in being closest in shape to a circle. Even the 4-healthy phase non-adjacent operation considering loss of phases separated by 180^0 *e* , the 4-healthy phase adjacent phase-loss operation and the 3-healthy phase non-adjacent phase-loss operation exhibit relatively lower amount of torque ripple content when compared to the standard two-phase operation of a three-phase motor.

Table 6-4 gives a comparison between the rms values of phase currents in the various cases studied given earlier in this chapter, in which the motor was developing an average torque of 30Nm approximately:

CONDITION	RMS VALUE OF PHASE CURRENT (A)
Healthy 6-phase	6.8
5-healthy phase and one faulty phase with loss of phase A	10.92
4-healthy phase and two faulty phase with loss of adjacent phases A and B	13.496
4-healthy phase and two faulty phase with loss of non-adjacent phases A and C	12.8
4-healthy phase and two faulty phase with loss of non-adjacent phases A and D	9.8995
3-healthy phase and three faulty phase with loss of adjacent phases A ,B and C	24.3245
3-healthy phase and three faulty phase with loss of non-adjacent phases A ,C and E	12.1662
3-healthy phase and three faulty phase with loss of non-adjacent phases A ,B and D	25.3568
2-healthy phases and one faulty phase of a 3-phase motor	12.6572

Table 6-4: RMS values of phase currents under the various cases considered.

From Table 6-4 it can be observed that the rms value of phase current increases under phase-loss conditions. A solution to this issue involving a derating of the motor output torque and power is suggested in the next section. This is in order to prevent winding overheating and hence preserve the thermal integrity of the motor.

6.5.2 DISCUSSION REGARDING DERATING OF THE MOTOR OUTPUT UNDER VARIOUS FAULT SCENARIOS

It is well known that as the current increases in the phases, the motor is prone to overheating and thermal degradation . Under very high currents , the motor windings may even burn. In order to overcome this problem, it is necessary to derate the motor output under fault conditions, while permitting the running of the motor for limited periods for “limp-home” purposes. The concept of derating can be explained as follows:

The total electromagnetic power in a 6-phase machine is given by ,

$$P_{em} = 6 I_2^{\,2} (R_2 / s) \qquad (6\text{-}1)$$

where I_2 = the equivalent rms value of the rotor current /phase referred to the stator side.

R_2 = the equivalent rotor resistance /phase referred to the stator side.

and s is the slip.

Here, the total developed power is as follows:

$$P_{dev} = 6 I_2^{\,2} (1 - s/s) R_2 \qquad (6\text{-}2)$$

For the purposes of this discussion, it can be assumed that the stator current per phase , $I_1 \approx I_2$. Therefore, the total ohmic loses in a 6-phase machine can be given as follows:

$$P_{ohmic} = \sum I_1^{\,2} R_2 = I_a^{\,2} R_2 + I_b^{\,2} R_2 + I_c^{\,2} R_2 + I_d^{\,2} R_2 + I_e^{\,2} R_2 + I_f^{\,2} R_2 \qquad (6\text{-}3)$$

where $I_a, I_b, I_c, I_d, I_e, and\ I_f$ are the values of the phase currents in phases *A,B,C,D,E* and *F*.

From the standpoint thermal heating considerations, the ohmic losses in the machine can be taken indirectly proportional to the developed or output power , that is,

$$P_{output} \text{ or } P_{rating} \propto \frac{1}{P_{ohmic}} \tag{6-4}$$

The heating in a machine is directly dependent on the ohmic losses, which means that as the ohmic losses increases, the heating in the machine also increases .Therefore, the so-called “heat index” for the machine can be defined as follows:

$$Heat\ Index = \sum I_{ph\ rms}{}^2 \tag{6-5}$$

From Equations 6-3 and 6-4 , one can write the following for the six-phase case:

$$P_{rating} \propto \frac{1}{\sum I_1{}^2 R_2} \propto \frac{1}{I_{a_6}{}^2 R_2 + I_{b_6}{}^2 R_2 + I_{c_6}{}^2 R_2 + I_{d_6}{}^2 R_2 + I_{e_6}{}^2 R_2 + I_{f_6}{}^2 R_2} \tag{6-6}$$

Accordingly, for the six-phase healthy condition Equation 6-6 can be rewritten as follows:

$$P_{rating(healthy)(six-phase)} \propto \frac{1}{\sum I_1{}^2 R_2} \propto \frac{1}{I_{a_6}{}^2 R_2 + I_{b_6}{}^2 R_2 + I_{c_6}{}^2 R_2 + I_{d_6}{}^2 R_2 + I_{e_6}{}^2 R_2 + I_{f_6}{}^2 R_2} \tag{6-7}$$

For the faulty case , considering the 5-healthy phase and one faulty phase condition , where there is loss of phase A , one can write

$$P_{rating\,new(\,faulty)(5-healthy\,and\,one\,faulty)} \propto \frac{1}{\sum I_1{}^2 R_2} \propto \frac{1}{I_{b_5}{}^2 R_2 + I_{c_5}{}^2 R_2 + I_{d_5}{}^2 R_2 + I_{e_5}{}^2 R_2 + I_{f_5}{}^2 R_2} \tag{6-8}$$

Dividing Equation 6-8 by Equation 6-7 , one obtains

$$\frac{P_{rating\,new(\,faulty)(5-healthy\,and\,one\,faulty)}}{P_{rating(healthy)(six-phase)}} = \frac{I_{a_6}{}^2 R_2 + I_{b_6}{}^2 R_2 + I_{c_6}{}^2 R_2 + I_{d_6}{}^2 R_2 + I_{e_6}{}^2 R_2 + I_{f_6}{}^2 R_2}{I_{b_5}{}^2 R_2 + I_{c_5}{}^2 R_2 + I_{d_5}{}^2 R_2 + I_{e_5}{}^2 R_2 + I_{f_5}{}^2 R_2} \tag{6-9}$$

Or

$$\frac{P_{rating\,new(\,faulty)(5-healthy\,and\,one\,faulty)}}{P_{rating(healthy)(six-phase)}} = \frac{I_{a_6}{}^2 + I_{b_6}{}^2 + I_{c_6}{}^2 + I_{d_6}{}^2 + I_{e_6}{}^2 + I_{f_6}{}^2}{I_{b_5}{}^2 + I_{c_5}{}^2 + I_{d_5}{}^2 + I_{e_5}{}^2 + I_{f_5}{}^2} \tag{6-10}$$

Therefore, from Equation 6-5,

$$\frac{P_{rating\,new(\,faulty)(5-healthy\,and\,one\,faulty)}}{P_{rating(healthy)(six-phase)}} = \frac{Heat\ Index_{(healthy)(six-phase)}}{Heat\ Index_{(\,faulty)(5-healthy\,and\,one\,faulty)}} \tag{6-11}$$

Equation 6-10 is a more conservative formula which can be modified in order to include the worst condition possible, where all the currents in phases of the faulty case are assumed to be equal to the maximum value of the unbalanced phase currents in the faulty case. With this conservative notion, Equation 6-10 can be simplified and rewritten as follows:

$$P_{rating\,new(\,faulty)} = \frac{6 \times I_{ph\ rms_6}^{\ 2}}{N_H \times [\max(I_{ph\ rms_{\ faulty}})^2]} P_{rating(healthy)(six-phase)} \tag{6-12}$$

where , N_H is the number of healthy phases,

and $[\max(I_{ph\ rms_{\ faulty}})]$ is the highest value of rms current in the remaining healthy phases.

For the faulty case , considering the 5-healthy phases and one faulty phase condition , where there is a loss of phase A , Equation 6-12 becomes

$$P_{rating new(5-healthy and one faulty phase)} = \frac{6 \times I_{ph\ rms_6}^{\ 2}}{5 \times [\max(I_{ph\ rms_{5-healthy and one faulty\ phase}})^2]} P_{rating(healthy)(six-phase)} \tag{6-13}$$

Since the $P_{rating(healthy)(six-phase)}$ is known , From Equation 6-11, the new $P_{rating\,new(\,faulty)}$ for the faulty case can be found such that , if the motor is derated to operate at the new value of the calculated output power , the highest current in the phases would be nearly maintained at the same value as in the six healthy phase case , thus avoiding the thermal overstress of winding insulation and possible damage to the motor, and ensuring a safe “limp-home” operation.

6.5.2.1 VERIFICATION OF DERATING OF THE MOTOR FOR THE 5-HEALTHY PHASE AND ONE FAULTY PHASE CONDITION WITH LOSS OF PHASE A BY TIME-STEPPING FINITE-ELEMENT SIMULATION

For the case study 5-hp six-phase machine , $I_{ph\ rms_6} = 6.8\,A$, according to the nameplate and design data.

From the TSFE simulation, the maximum rms phase current value under rated condition is ,

$$\max(I_{ph\ rms_{5-healthy\ and\ one\ faulty\ phase}}) = 10.98\,A$$

Therefore , from Equation 6-13 ,

$$P_{rating\,new(5-healthy\,and\,one\,faulty\,phase)} = \frac{6 \times I_{ph\ rms_6}{}^2}{5 \times [\max(I_{ph\ rms_{5-healthy\,and\,one\,faulty\ phase}})^2]} P_{rating(healthy)(six-phase)}$$

For this motor, $P_{rating(healthy)(six-phase)}$ = 3728.5 W. Therefore, according to Equation 6-13 for the 5-healthy phases/one faulty phase condition, one can write the following:

$$P_{rating\,new(\,faulty)(5-healthy\ and\ one\ faulty)} = \frac{6 \times 6.8^2}{5 \times 10.98^2} \times 3728.5$$

$$P_{rating\,new(\,faulty)(5-healthy\ and\ one\ faulty)} = 1716.04\ \text{W}$$

Hence, the new value of torque that the motor would be operating at to produce the rated current would be

$$T_{new} = \frac{P_{rating\,new(\,faulty)(5-healthy\,and\,one\,faulty)}}{\omega}$$

where ω is the rated speed in mech. rad/sec.Since the rated speed is 1165 r/min for the case-study 5-hp induction motor, That is

$$\omega = 1165 \times \frac{2\pi}{60} = 122\ mech.rad/\text{sec}$$

Hence,

$$T_{new} = \frac{P_{rating\,new(\,faulty)(5-healthy\,and\,one\,faulty)}}{\omega} = \frac{1716.04}{122} = 14\,Nm$$

Therefore , after derating the 6-phase motor under loss of one phase , to the new value of the calculated power , the motor would produce a developed average torque of 14 Nm , without exceeding the rated design value of current in the phases. Figures 6-107 and 6-108 shows the TSFE simulation results of the phase currents in the 5-healthy and one faulty phase case, with the loss of phase A , before and after derating the motor , that is for a torque of 30Nm and 14Nm, respectively.

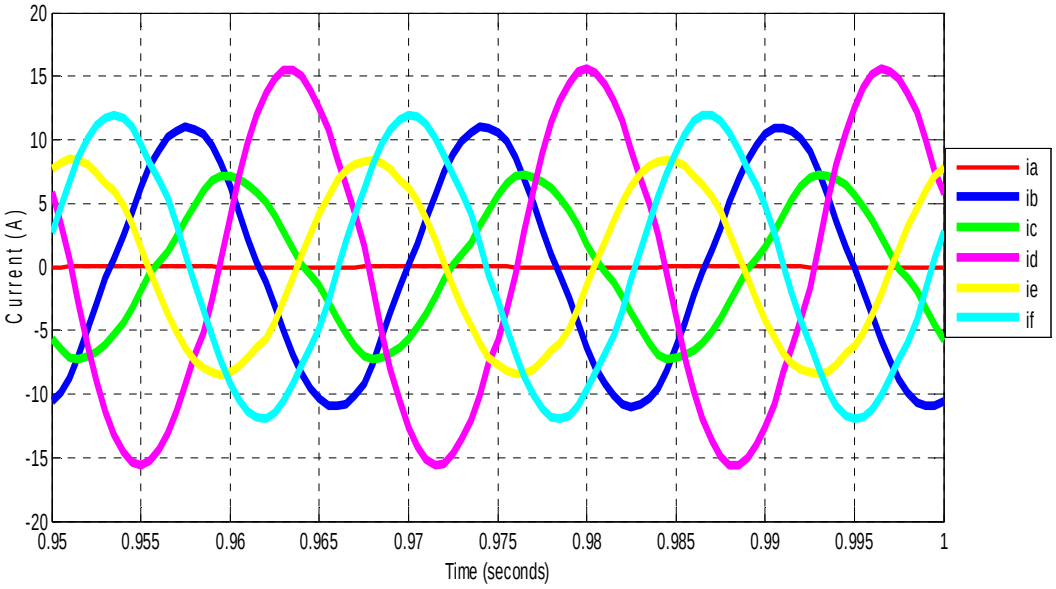

Figure 6-107: Phase currents in the 5-healthy and one faulty phase with loss of phase A before derating the motor from TSFE simulation.

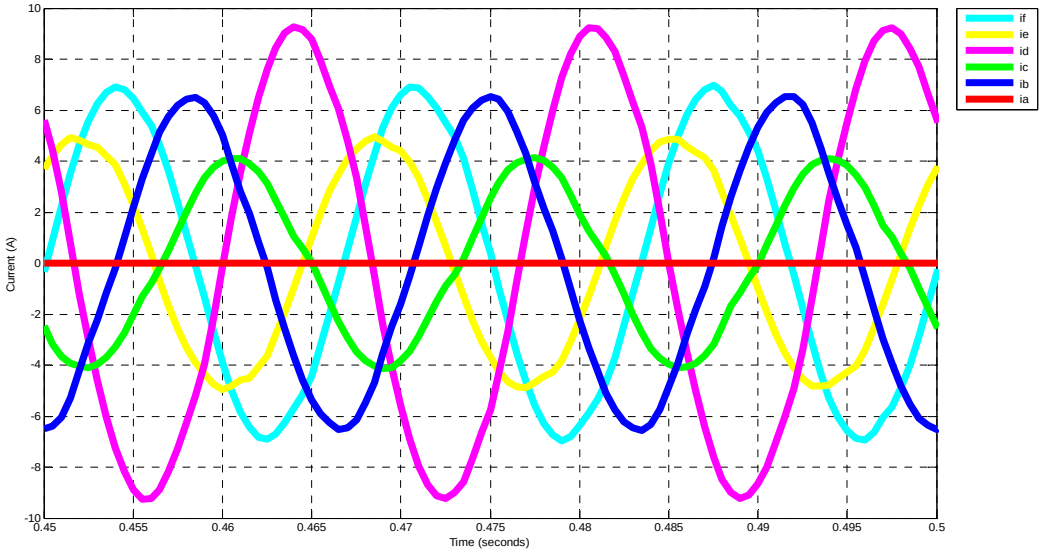

Figure 6-108: Phase currents in the 5-healthy and one faulty phase with loss of phase A after derating the motor from TSFE simulation.

From Figures 6-107 and 6-108 , it can be observed that the rms value of the highest value of phase currents after derating the motor has dropped to 6.4 A which is below the rated current value of 6.8 A, of the original design.

Similarly , the motor can be derated under the other faulty cases as well , to bring down the current in the phases under "limp-home" operation scenarios to values close to the rated current of 6.8A, thus avoiding any potential winding overheating, damage to the motor. Accordingly, for the 4-healthy phases and the two faulty phase operation scenario with the loss of two adjacent phases A and B ,

Upon applying Equation 6-12 for derating the motor output as discussed earlier, it is found that,

$$P_{rating new(4-healthy and two faulty phase)} = \frac{6 \times I_{ph\ rms_6}{}^2}{4 \times [\max(I_{ph\ rms_{4-healthy and two faulty\ phase}})^2]} P_{rating(healthy)(six-phase)}$$

The maximum rms phase current was found to be 13.484 A, hence,

$$P_{rating new(\ faulty)(4-healthy\ and\ two\ faulty)} = \frac{6 \times 6.8^2}{4 \times 13.484^2} 3728.5$$

$$P_{rating new(\ faulty)(4-healthy\ and\ two\ faulty)} = 1422.34 \text{ W}$$

and the new value of the developed torque would be ,

$$T_{new} = \frac{P_{rating new(\ faulty)(4-healthy and two\ faulty)}}{\omega} = 11.65 \text{ Nm}$$

For the 4-healthy phase and the two faulty phase operation scenario with the loss of two non-adjacent phases A and C,

Upon applying Equation 6-12 for derating the motor output as discussed earlier, it is found that,

$$P_{rating new(4-healthy and two faulty phase)} = \frac{6 \times I_{ph\ rms_6}{}^2}{4 \times [\max(I_{ph\ rms_{4-healthy and two faulty\ phase}})^2]} P_{rating(healthy)(six-phase)}$$

The maximum rms phase current was found to be 12.94 A, hence,

$$P_{rating\,new(\,faulty)(4-healthy\ and\ two\ faulty)} = \frac{6\times 6.8^2}{4\times 12.94^2}3728.5$$

$$P_{rating\,new(\,faulty)(4-healthy\ and\ two\ faulty)} = 1544.45 \text{ W}$$

and the new value of the developed torque would be ,

$$T_{new} = \frac{P_{rating\,new(\,faulty)(4-healthy\,and\,two\,faulty)}}{\omega} = 12.65 \text{ Nm}$$

For the 4-healthy phase and the two faulty phase operation scenarion with the loss of two non-adjacent phases A and D,

Upon applying Equation 6-12 for derating the motor output as discussed earlier, it is found that,

$$P_{ratingnew(4-healthyand\,two\,faulty\,phase)} = \frac{6\times {I_{ph\ rms_6}}^2}{4\times[\max(I_{ph\ rms_{4-healthyand\,two\,faulty\ phase}})^2]}P_{rating(healthy)(six-phase)}$$

The maximum rms phase current was found to be 10.04 A, hence,

$$P_{rating\,new(\,faulty)(4-healthy\ and\ two\ faulty)} = \frac{6\times 6.8^2}{4\times 10.04^2}3728.5$$

$$P_{rating\,new(\,faulty)(4-healthy\ and\ two\ faulty)} = 2565.5 \text{ W}$$

and the new value of the developed torque would be ,

$$T_{new} = \frac{P_{rating\,new(\,faulty)(4-healthy\,and\,two\,faulty)}}{\omega} = 21.02 \text{ Nm}$$

For the 3-healthy phase and the three faulty phase operation scenario with the loss of three adjacent phases A, B and C

Upon applying Equation 6-12 for derating the motor output as discussed earlier, it is found that,

$$P_{ratingnew(3-healthyand\,three\,faulty\,phase)} = \frac{6\times {I_{ph\ rms_6}}^2}{3\times[\max(I_{ph\ rms_{3-healthyand\,three\,faulty\ phase}})^2]}P_{rating(healthy)(six-phase)}$$

The maximum rms phase current was found to be 25.23 A, hence,

$$P_{rating\,new(\,faulty)(3-healthy\ and\ three\ faulty)} = \frac{6\times 6.8^2}{3\times 25.23^2}3728.5$$

$$P_{rating\,new(\,faulty)(3-healthy\ and\ three\ faulty)} = 541.6 \text{ W}$$

and the new value of the developed torque would be ,

$$T_{new} = \frac{P_{rating\,new(\,faulty)(3-healthy\,and\,three\,faulty)}}{\omega} = 4 \text{ Nm}$$

For the 3-healthy phase and the three faulty phase operation scenario with the loss of three non-adjacent phases A, C and E

Upon applying Equation 6-12 for derating the motor output as discussed earlier, it is found that,

$$P_{rating new(3-healthy and three faulty phase)} = \frac{6\times I_{ph\ rms_6}{}^2}{3\times[\max(I_{ph\ rms_{3-healthy and three faulty\ phase}})^2]} P_{rating(healthy)(six-phase)}$$

The maximum rms phase current was found to be 12.17 A, hence,

$$P_{rating\,new(\,faulty)(3-healthy\ and\ three\ faulty)} = \frac{6\times 6.8^2}{3\times 12.17^2}3728.5$$

$$P_{rating\,new(\,faulty)(3-healthy\ and\ three\ faulty)} = 2328.09 \text{ W}$$

and the new value of the developed torque would be ,

$$T_{new} = \frac{P_{rating\,new(\,faulty)(3-healthy\,and\,three\,faulty)}}{\omega} = 19.08 \text{ Nm}$$

For the 3-healthy phase and the three faulty phase operation scenario with the loss of three non-adjacent phases A, B and D

Upon applying Equation 6-12 for derating the motor output as discussed earlier, it is found that,

$$P_{rating new(3-healthy and three faulty phase)} = \frac{6\times I_{ph\ rms_6}{}^2}{3\times[\max(I_{ph\ rms_{3-healthy and three faulty\ phase}})^2]} P_{rating(healthy)(six-phase)}$$

The maximum rms phase current was found to be 18.66 A, hence,

$$P_{rating\,new(\,faulty)(3-healthy\ and\ three\ faulty)} = \frac{6\times 6.8^2}{3\times 18.66^2}3728.5$$

$$P_{rating\,new(\,faulty)(3-healthy\ and\ three\ faulty)} = 990.28 \text{ W}$$

and the new value of the developed torque would be ,

$$T_{new} = \frac{P_{rating\,new(\,faulty)(3-healthy\,and\,three\,faulty)}}{\omega} = 8.11 \text{ Nm}$$

In summary to the above discussion on derating the motor output under various fault scenarios, Table 6-5 gives the power rating of the motor and the torque developed after derating of the motor output under the various faulty cases:

CONDITION	POWER RATING (W)	TORQUE (Nm)
6-Healthy phases	3728.5	30
5-Healthy and one faulty phase	1716.05	14
4-Healthy and two adjacent faulty phase with loss of phases A and B	1422.64	11.65
4-Healthy and two non-adjacent faulty phase with loss of phases A and C	1544.45	12.65
4-Healthy and two non-adjacent faulty phase with loss of phases A and D	2565.5	21.02
3-Healthy and three adjacent faulty phase with loss of phases A , B and C	541.6	4
3-Healthy and three non-adjacent faulty phase with loss of phases A C and E	2328.09	19.08
3-Healthy and three non-adjacent faulty phase with loss of phases A B and D	990.28	8.11

Table 6-5 : Power rating and the corresponding torque under various conditions after derating the motor.

It can be observed that by derating the motor under the various faulty cases, the operation of the motor can be continued for a sufficient amount of time for “limp-home” purposes without exceeding the rated current. This would definitely be useful in cases where reliability is a huge concern. Also since most of the practical motor operations are carried out at or below 60% of the full load capacity of such motors, the problem related to excessive currents is quite rare. Also it is important to note that the faulty cases studied in this work are limited to faults that would necessitate taking out one or more of the motor phases because of faults occurring in the drive or between the drive and the motor terminals, and not faults occurring in the actual motor winding turns inside the core of the machine.

CHAPTER 7: CONCLUSIONS AND RECOMMENDATIONS

7.1 CONCLUSIONS

In this thesis, a unique and useful design for a reversible three-phase to six-phase induction machine was developed. The main aim of this design was to introduce multiple phases in order to improve the reliability of the motor under loss of phase or phases due to external fault conditions to the motor. The design approach was to maintain the same structure / core for both the three-phase and the six-phase operations. Thus, by reconnecting the coils available at the terminals , both of the three-phase and six-phase operations could be achieved. Both configurations were TSFE simulated for their performance characteristics and parameters to check whether the reconfigured six-phase case meets the required specifications. The TSFE simulation results were verified by experimental data for the three-phase operation. More specifically, effects of different types of phase-loss scenarios on the torque of the six-phase motor were studied and a comparitive analysis of the various phase-loss conditions with respect to the healthy case was presented.

The analysis of the ripple content in the torque under various loss of phase / phases conditions were presented and reasoned by using the concept of locus of current space-vector, which pictorially and effectively reflects the deterioration of the quality of the torque-profile under the different cases. The closer the locus is to the shape of a circle the better the quality of the torque developed by the motor. Also the harmonic analysis of the time-domain torque profiles

under these various faulty-phase cases reveals the effect of the magnitude of the second order harmonic on the ripple content in the torque.

Overall , It was shown that the six-phase motor exhibits better performance under the loss of phases than the three-phase motor without any external control techniques. Moreover, some of the cases gave results which were very close to the healthy operation.

Although , there are some thermal issues with regard to excessive phase currents under loss of phase conditions, these issues have been addressed here. Namely, one of the solutions to this issue presented in this work is the concept of derating the motor output. It was shown that this method of derating is an effective way to minimize the current in the phases thereby rendering a safe operation. It is important to note that these thermal issues come into play only under full-load conditions. But since most of practical motor operations are carried out at or below 60 % of the rated condition, it is quite rare that this problem would be encountered under many of these loss of phase/phases scenarios. Thus , the reversible three-phase/six-phase motor design was successfully achieved, and serves the purposes of maintaining performance quality under faulty conditions far better than the conventional three-phase design.

7.2 RECOMMENDATIONS FOR FUTURE WORK

In this work , the main focus was given to the design aspects of the reversible three-phase to six-phase induction motor. The six-phase configuration was then studied under different types of phase-loss conditions under direct line energization. This work can later be applied to study the limp-home stratergies under operation from a six-phase open-loop and closed-loop inverters . Also exploration of different inverter control algorithms for enhanced performance under faulty conditions should be explored in light of the possible use of the additional degrees of freedom (phase currents and voltages) available , where one can / might effectively improve the overall performance of the motor , in so far as achieving the least amount of ripple in the steady state

torque, even under some of the loss of phase cases presented in this thesis, with possible minimization of the imbalance between the phase currents through drive control techniques.

REFERENCES

[1] T.M. Jahns. "Improved Reliability in Solid-State AC Drives by Means of Multiple Independent Phase-Drive Units." *IEEE Transactions on Industry Applications*,Vol. IA-16, pp. 321-331. May/June,1980.

[2] E.A. Klingshirn, "High phase order induction motors - Part I –Description and theoretical consideration," IEEE Transactions on PowerApparatus and Systems, vol. PAS-102, n° 1, January 1983, pp.47 -53.

[3] G.K. Singh, "Multi-phase induction machine drive research – a survey," *Electric Power Systems Research,* vol. 61, no. 2, pp.139-147, 2002.

[4] H.A. Toliyat and H. Xu, "DSP-based direct torque control (DTC) for five-phase induction machines," *Proc. Int. PowerElectronics Conf. IPEC,* Tokyo, Japan, pp.1195-1200, 2000.

[5] E. Levi, S.N. Vukosavic and M. Jones, "Vector control schemes for series-connected six-phase two-motor drive systems," *IEE Proc. – Electric Power Applications,* vol. 152, no. 2, pp. 226-238, 2005.

[6] R. Bojoi, F. Farina, G. Griva, F. Profumo and A. Tenconi, "Direct torque control for dual three-phase induction motor drives," *IEEE Trans. on Industry Applications,* vol. 41, no. 6,pp.1627-1636, 2005.

[7] Peter Vas, Sensorless Vector and Direct Torque Control,Oxford University Press, 1998.

[8] B. K. Bose, Power Electronics and AC Drives, Prentice-Hall,Englewood Cliffs, New Jersey, 1986.

[9] J.B. Wang, K. Atallah and D. Howe, "Optimal torque control of fault-tolerant permanent magnet brushless machines," *IEEE Trans. on Magnetics*, vol. 39, no. 5, pp. 2962-2964, 2003.

[10] B.C. Mecrow, A.G. Jack, D.J. Atkinson, S.R. Green, G.J.Atkinson, A. King and B. Green, "Design and testing of a Four phase fault-tolerant permanent magnet machine for an engine fuel pump," *IEEE Trans. on Energy Conversion,* vol.19, no. 3, pp. 671-678, 2004.

[11] G.J. Atkinson, B.C. Mecrow, A.G. Jack, D.J. Atkinson, P.Sangha and M. Benarous, "The design of fault tolerant machines for aerospace applications," *Proc. IEEE Int. Electric Machines and Drives Conf. IEMDC*, San Antonio, TX, pp.1863-1869, 2005.

[12] A.J. Mitcham, G. Antonopoulos and J.J.A. Cullen, "Favourable slot and pole number combinations for fault-tolerant PM machines," *IEE Proc. - Electrical Power Applications,* vol.151, no. 5, pp. 520-525, 2004.

[13] J. R. Fu and T.A. Lipo, "Disturbance free operation of a multiphase current regulated motor drive with an open phase", *IEEE Trans on .Ind Applications,*Vol. 30, Issue.5, Sep. – Oct. 1994, pp.1267 -1274.

[14] Leila Parsa, Hamid A. Toliyat, "Fault-Tolerant Interior-Permanent-magnet Machines for Hybrid Electric Vehicle Applications" , *IEEE Transactions on Vehicular Technology*, Vol.56,No.4,July 2007,pp.1546-1552.

[15] T. H. Liu, J. R. Fu, and T. A. Lipo, "A strategy for improving reliability of field oriented controlled induction motor drives," 1991 *IEEE U S Annu. Meet. Conf. Rec.,* vol. 1, pp. 449-455, 1991.

[16] C. B. Jacobina, R. S. Miranda, M. B. de R. Corrêa, A. M. N. Lima, "Disturbance-Free

operation of a six-phase AC motor drive system", *IEEE Power Electronics Specialist Conference*, Aachen Germany, 2004.

[17] H. A. Toliyat, "Analysis and simulation of multi-phase variable speed induction motor drives under asymmetrical connections", *APEC '96*, Volume 2, 3-7 March 1996 , pp.586 -592.

[18] Yifan Zhao, Thomas A. Lipo, "Modeling and control of a multi-phase induction machine with structural unbalance", *IEEE Transactions on Energy Conversion*, vol.11,No.3,September 1996, pp.578-584.

[19] Gerard Aroquiadassou, Humberto Henao, "Experimental Analysis of the dqo stator current component spectra of a 42V fault-tolerant six-phase induction machine drive with opened stator phases", *Diagnostics for Electric Machines, Power Electronics and Drives, 2007*. September 2007 , pp. 52-57.

[20] J. P. Martin and F. Meibody-Tabar, "Multi-phase permanent magnet synchronous machine supplied by VSIs, working under fault conditions", *IEEE Industry Applications Conference*, Volume 3, 8-12 Oct. 2000, pp.1710-1717.

[21] N.A.O. Demerdash, "Design and Analysis of Electric Motors in Adjustable Speed Drives" Class Notes for EECE 185, Department of Electrical and Computer Engineering, Marquette University, Milwaukee, Wisconsin, Fall 2007.

[22] C. B. Jacobina, R. S. Miranda, and A. M. N. Lima, "Reconfigurable Fault Tolerant Dual-Winding AC Motor Drive System,"IEEE Trans. On Power Electron. , 2005 Page(s):1574 – 1579.

[23] R. Peuget, S. Courtine, and J. P. Rognon, "Fault detection and isolation on a pwm inverter by knowledge-based model," *IEEE Trans. Ind. Aplicat.*, vol. 34, pp. 1318–1326, Nov./Dec. 1998.

[24] R. Ribeiro, C. Jacobina, E. da Silva, and A. Lima, "Fault detection in voltage-fed pwm motor drive systems," in *Conf. Rec. PESC*, pp. 242–247, 2000.

[25] M. Correa, C. Jacobina, E. da Silva, and A. Lima, "An induction motor drive system with

improved fault tolerance," *IEEE Trans. Ind. Applic.*, vol. 37, pp. 873–879, May/June 2001.

[26] Chia-Chou Yeh, and Nabeel A. O. Demerdash, "Fault Tolerant Operations in Adjustable-Speed Drives and Soft Starters for Induction Motors," IEEE Trans. On Power Electronics, 17-21 June 2007 Page(s):1942 - 1949

[27] Ahmed Sayed-Ahmed, Chia-Chou Yeh, Behrooz Mirafzal, and Nabeel A. O. Demerdash, "Analysis of Stator Winding Inter-Turn Short-CircuitFaults in Induction Machines for Identification of the Faulty Phase," *IEEE Trans. Ind. Applications*, Volume 3, 8-12 Oct. 2006 Page(s):1519 – 1524.

[28] Sarani, E., Abbaszadeh, K., and Ardebili, M, "Modeling and simulation of turn-fault and unbalance magnetic pull in induction motor based on magnetic equivalent circuit method", *Electrical machines and Systems, 2005, ICEMS 2005.Proceedings of the Eighth Intenational Conference on*, vol. 1, pp. 52-56, 27-29 Sept. 2005.

[29] Gennadi. Y. Sizov, "Analysis, Modeling, and Diagnostics of Adjacent and Nonadjacent Broken Rotor Bars in Squirrel-Cage Induction Machines", M.S. Thesis , Marquette University , Wisconsin , U.S.A., 2007.

[30] Behrooz Mirafzal, "Incipient Fault Diagnosis In Squirrel-Cage Induction Motors", Ph.D. dissertation, Marquette University, Milwaukee, WI, 2005.

[31] S.C. Tandon, A.F. Armor, and M.V.K. Chari, "Nonlinear Transient Finite Element Field Computation for Electrical Machines and Devices", IEEE Transactions on Power Apparatus and Systems, Vol. PAS-102, No. 5, pp. 1089-1096 May 1983.

[32] M.V.K. Chari, G. Bedrosian, J. D'Angelo, and A. Konrad, "Finite Element Applications in Electrical Engineering", IEEE Transactions On Magnetics, Vol. 29**,** No. 2, pp. 1306-1314 March 1993.

[33] P. Silvester, and Madabushi V. K. Chari, "Finite Element Solution of Saturable Magnetic

Field Problems", IEEE Transactions On Power Apparatus and Systems, vol. PAS-89, no. 7, pp. 1642-1651 September/October 1970.

[34] Demerdash, N. A., Bangura, J. F., Isaac, F. N. and Arkadan, A. A., "A Time-Stepping Coupled Finite Element-State-Space Model for Induction Motor Drives-Part 1: Model Formulation and Machine Parameter Computation and Part 2 Machine Performance Computation and Verification," *Papers No. 376 and 377 Presented at the* IEEE-IEMDC, *May 1997. and Accepted for Publication in the IEEE Transactions on Energy Conversion.*

[35] J. F. Bangura, "A time-stepping coupled finite element-state space modeling for on-line diagnosis of squirrel-cage induction motor faults," Ph.D. dissertation, Marquette University, Milwaukee, WI, 1999.

[36] N. A. Demerdash and J. F. Bangura, "A time-stepping coupled finite element-state space modeling for analysis and performance quality assessment of induction motors in adjustable speed drives applications,"presented at the Naval Symposium on Electric Machines, Newport, RI, 1997.

[37] J. F. Bangura and N. A. Demerdash, "Diagnosis and characterization of effects of broken rotor bars and connectors in squirrel-cage induction motors by a time-stepping coupled finite-element-state space modeling approach," *IEEE Trans. Energy Conv.*, vol. 14, pp. 1167–1175, Dec. 1999.

[38] J. F. Bangura and N. A. Demerdash, "Simulation of inverter-fed induction motor drives with pulse-width modulation by a time-stepping coupled finite element-flux linkage-based state space model," *IEEE Trans. Energy Conv.*, vol. 14, pp. 518–525, Sept. 1999.

[39] J. F. Bangura and N. A. O. Demerdash, "Effects of broken bars/end-ring connectors and airgap eccentricities on ohmic and core losses of induction motors in ASDs using a coupled finite element-state space method," *IEEE Trans. Energy Conv.*, vol. 15, pp. 40–47, Mar. 2000.